Advances in High-Power Wireless Charging Systems: Overview and Design Considerations

Hao Feng, *Member*, *IEEE*, Reza Tavakoli, *Member*, *IEEE*, Omer C. Onar. Zeljko Pantic, *Member*, *IEEE*, and Omer C. Onar, *Senior Member*, *IEEE*

***Abstract*—Wireless charging systems are foreseen as an effective solution to improve the convenience and safety of conventional conductive chargers. As this technology has matured, recent broad applications of wireless chargers to electrified transportation have indicated a trend toward higher power, power density, modularity, as well as scalability of designs. In this paper, commercial systems and laboratory prototypes are reviewed, focusing mostly on the advances in high-power wireless charging systems. The recent endeavors in magnetic pad designs, compensation networks, power electronics converters, control strategies, and communication protocols are illustrated. Both stationary and dynamic (in-motion) wireless charging systems are discussed, and critical differences in their designs and applications are emphasized. On that basis, the comparison among different solutions and design considerations are summarized to present the essential elements and technology roadmap that will be necessary to support large-scale deployment of high-power wireless charging systems. The review is concluded with the discussion of several fundamental challenges and prospects of high-power wireless power transfer (WPT) systems. Foreseen challenges include utilization of advanced materials, electric and electromagnetic field measurement and mitigation, customization, communications, power metering, and cybersecurity.**

***Index Terms*—Wireless charging systems, high-power wireless chargers, transportation electrification.**

I. Introduction

THE last decade has witnessed a rapidly growing market of consumer electronics, industrial electronics, and electric vehicles (EVs). However, battery technology remains the major impediment to their further development. On the one hand, the capacity of commercialized lithium-ion (Li_Ion) battery severely restricts the vehicle range. As an illustration, the energy density of Li_Ion batteries is only 100–250 Wh/kg, compared to 12000 Wh/kg of gasoline [1]. On the other hand, the batteries are heavy and costly, with an average cost of approximately 200-400 USD/kWh [1]. The enhancement of cruising range is mostly dependent on adding more battery cells and modules, which further increases vehicle weight and cost.

To solve the capacity constraint without a significant investment in battery systems, a flexible, efficient, and ubiquitous charging solution is needed. Apart from the conductive charging techniques, the wireless power transfer (WPT) technology is an alternative charging method that has been introduced and studied extensively in recent years. The concept of WPT was proposed by scientist Nikola Tesla more than a hundred years ago, but it took time for the technology to mature and become a technically feasible and commercially competitive solution. The new technology replaces the wired interface by a pair of physically separated couplers, allowing energy to be transferred in a contactless manner. Compared with traditional conductive power transfer, WPT technology features high application convenience and adaptability. It eliminates the need for heavy charging cords and connectors, and is weather-resistant and vandalism proof. In addition, wireless charging systems offers high operational flexibility since the power supply and the powered device are coupled through the magnetic field, allowing the device to be charged anytime and anywhere, even while the vehicle is moving [3]. Therefore, it is a practical means to solve the range anxiety of electrified transportation and electronic devices [4]. Insulation and worn conductor issues caused by contact friction in a variety of harsh environments, such as underwater, underground, and aerospace, are eliminated, which significantly improves the safety and reliability of charging systems [5]. Given the above advantages, WPT applications cover a wide range from low-power electronic devices to high-power transportation systems. Furthermore, it can be extended to scenarios where reliable, automated, and space-isolated power transfer is demanded [6].

The advantages of WPT technology makes it suitable for large-scale deployments to enable convenient and safe charging, such as the charging infrastructure in electric and electrified transportation. Nowadays, the high-power Stationary Wireless Charging (SWC) technology has gradually matured [1]. On this basis, Dynamic Wireless Charging (DWC) was proposed and quickly became trending research for EV wireless charging [7]. DWC envisages embedding wireless

Hao Feng, Reza Tavakoli, Zeljko Pantic are with Electrical and Computer Engineering Department, North Carolina State University, Raleigh, NC USA. (e-mail: hfeng6@ncsu.edu, stavako@ncsu.edu, zpantic@ncsu.edu).

Omer C. Onar is with the Power Electronics and Electric Machinery Research Group in the Electrical and Electronic Systems Research Division of Oak Ridge National Laboratory, Oak Ridge, TN, 37830 USA. (e-mail: onaroc@ornl.gov)

charging pads in a small section of the road to provide an opportunity charging for a moving EV. In theory, the DWC approach can solve the problem of limited cruising range [8]-[9]. Practically, the implementation of this concept faces challenges at high vehicle speeds and demands a costly initial capital investment. Alternatively, the quasi-dynamic charging concept assumes the long-time manual charging to be replaced by fully automatic distributed charging at bus stops, commercial centers, or even traffic lights where EVs densely gather or make stops along the route [10]-[11]. DWC not only solves the range anxiety but also helps reduce the battery capacity requirements and expands the battery life due to shallow discharging patterns brought by opportunity charging, thereby reducing the EV cost. The literature [12] points out that the long-term benefits of adding DWC facilities can make up for its initial infrastructure costs, and the overall cost will not increase significantly, making dynamic wireless charging an economically viable solution.

The WPT system can be realized based on different physical principles. According to the medium for power accumulation and transfer, the WPT technology is mainly divided into three categories: microwave radiation type, electric field-coupled type, and magnetic field-coupled type [13]-[15].

Microwave-based WPT systems transfer energy through spatial microwave directional radiation. The principle is illustrated in Fig. 1. An RF power amplifier converts a DC signal to microwaves. The microwave beam is then sent out by the transmitting antenna. The receiving antenna is oriented to receive microwaves and finally rectifies them into DC power that can be used by the equipment. Owing to its characteristics such as long transmission distance and possible high power capacity, the microwave-based WPT is mainly used in long-distance and high-power WPT applications. Previous demonstrations include space solar power stations, microwave aircrafts, and inter-island wireless transmissions [16]-[17]. As early as 1988, there were some attempts to power an aircraft model by using microwaves at 2.45 GHz. The system is rated at 10 kW, which was able to drive a 2.9 x 4.5 m^2 model aircraft, 150 meters above the ground [17]. For EV charging applications, Mitsubishi Electric worked with Kyoto University to develop a commercial EV microwave charging system. They used magnetron-based 2.45 GHz microwaves to transfer 1 kW to the receiving antenna mounted on the vehicle chassis [17]. The end-to-end efficiency obtained by the experiment was above 70%. The major issues in implementing this technology to EV charging are the potential influence of microwave radiation on the human body and the complexity of safely orientating the microwaves. Moreover, the efficiency of such systems needs to be improved for broader applications in high-power charging systems [18].

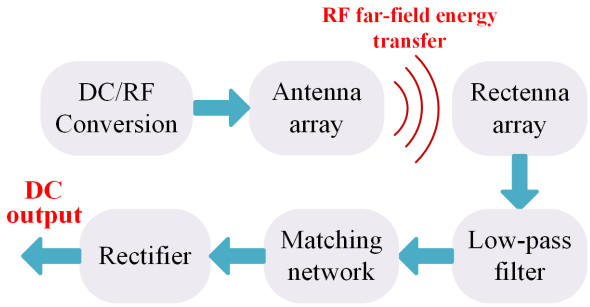

Fig. 1. Diagram of WPT based on microwave technology.

WPT via near-field magnetic coupling is the most widely studied and employed WPT method. In magnetically coupled systems, the receiver coil picks up the magnetic field generated by the high-frequency current in primary coils and converts it into DC current to charge. A near-field magnetically-coupled coils can be considered as a loosely coupled transformer with its primary and secondary windings separated by a significant distance [21].

Due to the large air gap, the leakage of loosely coupled coils is much higher than in conventional transformers, and the corresponding coupling factor is usually below 0.3. Given the low coupling, efficient power transfer can still be realized if the quality factor of coils is properly optimized [22]. The state-of-the-art WPT efficiency is commensurate to that of conductive charging. The power level has already reached hundreds of kilowatts, and megawatts of power are also achievable through paralleling multiple modules or deploying polyphase systems [23]. Besides, the vertical air gap and horizontal allowable misalignment reach several tens of centimeters, and is comparable to half of the coil diameter. The magnetic resonance principle was proposed in 2008 for WPT systems [24]. However, it is essentially a special case when the quality factor of an air-core coil is enhanced by the MHz-range excitation to compensate for the drop of coupling factor so that the high-efficiency power transfer can be achieved even at large air gaps [25].

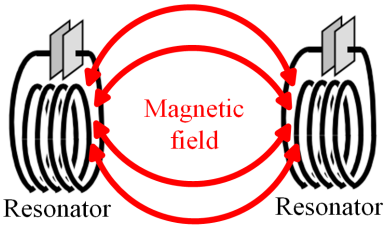

Fig. 2. Principles of magnetic coupled WPT.

Electric field-coupled WPT systems referred to as capacitive power transfer (CPT) systems, utilize two pairs of plates to form an equivalent capacitor for transferring power, as outlined in Fig. 3. Owing to its unique operating principle, the CPT can be used in applications that require power transfer through metallic materials since a capacitor is formed from each conductor plate to the metallic surface [26]. Furthermore, it features favorable characteristics such as lightweight and cost-effective couplers than couplers in magnetically coupled WPT systems; and the power transfer is less sensitive to the misalignment as the electric field between plates “bends” with the misalignment of the plates. However, the capacitance composed by paralleled plates is usually very small which

adversely affects the power transfer capabilities of couplers [27]. To solve that issue, high operating frequency in the MHz range is demanded to reduce the impedance of the power flow channel. In [29], a stacked, four-layer structure is applied with LCL compensation to transfer 1.88 kW at a 150-mm air-gap. In [27], a six-plate coupler is set up to reduce the electric field emission. A 1.97-kW power transfer is achieved at a 150-mm air-gap. Reference [31] describes a CPT system transferring 2.4 kW at a 150-mm air gap. Generally, the power level of several kilowatts is achievable using CPT. However, one of the major barriers of a high-power CPT system is the power density constraint. To deliver power efficiently for a large air gap, the dimension of coupler should usually be much larger than the air gap, which may not be practical in many scenarios. With dedicated coupler integration in [29], the reported power density is still as low as 11.88 kW/m^2. Reference [28] increases the power density to 29.5 kW/m^2 by pushing the frequency to 13.56 MHz. As a comparison, the state-of-the-art surface power density of magnetically coupled wireless power transfer can reach up to 1.6 kW/dm^2 (160 kW/m^2), according to [38], and higher power densities are possible with polyphase couplers. One feasible solution is to further increase the operating frequency. However, ultrahigh switching frequency and high power capability are hampered by the existing technology of semiconductor devices. Moreover, frequency from the HF frequency range can cause excessively high-voltage stress on compensation networks. The enhancement of Gallium Nitride (GaN) switch technology and multiphase modular design are expected to boost the future development of high-power CPT charging systems [32].

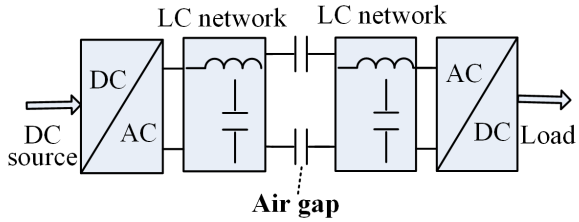

Fig. 3. Diagram of an electrical field-based (capacitive) WPT system.

A comparison of the discussed WPT techniques is presented in , considering factors such as efficiency, controllability, safety, and cost. Currently, the near-field magnetic coupling is still the most practical and prevailing means to enable high power transfer.

Through numerous research efforts and prototype demonstrations, the large-scale deployment of WPT systems has become feasible. Moreover, accompanied by the rapidly growing demand for fast charging facilities, the recent development of WPT systems presents a trend towards a higher power, high power density, and higher flexibility and scalability. Bombardier Primove initiated several 200-kW wireless charging systems for electric buses equipped by 60 kWh and 90 kWh battery packs. The electric buses are charged in the very few minutes of dwell time spent at the end station, and the reported AC to DC efficiency is higher than 90% [35]. Momentum Dynamics also developed a WPT system for electric trucks and vans with a power level of up to 200 kW [36]. In [37], a 1-MW WPT system is designed and tested for plug-in hybrid vessels, which allows for reliable onshore charging in a damp environment. Researchers at ETH provided a comprehensive design consideration regarding a Silicon Carbide (SiC)-based 50-kW wireless charger [38]. The efficiency, power density, and leakage field were optimized jointly, accounting for the thermal and size limitation. Conductix cooperated with the University of Auckland to test a 60 kW charger on electric buses [39]. WAVE designed and tested a 250-kW wireless charger for electric fleets in Southern California. The newly granted DOE project envisages a 500 kW wireless charging system for drayage trucks [40]. WiTtricity presented a series of products up to 11 kW and is further developing prototypes supporting 25 kW power transfer. The prototype described in [41] realized a full SiC-based operation and showed a grid to battery efficiency of 91% to 93%. Fraunhofer Institute in Germany demonstrated a full power electronics prototype for a 22-kW bidirectional wireless charger. The highest efficiency reached more than 96% (dc-to-dc; from primary-side inverter input to the secondary-side rectifier output) owing to a novel controller design [42]. Recently, Oak Ridge National Laboratory (ORNL) developed a single-phase 100-kW wireless charger, reaching an efficiency of around 97% for 5 inches air gap with a single transmitter and receiver without paralleling multiple units [43]. Toshiba tested a 44-kW modularized WPT system for electric buses and evaluated its EMI performance to comply with the International Commission on Non-Ionizing Radiation Protection (ICNIRP) leakage field emission guideline [46]. In [47], a 25-kW wireless charging module is built based on three paralleled half-bridge cells, and 95% dc-to-dc efficiency is achieved.

Regarding the dynamic charging system, Korean Advanced Research Institute (KAIST) has completed a series of large-scale demonstrations on railway transit and EVs, in which they propose various magnetic coupler structures to improve the compactness, EMC performances, and compatibility to roadway construction [48]. A 1-MW prototype for high-speed trains is designed by Korean Railroad Research Institute (KRRI), which is tested up to 800 kW [23]. Bombardier Primove has developed a DWC system at 250 kW for trams [49]. Integrated Infrastructure Solutions (INTIS) research team set up a 25-m track to test the performance of DWC of EVs at 200 kW [50]. They also deploy a DWC for industrial movers at 30 kW [51]. In [52], Utah State University demonstrated a 25 kW dynamic charging system that allowed 15 cm of lateral

TABLE I
THE COMPARISON OF DIFFERENT WPT PRINCIPLES

WPT principle	Advantages	Disadvantages
Microwave	• Ultra-long transfer distance	• High radiation and losses • Antenna and rectenna orientation needed • Complex equipment
Electric field coupling	• Light and low-cost couplers • Can transfer power through metal • Better misalignment tolerance than magnetic WPT	• Limited power due to low capacitance of plates • Very high electric field requirement
Magnetic field coupling	• Highest efficiency • Can adapt to power transfer widely ranging from up to MW level to several watts	• Short power transfer distance. Larger distance can be achieved by increasing the quality factor to compensate the weak coupling

misalignment while still delivering full power. Besides, IK4-Ikerlan Research Center in Spain also initiated a 50-kW dynamic charging project [53]. In Table II, recent commercial products and laboratory prototypes of high-power wireless chargers are summarized. Only SWC systems are included as the efficiency and power density of DWC are hard to quantify using regular definition.

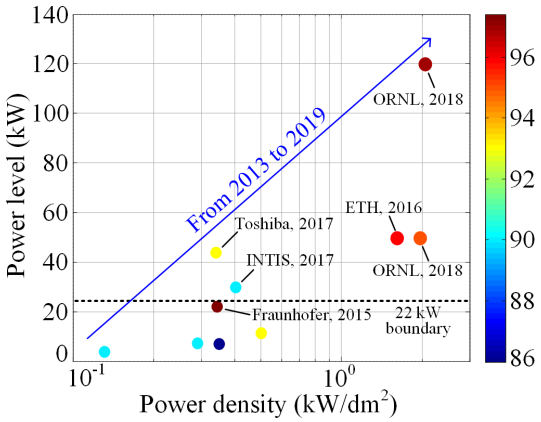

Fig. 4. Trend in power level, power density, and efficiency of some recently developed wireless chargers.

The representative cases are illustrated in Fig. 4 regarding their power level, efficiency, and area-related power density. As can be perceived, significant improvement has been made in all aspects during recent years. For high-power wireless charging systems, the highest dc-to-dc efficiency reaches over 97%, and optimal power density is around 2 kW/dm^2. Since 2016, most of the stationary charging systems have been aiming for power levels higher than 22 kW, which have not yet been covered in WPT standardization development by SAE J2954. The motivation towards higher power charging has also been encouraged by policy suggestions or targets set by governments. In 2017, DOE set up a goal to reduce the charging time to 15 minutes or less, which requires a power level of 350 to 400 kW for the charging system [55]. In order to fill the demand gap, it is expected that the power level of wireless charging systems will further increase to accommodate ever-growing EV penetration and to provide a charging experience paralleled to fossil fuel based refueling.

Recent demonstration projects of high-power charging systems significantly accelerate the commercialization of WPT systems. The standard to accommodate the specific power range is still under development by SAE J2954 [72]. However, novel concepts in terms of magnetic pad design, compensation topology, power conversion architecture, and control algorithms have already been proposed to improve the overall performance of high-power WPT systems. Throughout these projects, challenges emerge, such as thermal management, EMI compatibility, real-time communication, and others, which requires design guidelines to further optimize high-power WPT systems and promote their applications. Recent surveys have partially summarized the advances in high power WPT systems. In [18], a review of wireless power transfer for vehicular applications is presented. However, emerging topics, such as pervasive applications of WBG devices, the growing trend of CPT systems, mechanical issues inherent to road integration, the impact of DWC on the power grid, and measurement precision are not discussed. In [19], the wireless power transfer for general applications is reviewed with an emphasis on low power midrange applications. The major limitation of this paper lies in the scarcity of critical topics, such as power electronics, couplers, and communications. Literature

TABLE II RECENT COMMERCIAL AND LABORATORY PROTOTYPES IN HIGH POWER WIRELESS CHARGERS

Institution	Power level	Performance	Year
WiTricity [34]	3.7 kW (WiT-3300)	Primary coil: 500 mm x 500 mm x 37.5 mm (12.5 kg) Power density: 0.13 kW/dm^2 DC-DC efficiency 90% at 180 mm air gap	2013
Toshiba [33]	7 kW	Coil size: 600 mm × 400 mm, air gap 160 mm	2014
BOSCH [192]	7 kW	Primary coil: 360 mm x 560 mm (2.8 kg) Secondary coil: 260 mm x 260 mm (1.8 kg) Power density: 0.35 kW/dm^2 DC-DC efficiency > 86%	2015
Bombardier Primove [35]	200 kW	Grid to battery efficiency > 90%	2015
Fraunhofer Institute for Solar Energy Systems (ISE) [42]	22 kW	Primary coil: 800 mm x 800 mm x 32 mm (38.2 kg) Air gap: 130 mm; DC-DC efficiency: 97.4%	2015
WiTricity [41]	11 kW	9-28 cm; Grid to battery efficiency: 91% to 93%	2016
ETH [38]	50 kW	Coil size: 410 mm x 760 mm x 60 mm DC-DC efficiency: 95.8% under 160 mm air gap Power density: 1.6 kW/dm^2	2016
Toshiba [46]	44 kW	Maximum misalignment tolerance: ± 10 cm minimum Air gap: 10 cm minimum	2017
INTIS [44]	30 kW	Air gap: 14 cm; Gross battery capacity: 22.5 kWh Pick-up dimensions: 880 x 860 x 25 mm	2017
ORNL [200]	50 kW	Air gap: 150 mm; DC-DC efficiency: 95% Power density: 1.95 kW/dm^2	2018
ORNL [45]	120 kW	Air gap: 5 inches; DC-DC efficiency: 96.9% at 50 kW Power density: 2.04 kW/dm2	2018
WAVE [40]	500 kW	N/A	2019

[20] gives an overall review of recent research and industrial projects. However, the overview is limited to the level of introducing the progress and lacks technical discussion of critical subsystems, such as compensations and power electronics.

This paper focuses on the high-power magnetic field-based wireless charging systems. It should be noted that the definition of high-power varies from case to case, depending on the application and medium. The definition of high-power in this paper refers to the power level higher or equal to WPT1 defined by SAE J2954, namely 3.7 kVA. Whereas the content will mostly focus on the technologies that contribute to upcoming WPT4 deployment. This review will cover recent high-power prototypes and commercial endeavors regarding magnetic pad designs, compensation networks, power electronics topology and architectures, control, monitoring, and communication systems. The designs are evaluated, and the advantages and drawbacks of previous solutions are identified. Finally, the future challenges and prospects of high-power wireless charging are discussed.

II. Theory of Operation

A. Governing Principle

The principle of operation of near-field magnetic-based wireless power transfer can be explained by the notion of Ampere's and Faraday's laws, as indicated in Fig. 5.

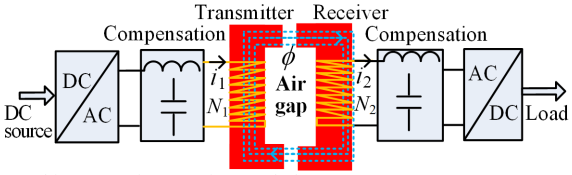

Fig. 5. Architecture of magnetic-coupled WPT systems.

On the primary-side, according to Ampere's law, an AC current generates a time-varying magnetic flux around the conductor. The flux is linked to the secondary-side coupler and induces a voltage across the conductor. The magnetic field generated by primary is proportional to the current and length of the primary coil (number of turns) as governed by Ampere's Law. The amplitude of the induced voltage is proportional to the coupled flux and the number of turns in the conductor, as governed by Faraday's Law:

$$\oint_C B \cdot dl = \mu_0 N_1 I \qquad \vartheta = -N_2 \frac{d\phi}{dt} \tag{1}$$

where N_1 and N_2 are the number of turns on the primary and secondary-sides, B is the magnetic field, C is the boundary of curve for integration. μ_0 is the permeability of air. I is the primary coupler current, ϑ is the voltage induced on the secondary-side, and ϕ is the flux coupled to the secondary-side.

A conceptual wireless charging system contains a pair of coils separated from each other, and because of that, it is commonly referred to as a loosely coupled transformer. Due to a large air gap, only a portion of the magnetic flux generated by the primary-side is coupled to the secondary, which leads to high leakage and low magnetizing inductances of the coils and introduces a large amount of reactive power circulating in the resonant network [54]. The increased reactive power causes higher electric stress on switching devices and passive components and raises thermal concerns for high-power charging systems. Therefore, one or more passive elements, referred to as a compensation network [56], are set up to provide a local path for the reactive power, preventing its circulation through the power source. Moreover, the compensation network also cancels the high inductive reactance of the coils at the resonant frequency, reduces the impedance of the coil, and enables injecting high current into the winding. As shown in Fig. 5, the high-frequency AC excitation is usually acquired by inverting DC source at a high switching frequency. The high-frequency alternating current at the secondary side is then rectified into DC current, filtered, and fed to the load.

B. Circuit Models and Analysis Methods

Different perspectives exist for understanding WPT systems. At the early developing stage of WPT systems, capacitors are deployed on both sides of a loosely coupled WPT coupler, and the operating frequency is tuned to approach the resonance frequency. The existence of a dual-sided resonant tank is considered to be analogous to a resonance system with two objects resonating at the same resonance frequency, which allows the amplitude of resonance to be amplified and power transferred more efficiently, as in a pair of pitchfork [25]. Despite its physical intuition, this explanation lacks the description of a circuit model and its operating modes, thereby not being instructive from an electrical point of view. The concept of magnetic resonance is brought up by MIT using coupled-mode theory [24]. However, the physical essence of magnetic resonance is not intuitive from a circuit point of view, and the mathematical derivation of a resonator is not straightforward.

Another view considers WPT systems as a conventional resonant converter that utilizes the resonance of an inductor and a capacitor to produce zero-crossing conditions, which facilitates the device soft-switching [57]. However, the WPT resonant network is typically composed of multiple L and C elements, resulting in multiple resonant modes, which is different from conventional ones that only contain a single LC resonance.

Given the diverse models and methods to describe the system, a simple and intuitive model is demanded to unify the understanding of the system and identify the physical meaning of WPT.

1) Mutual Inductance Model (Coupled Coils Model)

The mutual inductance model is the most commonly adopted model in wireless charging systems, in which the T-type transformer is transformed into a two-port network, and the coupling between the primary and secondary-sides is represented by the mutual inductance M, as indicated in Fig. 6. Compared to the transformer model, it features higher simplicity as it removes the leakage inductance and the turn ratio from the model, so that the number of variables is reduced.

The mutual inductance model can be expressed using the following circuit expressions:

$$\begin{bmatrix} V_{inv} \\ 0 \end{bmatrix} = \begin{bmatrix} Z_1 & -j\omega M \\ -j\omega M & Z_2 \end{bmatrix} \begin{bmatrix} I_1 \\ I_2 \end{bmatrix} \tag{2}$$

in which the primary-side impedance is simplified as $Z_1=R_1+j(\omega L_1-1/\omega/C_1)$, and the secondary-side impedance is

$Z_2=R_{eq}+R_2+j(\omega L_2-1/\omega/C_2)$. Therefore, the input impedance of the resonant tank can be solved as

$$Z_{in}=\frac{V_{inv}}{I_1}=\frac{Z_1Z_2+(\omega M)^2}{Z_2}=Z_1+\frac{(\omega M)^2}{Z_2} \tag{3}$$

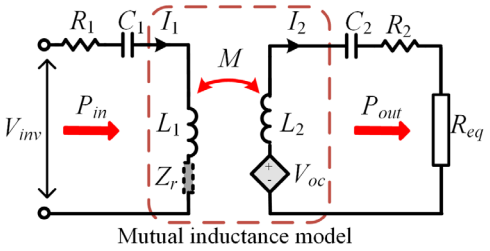

Fig. 6. Circuit diagram of the mutual inductance model.

The second term in (3) represents the reflected impedance from the secondary-side to the primary. Based on the above derivations, the equivalent mutual inductance model can be acquired as shown in Fig. 6. The reflected impedance Z_r and the secondary open-circuit voltage V_{oc} represent the coupling effect of the primary and secondary-side. With this definition, the input power of the system and the power received by the load are given below, respectively:

$$\begin{cases} P_{in}=\mathrm{Re}\left(\dfrac{V_{inv}^{\ 2}}{Z_{in}}\right)=\mathrm{Re}\left(\dfrac{V_{inv}^{\ 2}}{Z_1+(\omega M)^2/Z_2}\right) \\ P_{out}=P_{R_{eq}}=|I_2|^2R_{eq}=\dfrac{V_{inv}^{\ 2}(\omega M)^2R_{eq}}{|Z_1Z_2+(\omega M)^2|^2} \end{cases} \tag{4}$$

The apparent power between the primary side and the secondary side is expressed as:

$$S_{12}=|V_{oc}I_2|=|\omega MI_1I_2|=\left|\frac{V_{inv}^{\ 2}(\omega M)^2Z_2}{[Z_1Z_2+(\omega M)^2]^2}\right|=P_{out}\frac{|Z_2|}{R_{eq}} \tag{5}$$

According to (5), only when the secondary side is fully compensated as $Z_2=R_{eq}+R_2$, then purely active power is transferred between two sides. Moreover, the primary-side only provides active power when it is fully compensated. Therefore, equations (4) and (5) present an analytical tool to evaluate the power transfer characteristics and efficiency. It also provides insight on how to design the compensation network to improve the power transfer capability and efficiency.

2) Transformer Model

The transformer model is commonly used in the mode analysis of resonant converters. As shown in Fig. 7 (a), the circuit is described by a magnetizing inductance, physical turns ratio and leakage inductance on both sides. It largely facilitates the analysis of compensation relations between passive components, thereby helping formulate new compensation topologies that target different design objectives. Fig. 7 (b) presents another form of transformer model where all the parameters are reflected to the primary-side. L_k, L_{me}, and N_e stand for equivalent leakage, magnetizing inductance and turns ratio respectively. This is often seen in analysis of resonant converter built on regular transformer, such as the series resonant LLC converter. The low number of elements in this model enables simple selection of compensation topology and component value.

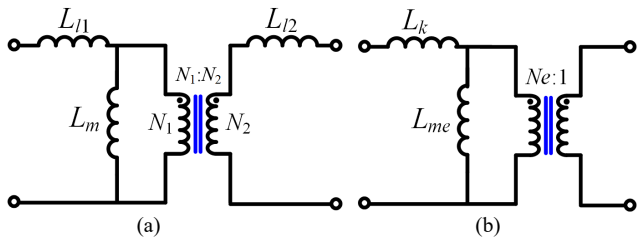

Fig. 7. The transformer model of loosely coupled transformer. (a) The transformer model that includes the primary leakage, secondary leakage and the physical turns ratio. (b) The model that reflect all leakage and magnetizing inductance to primary-side, and Ne represents equivalent turns ratio.

To correlate two different models, the equivalency of the two models is utilized to derive their parametric relationship. Using the Kirchhoff's Voltage Law (KVL) on both sides and observe from the input and output port, the mutual inductance model and the transformer model can be converted mutually. The following conclusion regarding the relationship between self-, leakage, magnetizing inductances and turns ratio can be expressed as:

M-model to T-model in Fig.7(a)

$$\begin{cases} L_1=L_{l1}+L_m \\ L_2=L_{l2}+L_m/N^2 \end{cases} \qquad L_m=NM \tag{6}$$

M-model to T-model in Fig.7(b)

$$\begin{cases} k=M/\sqrt{L_1L_2} \\ L_k=(1-k^2)L_1 \\ L_{me}=k^2L_1 \end{cases} \qquad N_e=k\sqrt{\frac{L_1}{L_2}} \tag{7}$$

Taking into account (6) and (7), the mutual inductance model and transformer model can be analyzed in a unified manner.

3) Coupled-mode Model

Marin Soljacic's research team at the MIT School of Physics was the first to propose the magnetic resonance WPT model [24]. The demonstrated magnetic resonant system uses two resonant coils of the same resonant frequency to generate a strong resonant coupling to achieve wireless power transfer. By increasing the frequency to MHz range, magnetic resonance WPT is more suitable for longer transfer distances since it uses high-Q coils to compensate for the lack of coupling.

In terms of modeling the power transfer process, magnetic resonant WPT utilizes the coupled-mode theory:

$$\dot{a}_m(t)=-(i\omega_m+\Gamma_m)a_m(t)-\sum_{n\neq m}i\kappa_{mn}a_n(t)+F_m(t) \tag{8}$$

The subscripts m, n represent individual resonators. $a_m(t)$ is defined as the energy in the m^{th} resonator, ω_m represents the free resonant frequency of the resonator. Γ_m is the inherent attenuation constant (related to ohmic and radiative losses). κ_{mn} is the coupling between the resonator m and resonator n. Finally, $F_m(t)$ is the excitation coefficient of the resonator m. It can be seen that the energy within the resonators is characterized by resonant frequency, damping factor (load condition), coupling factor, and excitation. Therefore, it shares the same physical meaning with the mutual-inductance model. The coupled-mode theory is essentially another mathematical formulation of the same wireless power transfer process.

A detailed comparison between models is illustrated in Table III.

TABLE III
THE COMPARISON BETWEEN MODELS FOR WPT SYSTEM

Models	Characteristics
Mutual inductance model	• Simplicity • Suitable for general math description • Cannot intuitively explain the compensation relation
Transformer model	• Easy to identify the compensation relation and explain the output source type • Helps generate new compensation networks for different design objectives • Requires a high number of elements in the equivalent circuit
Coupled-mode model	• Physical intuition • Complex math derivation • Not intuitive from an electric circuit point of view

C. *Frequency-domain Model*

Another relevant modeling category is the frequency-domain modeling, which is set up to characterize either the large-signal behavior to evaluate the transient envelop or the small-signal model to facilitate the controller design. The difficulty of WPT system modeling lies in being a high order system and massive external disturbance. In the recent efforts addressing the WPT system modeling, dynamic WPT (DWPT) systems are receiving growing attention recently due to its potential benefits in providing substantial range extension or charge sustaining driving for electric vehicles. In [58], a dynamic phasor model is built for analyzing the start-up process of a WPT system. Through Laplace transformation in phasor domain, the equivalent time-domain expression is acquired to calculate the inrush current. Hao *et al.* analyzed in detail the dynamics of an LCL-T-based WPT system in order to improve the tracking performance of an in-motion charging system [159]. A comprehensive WPT model is provided in [52] for a double-sided LCC compensation network. Using Generalized State-Space Averaging (GSSA), the system matrix (A matrix) is developed considering all the parasitic resistances, dc input filter, and secondary side dc/dc converter. In [60], GSSA is employed to model and control a series-series DWPT system. A designer can employ the A matrix to calculate the transfer function. In order to design a primary-side controller, a transfer function that is of significant importance is $G_{iv}(s) = I_{track}(s)/V_{inv}(s)$, where I_{track} is the RMS value of primary coil current and V_{inv} is the first harmonic of the inverter output voltage. The vehicle movement affects the mutual inductance time profile. Therefore, the controller bandwidth should be wide enough to incorporate the dynamics of power transfer variation caused by the highest vehicle speed. Fig. 8, taken from [52], compares the magnitude Bode plot of $G_{iv}(s)$ for a sample DWPT system at no-load and loaded conditions. One can observe that the secondary side adds several high-frequency dynamic modes to the system. However, it does not affect the frequency response at frequencies below 2 kHz. In other words, if the controller bandwidth is selected to be 2 kHz or below, the vehicle speed causing the variation of the reflected load to the primary may not affect the primary-side controller.

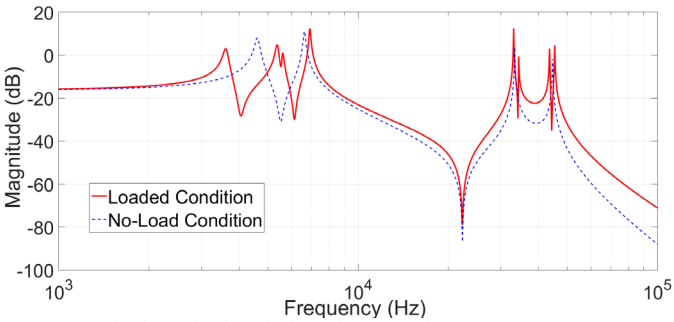

Fig. 8. Magnitude Bode plot of Giv(s) for a sample DWPT system [52].

Guo *et al.* studied the effect of vehicle speed on the induced voltage at the load side [61]. This induced voltage incorporates two factors: one is caused by the high-frequency time-varying magnetic field, and the other is created by the receiver coil movement. In [61], the authors considered the vehicle speed of 120 km/h and, based on their actual parameters, calculated the induced voltage. It was shown that the time-varying magnetic field induces 115 V, while the receiver movement only induces 1.6 mV. In other words, the vehicle speed does not play a significant role in transient analysis. In [62], mutual inductance is considered as a function of position, and the vehicle speed is included in the model to estimate system voltages and currents. Cui *et al.* modeled a DWPT system with constant mutual inductance [63]. However, in order to study the system instability caused by mutual inductance variations, they employed a mutual inductance observer and found that the system can maintain stability up to vehicle speeds of 200 km/h.

In dynamic charging systems, vehicle speed affects the amount of received energy. Therefore, Chen *at al.* included speed in their battery recharging plan [64]. They developed a model that helps the EV to select the charging lane and the required speed so that the trip time is minimized while ensuring completion of the trip without running out of charge [64]. In [12], the benefits of the dynamic charging system were demonstrated by analyzing how much the vehicle battery size can be reduced. In order to estimate the battery state-of-charge (SoC) during wireless charging, vehicle speed and charging time are essential parameters. Liu and Song optimized the location of DWPT pads and the vehicle battery size, simultaneously [65]. They considered speed as a predefined profile in a deterministic model for charging electric buses. Maximum efficiency tracking using the secondary side DC/DC converter can improve the DWPT power transfer efficiency. However, the mutual inductance information needs to be estimated in real-time in some of the control methods and implementations. In [66], a recursive least squares filter is used to estimate mutual inductance in a DWPT system, and the duty cycle of a buck converter at the secondary is controlled to maximize the efficiency. Dai *et al.* modeled a segmented DWPT system and considered mutual inductance variations in the system [67]. They used an equivalent circuit method and state-space averaging to build a dynamic model. In [68], a dc modeling approach is employed to analyze the dynamics of an *LCC* compensation network at the secondary side of a DWPT system. The modeling analysis shows that the dynamics of the resonant network have no impact on the control-to-output transfer function, but it affects the input-to-output dynamics.

TABLE IV
SUMMARIZATION OF J2954 STANDARD RECOMMENDED PRACTICE [72]

Maximum Power Level (at the input)	Z-Class (Distance (mm) from the surface of the secondary pad to the ground level)	Frequency range
• WPT1 3.7 kVA • WPT2 7.7 kVA • WPT3 11.1 kVA • WPT4 22 kVA (under development)	Z1 100-150 Z2 140-210 Z3 170-250	85 kHz center operating frequency within international frequency band of 79-90 kHz

Arteaga *et al.* calculated the WPT energy efficiency considering coupling factor k as a probability distribution [69]. They showed that the unpredictability of k can be considered as a stochastic variable, and its dynamic behavior can be modeled using a Probability Density Function (PDF). The PDF can be obtained by determining the probability distribution of the relative position between the transmitter and receiver coils [69]. A similar concept is employed in [52] where mutual inductance time profile is included as a random variable to estimate the expected value of DWPT energy efficiency.

D. Standards

Standards define the criteria that WPT systems should comply with. Unlike the area of low-power consumer electronics where two fully developed standards are available (Qi [70] and AFA Resonance [71]), the development of a standard for high-power WPT is still in progress. So far, the most commonly adopted international regulation for high-power WPT systems is SAE J2954. Although still being in the Recommend Practice phase, the document has already gone through a number of major revisions. It represents a sublimation of knowledge and excellent guidance for developing WPT systems for electrified transportation. The standard adopts the top-down approach defining the WPT charging system as well as its sub-systems and components. In its original draft, the design requirements and principles are defined, including the frequency range, power level classes (WPT1, WPT2, etc.), distances classes (Z1, Z2, etc.), reference pad models, maximum stray field levels, interoperability, etc. [240].

Some of these parameters are summarized in Table IV. More recently, SAE International has published the third version of recommended practice for SAE J2954, which specifies the requirements of WPT for EVs of up to 11 kW power levels [72]. The joint testing results from automotive manufacturers and research institutions show that the SAE J2954 WPT designs of two prevailing pad structures (circular and DD) are interoperable in terms of power and efficiency [73].

Another critical functionality described by J2954 is the communication protocol. J2954 relies on J2836/6, J2847/6, and J2931/6 to define the communication needs of a WPT system.

They incorporate the guidance and alignment communication to facilitate the manual or automatic vehicle positioning and the communication between ground assembly and vehicle assembly to achieve power transfer control and monitoring. The battery side measurements, such as voltage, current, temperature, SOC, can be measured by sensors or monitored from the battery management system's (BMS) controlled area network (CAN) bus and this information is wirelessly communicated to the primary-side or regulating the charging process or implementing a charge profile.

In addition to SAE J2954, there is also another standard development activity named SAE J2954/2 which focuses on high power WPT systems for medium and heavy-duty vehicles. SAE J2954 is expected to cover safety limits and performance targets, vehicle EVSE alignment methods, magnetic interoperability specifications, and verification testing up to 250 kW power levels. SAE J2954/2 is created to address the truck, bus, and rail applications of WPT systems at high-power levels. With relatively higher airgaps and higher power levels, possible issues related to the exposure to high electric and electromagnetic field levels require additional safety practices on coupler designs and shielding methodologies. Furthermore, due to higher ground clearances, the nature of foreign objects and detections challenges are different in the scope of J2954/2. The issues of interferences within the vehicle is different due to the differences in vehicle system components and susceptible electronic subsystems. Interference issues between vehicles are also different from the light-duty case because of differences in parking spaces and distances between charging system components. Similar to the J2954, J2954/2 is also expected to become a technical information report, then a recommended practice, and finally a standard.

Another available WPT standard is IEC 61980-3 [74], which is less common in practice, but it shares some similarities with SAE J2954. In addition to the regular definition of couplers, compensation circuits, and electrical performances of light-duty vehicles, it partially covers the design requirements of WPT systems for heavy-duty vehicles rated higher than 22 kVA. The mechanical air gap of such WPT systems is limited to up to 240 mm. Two recommended operating frequencies are 20 kHz and 60 kHz with small allowable variation ranges. The further amendment of IEC 61980 is ongoing simultaneously with J2954/2 development to complete the scarcity of the design guideline for heavy-duty vehicle WPT systems.

III. MAGNETIC COUPLERS

In most WPT systems, transmitter (Tx) and receiver (Rx) pads exchange power through an air medium. In the literature, these pads are commonly referred to as magnetic couplers and play a significant role in the entire WPT operation [77]. Therefore, many researchers have proposed pad structures to improve system coupling coefficient k, pads' quality factor Q, misalignment tolerance, coil-to-coil efficiency, and reduction in stray/fringe fields [77]. Magnetic couplers usually include Litz wires to reduce the skin effect losses and, flux guiding ferrite cores to increase the mutual inductance, and aluminum shielding to minimize leakage field.

A. Pad Structures

Fig. 9 shows the classification of lumped magnetic couplers and some common structures. Lumped magnetic couplers can

be categorized into a) single-sided or planar pads [78] or b) double-sided or solenoid couplers [78]-[80]. Single-sided couplers can be further classified into a) single-coil pads, such as Circular Pads (CP), Rectangular Pads (RP) [38],[81]-[82], or Double D (DD) pads [78], and b) multi-coil pads like Double D-Quadrature (DDQ) [78][83], Bi-Polar (BP) pads [84]-[86], or Tri-Polar (TP) pads [87]. Table V summarizes some of the common single-sided pad structures and their features.

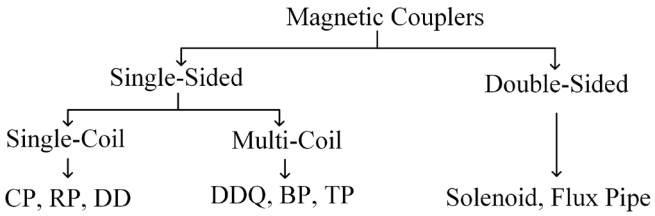

Fig. 9. Classification of lumped magnetic couplers in [88].

In order to increase the power transfer distance, intermediate coils can be employed to operate as repeaters and enhance power transfer between the source and the load [91]. Design procedures to maximize their benefits are discussed in the literature [92]-[95]. The intermediate coil can be placed in the same plane at the primary-side coil, which is often called a coplanar coil. It has been shown that coplanar coils can increase the system coupling coefficient, efficiency, and misalignment tolerance [96]-[97].

Furthermore, there have been efforts to make a WPT system more compact and efficient by integrating part of the compensation network into the magnetic couplers [98]-[103]. In this approach, the material or winding used for magnetic couplers is shared with the compensation network inductance such as the ones used with *LCL* or *LCC* type resonant tuning networks. In [98], the main WPT coils with the bipolar structure are integrated with rectangular compensation coils, and in [101], the main WPT magnetic couplers and compensation network inductors are made with a DD coil structure.

Recently, other unconventional structures have been proposed to improve magnetic couplers' performance. Tejeda et al. introduced a hybrid solenoid coupler to reduce flux leakage and losses and increase lateral misalignment tolerance [104]. This hybrid structure consists of a combination of an RP and a central solenoid. In [105], an unsymmetrical coupling structure is proposed to improve the capability of misalignment tolerance. In this structure, the primary-side coil height is much larger than in a conventional design. Pearce et al. proposed a ferrite-less DD pad that is lighter and has a lower leakage field, but the coil requires more current to transfer the same amount of power [106].

B. Pad Comparison

Many papers have compared different geometries under certain conditions. To compare different designs, many researchers have considered coupling factor k as the criteria for comparison [107]-[109], some have used kQ as the criteria [111], and some other studies employed uncompensated power P_{su} [86]. Based on the test conditions, different conclusions were derived. For example, the authors in [109] study three shapes, including a Square Pad (SP), an RP, and a CP, and conclude that the coupler surface area is more important than the shape itself. While in [108], it is shown that SP has a better performance than CP and DDP, and in [112], it is concluded that SP is a better option for WPT compared to CP. In [111], RP is selected compared to DDP, and in [78], it is shown that a

TABLE V
REVIEW OF SOME SINGLE-SIDED MAGNETIC COUPLERS [18], [88]-[90]

Circular Pad 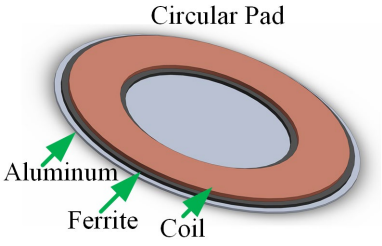 	Rectangular Pad 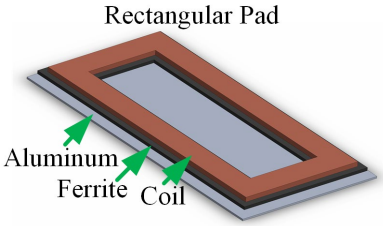 	DD Pad 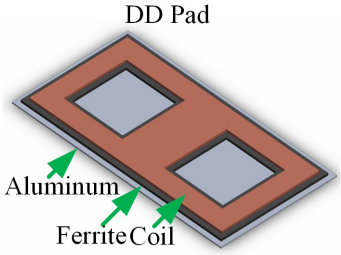
A CP is the most common pad for stationary WPT applications due to high efficiency and low leakage field.	An RP is the most common pad for dynamic WPT applications due to its cost-effective and compact structure.	A DD pad generates a parallel flux component that offers higher tolerance to horizontal misalignment. DD pads can be either single-coil or multi-coil pads.
Bi-Polar Pad 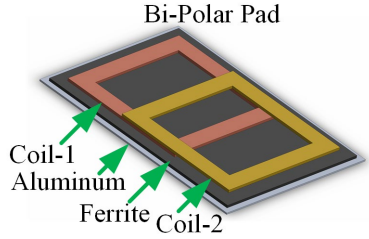 	DDQ Pad 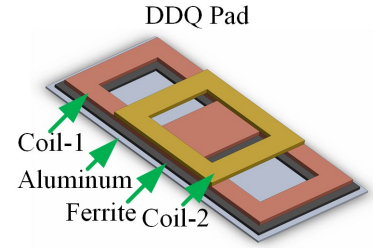 	Tri-Polar Pad 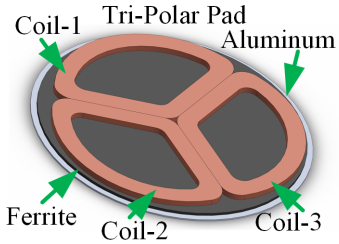
A BP pad is interoperable with other pads and offers good misalignment tolerance. In some designs with two independent windings, it requires two synchronized inverters for powering.	A DDQ pad is interoperable with other pads and offers good misalignment tolerance. In some designs with multiple windings, it requires two synchronized inverters for powering.	A TP pad demonstrates a higher coupling factor and lower leakage field compared to a CP. It requires three single-phase synchronized inverters or one three-phase inverter for powering.

DDP is superior over a CP. In [90], TP pad performance is evaluated compared to CP, and it is shown that the coupling factor and leakage magnetic field of TP pads are better than that of CP's.

To ensure a fair comparison between different structures, the magnetic couplers should be optimized under the same constraints [88]. However, most of the aforementioned studies lack such conditions. In [88], four major topologies are compared, including 1) CP, 2) RP, 3) DD-DD, and 4) DD-DDQ. Each geometry is optimized to maximize efficiency, volumetric power density, gravimetric power density, and misalignment tolerance. Some of the main comparison results are as follows: 1) CP shows the best efficiency and coupling factor for the same gravimetric power density, 2) CP uses the most ferrite and least copper for the same performance, 3) CP and RP outperform the polarized pads for the same power density, 4) polarized coils show better performance in specific misaligned directions, and 5) the CP and RP have lower stray fields compared to the polarized pads.

C. Pad Optimization

Once the coupler geometry is selected, the magnetic structure should be analyzed in detail, which means determining the wire position, the number of turns, separation between turns, size and position of ferrites, etc. This subject is commonly referred to as "pad layout design" or "pad optimization." Three general approaches can be distinguished: design flowcharts, parameter sweep, and evolutionary algorithms.

Design Flowchart - Some authors have tried to present design flowcharts to find the best magnetic pad structure. In [113] and [114], a modular design procedure is proposed for the entire WPT system, including magnetic pads. However, updating the coil design is based on a T-equivalent circuit model and does not consider nonlinearities in the design. In [94], the authors presented a systematic way to optimize the magnetic pad; however, their design is based on a linear analytical model of the system. A FEM-based optimization flowchart is introduced in [115], which focuses on three parameters in a CP design: the number of turns, separation between turns, and the outer coil diameter.

Parameter Sweep - A conservative method to find the pad optimum design is to simulate the design for all possible configurations by running a parameter sweep for all identified parameters. There are multiple variables that can affect pad performances, and each variable can have a wide acceptable range. This means that a parameter sweep for all variables requires a significant number of Finite Element Analysis (FEA) simulations. Researchers usually select a few parameters that have the most significant impact on the pad performances and run only a sweep of those parameters. For example, in [115], only three parameters (number of turns, line spacing, and the outer diameter) were selected for the design optimization of a CP. In [116], the authors tried to optimize a CP design based on efficiency and power density. To this aim, only three parameters (outer coil diameter, wire cross-sectional area, and operating frequency) have been chosen, and all possible configurations have been simulated. In [38], the authors employ a similar method to optimize an RP design.

Evolutionary Algorithms - Many researchers have proposed Evolutionary Algorithms (EA) to find an optimum solution for the pad design. The authors in [117] use the Genetic Algorithm (GA) to obtain an optimum layout for the coil design. At the same time, in [44], a Particle Swarm Optimization (PSO) approach is employed to optimize the shape of the ferrite structure in a CP. PSO helps to find Pareto fronts based on different figures of merits. Most of the researchers select a standard design and then use EAs to optimize different parameters without modifying the predefined shapes [119]-[122]. For example, in [121], a standard DDP design is optimized concerning power efficiency, material weight, and power density.

D. Three-Phase Pads

Recently, more attention is paid to the three-phase WPT system [123]-[125]. Three-phase WPT systems can increase power transfer density, and the use of a three-phase Voltage Source Inverter (VSI) may have some advantages compared to a single-phase VSI [125]-[128]. In [125], a three-phase WPT system is introduced, which energizes a 13-m-long test track. The proposed structure allows for a longer charging zone in dynamic wireless charging applications. A trifoliate pad structure is proposed in [128], which is energized with a three-phase VSI. The three-phase system model is developed in [129], and bi-directional operation is demonstrated in [127]. Matsumoto *et al*. compared single-phase and three-phase systems and confirmed that the systems with three-phase structures at both primary and secondary sides have higher efficiency and more uniform output power [130]. It has also been shown that a three-phase system requires smaller DC-link capacitors compared to single-phase systems [131]. It can be concluded that a three-phase VSI would be the best option if it is used with a three-phase magnetic coupler. Magnetic couplers demonstrated in [87] and [128] can be best used with a three-phase VSI.

E. Dynamic Charging Considerations

Vehicle movement adds new challenges to a WPT system. In this section, some insight is provided on selected research regarding magnetic coupler design in EV dynamic wireless charging applications. To extend the cruising range, some portion of the road needs to be equipped with transmitter (Tx) pads. KAIST researchers have focused on elongated rails for DWPT implementation, while others have studied the lumped transmitters or optimum length for segmented DWPT transmitters. Different On-Line Electric Vehicle (OLEV) generations employed various rail lengths, including 24 m, 60 m, and 240 m. On the other hand, segmented DWPT projects employ pads with the typical lengths of a few meters. Different rail configurations have been developed in KAIST OLEV projects, such as E-type, U-type, W-type, S-type, I-type, etc. The naming represents the cross-sectional view of the Tx rail, and a thorough review of this topic is given in [48]. The rail width can vary significantly, in KAIST OLEV designs, I-type and U-type transmitters have 10 cm and 140 cm minimum and maximum widths, respectively. Transmitters with lower widths are more desirable since they can potentially reduce the cost of construction and installation.

Optimum pad length - DWPT demonstrations have also been accomplished using segmented elongated pads. In [132], a 1.6×0.3 m^2 primary pad is reported for a DWPT application. Analytical derivations are provided in [133] to find the optimum length of the primary pad. The authors study mutual inductance as a function of primary pad length for different secondary sizes. It is shown that the mutual inductance peaks at a length of 1.2 m and plateaus after the length of 2.5 m for the transmitter analyzed in [133]. In [134], the authors studied the effect of EV speed on the optimum length, and it is shown that if one vehicle per pad is charged, the speed does not impact the optimum length. The optimum length of 3 m was reported based on the average coupling coefficient criteria. Buja *et al.* calculated the primary coil length and the distance between primary coils based on transferred energy [135]. Their goal was to transfer enough energy to allow an EV to drive in charge-sustaining mode.

The transition between pads - Power drop in the zone between two adjacent primary pads has been investigated in several studies. In [136], an array of four circular pads are used at the secondary side. Therefore, during the transition, some of the secondary coils have mutual inductance with the next primary pad while the rest still have mutual inductance with the previous primary pad. This scheme maintains designed mutual inductance between primary and secondary pad for all longitudinal misalignments. In [137], six rectangular primary pads are connected in parallel and the secondary pad length is optimized to achieve the minimum variation in the coupling coefficient. In this study, one inverter energizes six LCC compensation networks resulting in an output power pulsation of 7.5%. In [138], dimensions of DD pads are optimized to minimize the power drop between two adjacent primary pads. The optimization results in two unequal DD pads where the primary pad is shorter than the secondary pad. In [139], a DD pad is modified to be used on the DWPT primary-side. A crossed DD coil is proposed to achieve less variation in the coupling coefficient. In [140], the authors modified the primary pad edges to improve power transfer capability. In [141], a cascading feature is added to the primary pad design to increase the mutual inductance during transition. In [142], a DWPT configuration is demonstrated with two parallel secondary circuits, which helps maintain designed mutual inductance between the primary-side and the vehicle side through the transition. Furthermore, overlapped DD pads are studied to increase the magnetic field in the transition zone in [143].

F. Magnetic Shielding

The International Commission on Non-Ionizing Radiation Protection (ICNIRP) has released general public and occupational exposure levels to Electric and Magnetic Fields (EMF) [144]. This guideline is also referred by SAE J2954 and it sets the magnetic field limitation is set at 27 uT for a frequency range between 3 kHz to 100 kHz. The magnetic field around pads (where human can be present) should be suppressed to comply with the guideline. There are three methods for mitigating the EMF, including passive shielding, active shielding, and reactive resonant current loops [145]. Passive shielding is accomplished by either providing an alternate path for the magnetic flux using ferromagnetic materials (e.g. ferrite) or by generating a reverse magnetic field employing conductive materials (e.g. aluminum) through the eddy current phenomenon [145]. The SAE J2954 has recommended the specific shielding approach and defined the size of aluminum back plate shielding to be 800 mm x 800 mm or larger for WPT1 to WPT3 (see Table III for the definition of WPT1-3). While an aluminum back plate shielding can be very effective in suppressing the magnetic field emissions of unipolar circular or rectangular couplers, passive eddy current shielding of DD coils increases the magnetic field emissions [146]. While the Z-axis component of the field vector is dominant in unipolar (non-polarized) circular, square, or rectangular coils, the field vector of DD coils have a dominating XY-planar component [147]. In [149], power rails are enclosed between two vertical underground plates embedded in the road. Furthermore, metal brushes connect the chassis to the ground plates for extra shielding. Through the practice in the past decade, the conventional passive shielding method is preferred owing to its reliability, and it is proven to comply with the guideline under a wide range of power levels.

For WPT4 or higher power levels up to 100 kW and 350 kW, the stray field shielding is more challenging. Neither the magnetic field testing condition nor the shielding approach is defined for a WPT system rated higher than 22 kVA (at the input side). The lack of testing guidelines and requirements makes it difficult to design and evaluate the shielding. For the 100 kW WPT system described in [150], the shielding effect is evaluated 1 meter away from the center of the coil. As a comparison, the 50 kW system in [38] is shielded with both ferrite and aluminum plates and the stray field is tested at the 400 mm, 600 mm and 800 mm lateral to the air gap center point. An evaluation is given in [151] to compare the shielding effectiveness at different power levels. Using the shielding configuration from [150], the power level is further increased to 150 kW and 350 kW, and it was found that the system exceeds the exposure limits defined in the ICNIRP guideline. As expected, electromagnetic safety becomes a critical concern when the power level increases. Both the shielding method and testing principle should be reevaluated and further investigated to improve the shielding design.

Taking into account the extra weight and cost that would be brought due to the increased volume of ferrite and aluminum for higher power ratings, alternative active shielding method should be considered. It represents an alternative means of canceling EMF noise through an intentional generation of a magnetic field of the same magnitude and frequency but opposite phase [145]. The third method combines the advantages of active and passive shielding. The reactive resonant loop generates a magnetic field at the specified frequency to cancel the EMF noise without an extra power supply. This approach is realized in [145] by using a reactive current loop cable with capacitors and switch arrays to control the resonant frequency.

The recent development of CPT systems raises the problem of electric field shielding around the capacitive couplers. In inductively coupled systems, the electric field emissions around the resonant tuning capacitors might be high, too; especially in SS and SP tuned systems. In [148], phase-shifted shielding plates are supplied by multiple inverters to cancel the fringing field, but the solution is complex for implementation and provides limited improvement. In [30], two passive

shielding plates are added to a conventional lateral four-plate CPT system to constitute a six-plate system. Through capacitive coupling with main plates, the shielding plates are set to close-to-zero potential, effectively shielding the enclosed coupler plates and their field. However, this method is only applicable to four-plate lateral couplers, and its operation under misalignment has not been analyzed or tested. So far, there is no standardized solution for CPT shielding, and it represents an active research area.

IV. Compensation Networks

A. Design Requirement for Compensations

Compensation topology is a significant part of a WPT system. As indicated in section II.A), the compensation is primarily set up for reactive power compensation. In the meantime, a small portion of reactive power is still essential to achieve soft-switching under wide operating conditions, which is critical in achieving efficient operation in high-frequency converters.

Another compensation network design requirement emerges from the load change and coupling variation related to coils position. Moreover, different battery profiles require a wide output range from the charging system, which is even more challenging to accomplish under a wide load and coupling variation [154]-[155]. Therefore, the resonant network needs to compensate for output fluctuations due to a wide range of parameter drift and reduce the sensitivity to load and coupling variation [56].

Finally, the voltage and current stress on compensation components is exceptionally high under high power rating. According to previous research, the dielectric losses in capacitors, in addition to core and winding losses in inductors, can contribute up to 45% of the total loss [156]. Therefore, the simplicity of the compensation network is critical in maintaining overall high system efficiency. Moreover, considering the high resonant current and voltage requirements from resonant capacitors, multiple capacitor banks in series are normally paralleled so as to reduce the dielectric losses and offer a sufficient voltage and current margin, which makes the system costly and bulky. The volume of a compensation network alone has been reported to take almost 50% of the total footprint of a power stage in a specific mechanical layout [157]. Thus, the simplicity of compensation also corresponds to a more economical design of the system with high-power density, and therefore serves as a critical design metric. The other concern in more complex compensation topologies is the system order. On the one hand, the minor post-design frequency adjustment is widely adopted to compensate for parameter drift [38]. In that case, the multiple peaks in the voltage-gain-versus-frequency curve can easily cause converter instability or bifurcation [158]. On the other hand, some high-order systems may introduce sluggish response and unexpected system overshoots during transients [59]. This is particularly critical in high-power DWPT systems where even a short interval of charging time is counted in helping deliver power more efficiently [159]. In addition to the design principles mentioned above for magnetically coupled WPT systems, another critical requirement of CPT compensation is the reduction of voltage and current stress on passive components while maintaining the power transfer capability.

By extending the notion of resonance in WPT systems beyond the simple principle of "resonance" explained above, the compensation topology is no longer limited to the form of LC resonance. That opens the possibility of designing compensation networks to fulfill different objectives with a clear physical meaning. The compensation network design objectives are summarized as follows: i) to minimize the reactive power in the resonant tank; ii) to achieve a wide range of soft-switching operation; iii) to maintain a stable output profile against a wide range of load and coupling variation, and iv) to design a simple structure for high efficiency, low cost, compact design, and bifurcation tolerance. Whereas tradeoffs exist among these design objectives. For instance, complex compensations are reported to have lower requirement on capacitors' voltage and current rating, at the cost of additional inductors. For that reason, multi-resonant networks such as LCC-Series and LCC-LCC are also widely employed. Another consideration is the fault protection, such as the no-load condition of the secondary-side, which could happen if battery management system disconnects the battery. Some compensation methods on secondary-side can operate with no-load while others run into over-voltage issues depending on constant voltage or constant current behavior formed by the compensation network on the secondary-side. Generally, resonant tuning network should be selected based on the voltage and current requirements, efficiency, and functionalities such as load or coupling factor independent operations. In this section, the transformer model is used to better explain the relationship between compensation elements.

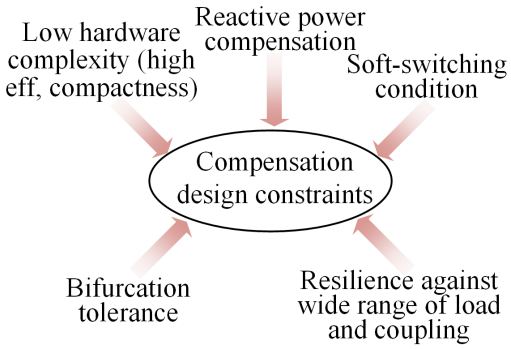

Fig. 10. Design constraints of the WPT compensation.

B. The Load-independent Compensations

A wide range of equivalent load conditions is commonly seen in charging systems where the output voltage and current gain characteristics can vary widely according to the state of batteries or supercapacitors. A suitable compensation is essential in preserving the stable output decoupled from the load condition. In some static charging systems with a fixed relative position or equipped with auxiliary positioning devices or parking guides, the coupling range is predetermined within a tolerance, and load-independent compensation can be readily achieved.

1) Single-element compensations

Conventional compensation methods include four schemes with a single compensation element on their primary and secondary sides, known as Series-Series (SS), Series-Parallel

(SP), Parallel-Series (PS), and Parallel-Parallel (PP). In [54], the method of selecting capacitance value to achieve a null reactive power condition of the resonant tank is analyzed, and the relationship between the load condition and the frequency-splitting phenomenon is pointed out. Since the voltage source is more commonly adopted to drive high-power converters, a paralleled capacitor cannot be used as a compensation on the primary side. Therefore, the following sections will focus on the series compensation on the primary side. Reference [160] points out that due to the duality of series and parallel compensations on the output profile, both primary and secondary sides can use different compensation methods to obtain desired output characteristics. This is demonstrated by an example in which the SS topology is applied to compensate for the self-inductance and generate a load-independent constant output current source. Similarly, the leakage inductance can be compensated for a load-independent constant output voltage source. In general, in the case of SS compensation, there are several "specific" operating frequencies regarding the voltage and current gains. Output characteristics can be switched between a constant current source and a voltage source by operating on different "specific" frequencies [161].

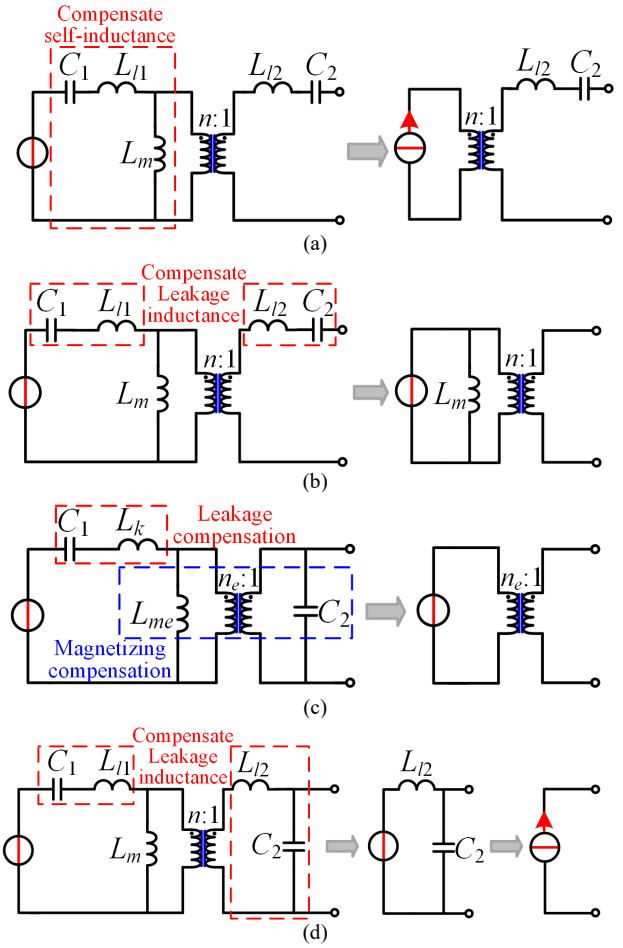

Fig. 11. Single-element compensation schemes. (a) Self-inductance compensated SS (constant current source). (b) Leakage-inductance compensated SS (constant voltage source). (c) Hybrid compensated SP (constant voltage source). Note that transformer model shown in Fig. 7(b) is used. (d) Leakage-inductance compensated SP (constant current source).

Similarly, there are different "specific" operation frequencies for the SP compensation, so that the system exhibits a constant voltage source or a constant current source output characteristics, which is equivalent to a hybrid compensation of leakage inductance or magnetizing inductance from the circuit point of view [162]. As shown in Fig. 11, using Norton-Thevenin transformation, series and parallel compensation methods can be expressed in a unified circuit form, and the duality of the compensation is noticeable from the complementary Norton-Thevenin equivalent circuits.

All of the above compensation structures eliminate the effect of load variation so that the controller only needs to deal with the coupling variation. However, since some single-element load-independent compensations rely on the parameters such as leakage inductance that are highly dependent on coil position, the constant output characteristic is diminished when the coupling factor drifts. In [163], it is reported that the voltage gain at the specific frequency of SS and SP compensations is proportional to the coupling coefficient, indicating a system's high sensitivity to the coupling variation. In [161], the impedance of the SS-type topology working at the fixed frequency is optimized to acquire a load-independent voltage gain. The frequency is designed to be as close as possible to the resonant frequency, which reduces the system reactive power. However, this method requires a compromise between the reactive power and output voltage stability, and it fails to fundamentally solve the interaction between the reactive power, the output voltage gain, and the varying coupling factor.

2) Multi-element compensations

Using series-parallel hybrid compensation with multiple elements is an effective approach to overcome the aforementioned design issues of single-element compensations. The LCL compensation is commonly adopted in some applications, as the output voltage is completely decoupled from the load. Furthermore, the unity power factor at the input port of the resonant network can be achieved regardless of the load and coupling condition [164]. Another improved LCC compensation is formed by adding a capacitor to the coil branch, and it preserves all merits of an LCL compensation. Besides, the achievable voltage gain is increased because the leakage inductance of the coil is partially canceled by the extra capacitor [165]. It should be noted that the output of the T-type compensation also demonstrates a duality relationship with respect to the secondary-side compensation method. Compared to the series compensation on the secondary side illustrated in Fig. 12, the secondary parallel compensation will change the output source characteristics, too [228]. A previous publication reports wide utilization of the LCL-P compensation cascaded by a boost converter for an EV charging [166]. In this case, the LCL-P compensation is considered as a current source to interface the boost inductor.

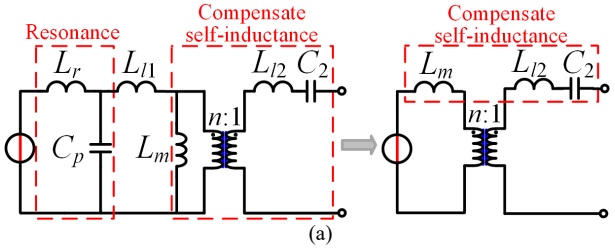

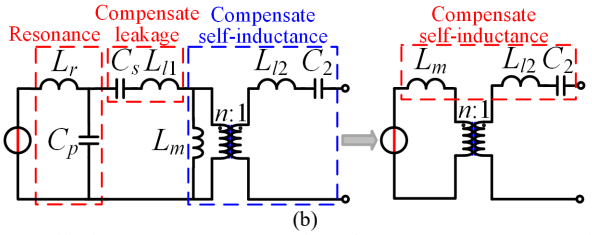

Fig. 12. Multi-element T-type compensation scheme. (a) LCL (constant voltage source). (b) LCC (constant voltage source).

The T-type compensation topology is further extended to the secondary side, as shown in Fig. 13. The starting point is to use the LCL compensation structure to achieve the unity power factor for the primary and secondary ports, and this characteristic has good parameter adaptability. In [167], an improved secondary LCL compensation is proposed. The equivalent inductance resulted from the rectified load is tuned by the series capacitor in the secondary inductor branch to guarantee the unity power factor, which constitutes the LCC compensation. Article [168] further applies LCC compensation to both sides where constant current source is acquired at the output. Moreover, to increase the compactness of the compensation network, the resonant inductors are further integrated into the main coils using a planar coil [99], [102]. However, despite the advantages of load-independent constant voltage/current output characteristics and the minimal reactive power decoupled from load and coupling conditions, the output sensitivity to the coupling factor still remains.

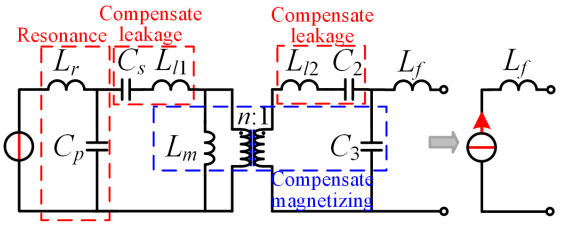

Fig. 13. Double-sided LCC compensation scheme from [168].

To improve the robustness of the above compensation to the coupling variation, work in [163] combines the characteristics of SS and SP and constructs an S/SP type compensation topology, as shown in Fig. 14.

The S/SP type realizes full compensation of the leakage inductance and magnetizing inductance, thus resulting in low reactive power. Stable output voltage gain is also acquired for a specific load and coupling factor range, as illustrated by the circuit simplification in Fig. 14. The drawback lies in the fact that the reactive power increases severely with decreasing coupling conditions, indicating an incomplete decoupling with the coupling factor.

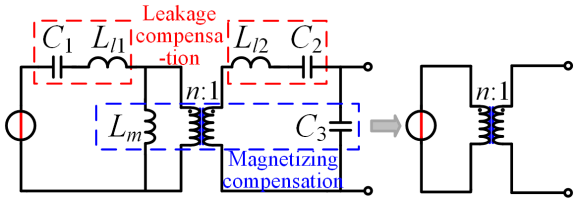

Fig. 14. S/SP compensation scheme from [163].

To summarize, the derivation of all load-independent compensations can be described by Norton-Thevenin equivalency using the transformer model and unified approach. However, the particularity of loosely coupled transformer determines that no compensation topology can well maintain the output stability and ensure the reactive power rejection under a wide operating range. Consequently, a design trade-off is needed to balance among design requirements (i) to (iv) listed in section IV(A). To conclude, the parameter design principles, load matching conditions, and output characteristics of several representative compensations are listed in Table VI, while the same can be developed for the other compensations, too. In the following expressions, Q_1 and Q_2 represent the quality factors of the primary coil and the secondary coil, while k_n stands for the nominal magnetic coupling designed for the load-independent characteristic. All variables are associated with the symbols in their corresponding circuit figures.

C. The Position-tolerant Compensations

In some applications, the relative coils position changes, causing the coupling factor to vary widely. Since the coupling factor impacts both the leakage and magnetizing inductances, its variation is not easy to compensate. Consequently, designs with an enhanced position tolerance are mostly considered through an adequate coil design and regulation in the early stages of a high-power wireless system design [38], [57].

Recently, researchers have exploited the characteristics of compensation networks to suppress the sensitivity to the coupling factor variation, and that way reduce the design complexity and additional material usage. As shown in Fig. 15(a), in [170], a CCL type compensation topology is proposed to transfer the rated power at a lateral offset of 25%, but the range of coupling coefficients is not indicated in the article. Literature [171] applies a four-coil configuration as in Fig. 15(b). The authors optimize the capacitance of each compensation element to obtain improved adaptability of the

TABLE VI
THE PERFORMANCE COMPARISON BETWEEN CONVENTIONAL COMPENSATIONS

	SS	SP	LCL/LCC-series	LCC-LCC
Parameter design principle	$C_1=1/(\omega_0^2L_1)$ $C_2=1/(\omega_0^2L_2)$	$C_1=1/\omega_0^2L_1(1-k_n^2)$ $C_2=1/(\omega_0^2L_2)$	$C_1=1/(\omega_0^2L_r)$ $C_2=1/(\omega_0^2L_2)$	$C_p=1/(\omega_0^2L_r)$ $C_{s1}=1/(\omega_0^2L_{l1})$ $C_2=1/(\omega_0^2L_{l2})$ $C_3=1/(\omega_0^2L_f)$
Load matching condition	$R_{eq}/\omega_0L_2\approx k$	$R_{eq}/\omega_0L_2\approx$sqrt($k^2$+1)/$k$	$R_{eq}/\omega_0L_2\approx k$	$R_{eq}/\omega_0L_2\approx k$
Output type	Load-independent constant current source	Load-independent constant voltage source	Load-independent constant voltage source	Load-independent constant current source
Reactive power compensation ability	Good within the entire load and coupling range; weakly coupled to the load and coupling when detuned for ZVS	Good at the nominal condition; degrade when drifting away from the nominal point	Good within the entire load and coupling range; weakly coupled to load and coupling considering ZVS constraints	Good within the entire load and coupling range

power curve against coupling, which helps in extending the effective charging region. In [172], the researchers use a switching capacitor array to track the maximum power delivery and achieve a stable energy transfer under variable distance, as shown in Fig. 15(c). However, the configurable resonant network introduces many new passive components and switches. Additionally, the reliability of such a system is also degraded due to the increased number of potential failure points. Similar comments apply to [173], where multiple resonant networks are activated through switches based on feedback signals. All the factors mentioned above make those active systems less practical for mitigating the impact of the coupling factor variation.

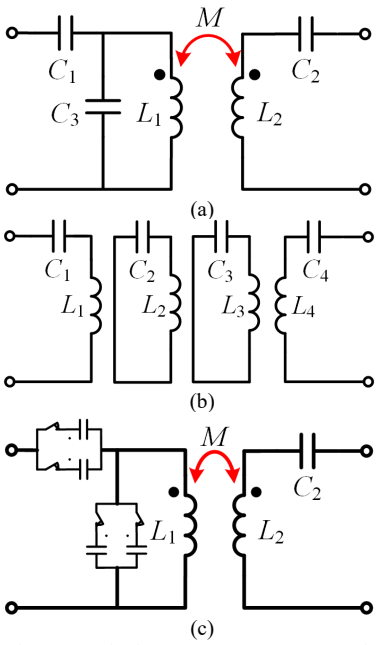

Fig. 15. Position-tolerant topologies. (a) SPS CCL type topology from [170]. (b) Four-coil compensation from [171]. (c) Switching capacitor compensation from [172].

In [174], a general method is discussed to derive a position-tolerant primary-side compensation circuit. Fig. 16 shows a sequential increase in the number of compensation elements where one-element [175], two-elements (L-type) [169], and three-elements (T-type) [176] compensations are proposed accordingly. The features of these topologies are reported to be able to keep the power transfer within 80% of its nominal value within a reasonably wide coupling factor variation (from $k_{\min}$ to $2k_{\min}$). Due to the high degree of freedom, the design requirements, such as the tolerance to coupling variation, full range ZVS, or reactive power suppression can be achieved simultaneously within a specified coupling range.

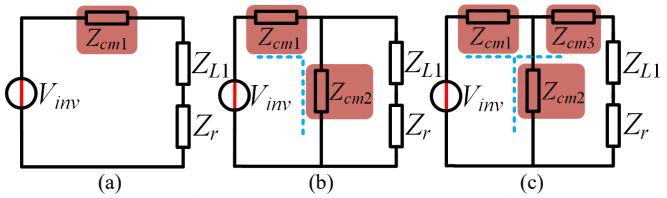

Fig. 16. Position-tolerant compensations: (a) One-element [175]. (b) Two-elements L-type [170]. (c) Three-elements T-type [176]. Z_{L1} represents the reactance of the coil and Z_r represents the impedance reflected to the primary coil branch from the secondary side. Compensation elements can be inductors or capacitors.

More recently, hybrid compensations combining different types of networks are proposed to acquire a more stable output. As illustrated in Fig. 17, in [177], the power transfer properties of LCC and SS compensations are synthesized to compensate each other. The resulting power transfer stability is improved compared to the single position-tolerant compensation family presented in [174]. Moreover, in [101], the resonant inductors of conventional double-sided LCC compensation are built in the form of planar auxiliary coils to participate in the power transfer process, termed as a dual-coupled compensation. The power transfer property is further improved owing to the complementary characteristics of both compensation and main winding flux paths.

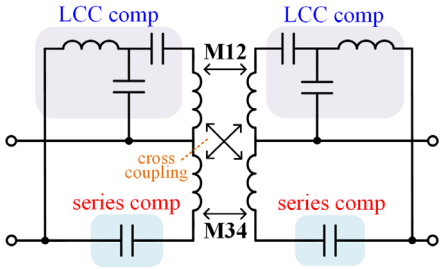

Fig. 17. Hybrid compensation paralleling LCC and SS compensations in one resonant tank in [177].

Generally, the position-tolerant compensations are more favorable in highly dynamic applications, such as DWPT chargers for EVs, industrial movers [181], or drones [182]. However, due to their distinct operational principle, the resilience to coupling variation is usually realized at the cost of losing the load-independent property. A summary of position-tolerant compensation topologies is given in Table VII.

TABLE VII
SUMMARY OF POSITION-TOLERANT COMPENSATIONS

Topology Principle	Advantages	Disadvantages
Impedance transformation	• High simplicity • Passive, without resorting to control or atypical pad designs	• Lower position tolerance compared to other approaches • Output property affected by load conditions
Complementary of different compensations	• High position tolerance • Passive	• Complex compensation structure • Coordination with the coupler design is needed in order to function properly • Output property affected by load conditions
Switching between compensation elements/topologies	• Highest position tolerance	• Control involved • Output property affected by load conditions

D. CPT Compensations

A CPT compensation network usually features a higher number of components. A typical configuration includes two pairs of coupling plates in a symmetric structure to produce two equivalent capacitors in the circuit. Therefore, conventional compensation is also built symmetrically. In [26], LCL compensation is applied to both sides of the coupling plates. Through resonance of inductors and capacitors, the voltage on the coupling plates is boosted to enable high-power transfer. However, the inductor required to resonate with a capacitance of several pF is extremely large. The fabrication of such an inductor operating in the MHz range is also challenging. In [178], LCLC compensation parallels external shunt capacitors to the coupling capacitors for lower series inductance, in this case, there is a total of eight external components added to the system. A 2.4-kW power transfer is achieved under an air gap of 150 mm. An attempt to simplify compensation is reported in [179], where an LC resonance is used to replace the LCLC one, at the cost of reduced power level. To further reduce the system complexity, literature [180] proposes a two-plate CPT system that utilizes the vehicle chassis and ground plane as the other two plates. In the proposed equivalent four-plate system, only a single inductor is needed to form the resonant tank. The previously reported compensations for CPT systems are illustrated in Fig. 18.

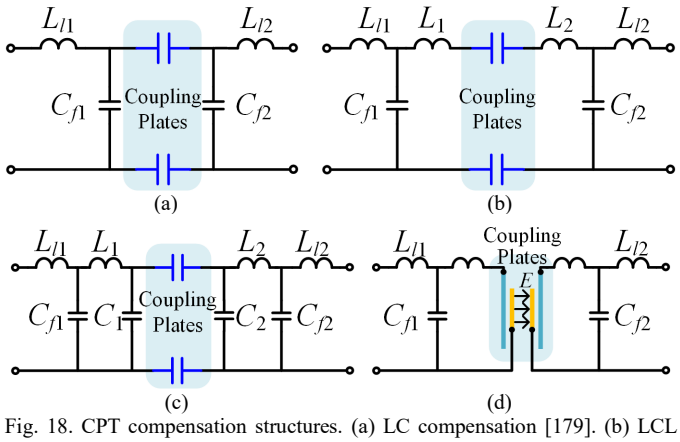

Fig. 18. CPT compensation structures. (a) LC compensation [179]. (b) LCL compensation [26]. (c) LCLC compensation [178]. (d) LCL compensation with vertically stacked coupling plates [29].

To summarize, existing CPT compensations mainly focus on the enhancement of power transfer capability and reduction of hardware complexity. These design objectives have already been solved in magnetically coupled WPT systems. Due to the scarcity of large-scale engineering practice in the high-power CPT field, there is no unified conclusion about which compensation is the most suitable for high-power CPT systems.

E. Performance-oriented Design

Depending on various application scenarios, the required performances may vary from case to case. Therefore, a performance-oriented design approach is essential in achieving multiple design objectives and reaching a balance between different performance indices. Taking into account the efficiency and controllability concerns of a high-power charging system, several candidates are discussed in terms of their practicality.

The traditional series-series (SS) compensation is the most commonly adopted compensation in charging systems. Resonant capacitors are selected to fully compensate the self-inductance at the resonant frequency. A theoretically ideal reactive power compensation is achieved, independent from the coupling and load due to the symmetry and duality between the primary and secondary sides. Accordingly, high efficiency can be achieved due to the superior reactive power compensation ability and its simple structure. Serving as a load-independent constant current source, it can adapt to a wide range of battery systems where a constant current charging period is needed. A span of the SS applications in prototypes or commercial products can be found in [38], [41], and [43]. Another advantage of the SS compensation comes from its symmetrical structure. In bidirectional wireless charging systems, the symmetry of compensation enables even distribution of the voltage and current stress at both sides of the magnetic coupler [183]. Moreover, it holds identical voltage or current gain characteristics in both power flow directions and facilitates their regulation. The downside of SS compensation is tuning sensitivity. The output characteristic, as well as the input impedance, both feature a high slope rate at the resonance point, which renders a high sensitivity to the least parameter shift. The consequence can be a losing the soft-switching and large output variation. To create the ZVS condition for the power stage, either the resonant tank is detuned slightly or the system operates slightly above the resonant frequency to introduce inductive loading at the inverter output. On the other hand, the above-mentioned issue still exists, though alleviated.

Another candidate for a high-power WPT system is the SP compensation in which the operating point is selected to realize a load-independent characteristic. The load-independent point of an SP topology also features with zero-phase-angle (ZPA), indicating that the reactive power in the resonant network can be entirely eliminated [116]. However, the merits mentioned above are fragile since the compensation capacitor is highly dependent on the magnetic coupling. Once the coupling drifts away from the specified nominal condition, the load-independent and ZPA properties are no longer hold. Besides, the voltage gain at the load-independent point is usually much higher than unity due to the boost mode of paralleled resonance. For the given input and output voltage, the SP compensation has to be designed with a very low turns ratio to keep the output voltage low. That is not preferred since the low number of secondary turns significantly decreases the quality factor of the secondary coil, resulting in the transmission efficiency degradation. The other option is to implement a high-frequency step-down transformer at the primary-side inverter output to eliminate the high voltage gain; however, this introduces another power conversion stage with additional losses. Another disadvantage of SP is that the required coil inductance for load matching is usually too low to dissipate the losses generated in a high-power WPT system [116]. However, for some applications where the relative position is fixed and the power is relatively low, the SP compensation may still be an ideal candidate.

For LCL compensation, the existence of the front-end inductor may largely limit the current flowing into the primary-side coil. Therefore, the voltage gain of the LCL-type resonant network is usually low, which makes it suitable for

low-voltage charging systems, for low-speed EVs, lift trucks, electric scooters [184], and distributed WPT system where multiple devices are supplied from a common rail, as in automatic guided vehicle (AGV) systems [77]. In EV charging scenarios, it can also be configured with a parallel compensation on the secondary side to boost the voltage. The practical concerns of LCL lie in the fact that a high-power, high-inductance inductors are usually required to match the coil's inductance to ensure ZPA and soft-switching [159], resulting in higher losses. From a fabrication point of view, it is not practical to build high-frequency resonant inductors with high inductance to handle high power, especially considering its counterparts in conventional resonant converters (LLC), which are usually less than 20 μH. Alternatively, the LCC compensation can largely alleviate the requirement of inductance value, which makes it possible to replace the LCL in some applications. Double-sided LCC also gains some applications in battery charging systems [155] and bidirectional WPT systems [185]. The parameter sensitivity is reported to be lower than in SS, which makes it more tolerant to parameter drift [186]. Double-sided LCC systems with identical primary and secondary-side components have unity voltage gain and the voltage gain is usually adjustable by adjusting the component values. The major drawback is the high number of compensation components.

In high-power wireless charging systems, efficiency, stability, and simplicity are major design concerns. From the above discussion, it is concluded that the SS compensation is an ideal solution for many applications, mainly due to its simplicity. To guarantee a stable and efficient operation of high-power wireless chargers, the real-time monitoring of the input impedance and minor frequency adjustments are recommended to account for the non-ZVS condition caused by the drift of operating conditions and parameters.

V. Power Electronics for High-Power Wireless Chargers

Power electronics play an important role in achieving high efficiency and high compactness of the converter, as well as the system reliability. Similar to conductive chargers, a typical wireless charging system also requires an AC-DC converter to interface with the grid, regulate the DC bus voltage, correct the power factor, and reduce the input harmonic distortions to comply with the power quality standards for grid-connection. Moreover, front-end and terminal DC-DC converters are sometimes adopted to regulate the charging process or perform impedance matching [187].

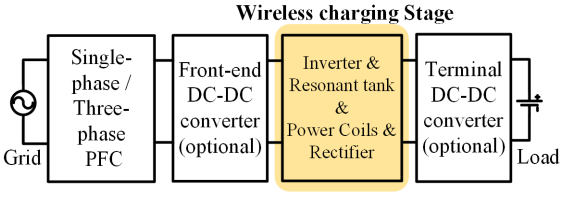

Fig. 19. Power electronics architecture of wireless charging systems.

The power conversion architecture is illustrated in Fig. 19, in which the wireless charging stage is considered as an intermediate stage that provides galvanic isolation through the large airgap separation. This section will focus on the isolated DC-DC wireless charging stage to investigate the applications of different power electronics topologies in high-power wireless charging systems.

A. Single-Phase Systems

A single-phase system is the most commonly adopted architecture. The primary side can be a full-bridge or half-bridge inverter fed by a voltage source or a current source, while the secondary side is configured as a full diode bridge, a voltage doubler, or a semi-active or active bridge, depending on the output voltage level and the power flow direction [188]-[190]. The existed single-phase power electronics are shown in Fig. 20.

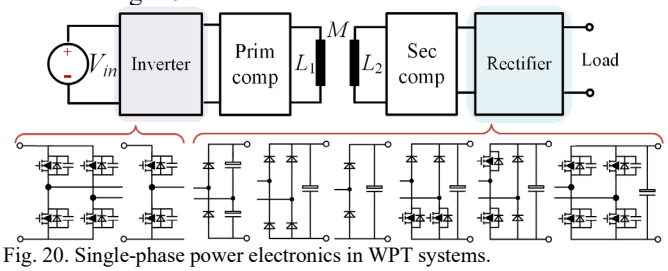

Fig. 20. Single-phase power electronics in WPT systems.

A voltage-source-driven converter is the mainstream in wireless charging systems. In vehicular applications, single-phase voltage source converters are applied widely for WPT1 to WPT3 chargers. WiTricity's first-generation WPT1 wireless charger utilizes a single-phase converter to deliver 3.3 kW at 90% efficiency. A recent prototype demonstrates a topology based on a single-phase bridgeless PFC and wireless charging stage with full SiC-based operation, providing 11 kW at 91-93% efficiency [41]. Fraunhofer Institute presented an 11-kW bidirectional wireless charger with single-phase power electronics using SiC devices [191]. Bosch developed a 7-kW prototype based on the single-phase semi-active bridge topology [192]. Generally, single-phase WPT systems prove to be able to accommodate most power ranges required by high-power charging, though 3-phase connection at the front-end is required at higher power since the single-phase grid is limited in maximum power. It is also preferred due to its simple power structure and auxiliary circuits.

To increase the system power capacity, multiple paralleled semiconductor devices are proposed to share the current stress and reduce the equivalent on-state resistance. A dedicated commutation loop design and a gate driver scheme are required to ensure the current sharing of devices and reliable operation of the system [38]. The introduction of wide bandgap devices, such as SiC that features limited gating voltage threshold and sensitive response to parasitic parameters, requires particular attention to the design procedure.

On the other hand, a current-fed converter has advantages such as lower current stress and inherent short circuit protection [193]. However, a dc inductor has to be scaled to form the current source at the inverter input. Moreover, the compensation needs to be adapted to the current source characteristics, which complicates the system structure. Therefore, there are very limited applications of current source converters in high-power wireless charging systems.

B. Multiphase Systems

Recent research in multiphase systems provides an alternative to single-phase ones. Specifically, three-phase

systems can provide a higher power rating and higher power density than single-phase systems with devices of the same current rating, as shown in Fig. 21 (a). Besides, three-phase magnetic couplers allow for different flux combinations to realize various design objectives. As early as 2007, a three-phase resonant converter was proposed to broaden the charging zone of a roadway vehicle charging system [125]. Driven by the idea of emulating the rotary magnetic field present in electrical machines, recent development of WPT systems has witnessed a proliferation of three-phase WPT systems. In [194] and [195], three-phase systems are deployed to cancel the magnetic field within the concerned area in order to improve EMC performance. Literature [196] presents a 22 kW three-phase system that adopts six coils on each side to effectively contain the stray field. A parameter design approach, as well as an optimized control strategy are presented in [197]. The smooth power transfer against rotary misalignment is achieved. Additionally, ZVS within the full coupling range is realized by adjusting the phase-shift angle between phases. In [198] and [199], the presented three-phase systems are applied to enhance misalignment tolerance in dynamic charging and bidirectional charging systems, respectively. In [200], a three-phase system is adopted for 50 kW EV wireless charging, which features the highest power density amid results reported so far. Except for the advantages mentioned above, high power density is achieved through system integration of couplers, and lower filter requirements are also reported due to the availability of interleaving operation provided by three-phase systems.

Generally, in a multi-phase WPT system, the orientation of the magnetic field can be manipulated to strengthen the flux coupled to receivers while minimizing the leakage to the surroundings. Thereby both the leakage field performance and position tolerance can be improved. Multiphase systems also enable devices of a lower rating to be used for high power transfer. Additionally, the multi-phase topology possesses the feasibility to integrate multiple coils to enhance the power density. The major concern is the cross-coupling among phases, which tends to alter the impedance of each phase, thereby increasing the reactive power, causing an uneven distribution of current stress among phases, which results in the ZVS failure. These issues are exacerbated by the misaligned position of the receiver. Therefore, most of the earlier studies aimed to cancel or minimize the cross-couplings between the phases. However, phase windings can have electrical as well as spatial phase shifts and multi layered windings can also be practiced and one may take the advantage of cross-couplings if the windings are designed and controlled such that their flux can support the flux of other windings or layers instead of causing cancellations. Therefore, the three-phase converter modulation and the flux path design remain to be studied to fully exploit its advantages. Furthermore, the resonant tuning circuitry can be designed to take the cross-coupling and mutual inductances between the phases into account.

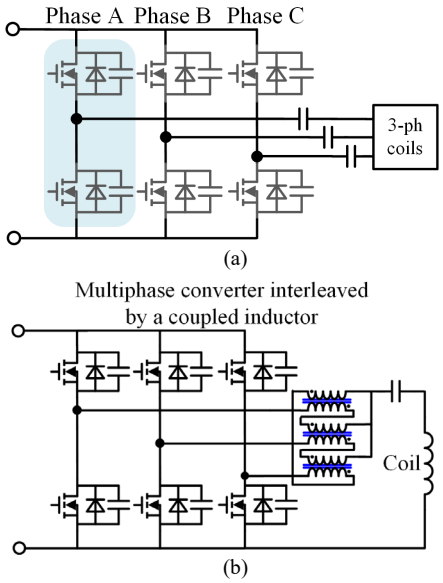

Fig. 21. (a) Primary-side topology of a three-phase WPT system. (b) Primary-side of multiphase WPT system paralleled by coupled inductors or intercell transformer.

In other cases, multiphase paralleled converters are applied to supply high power. More specifically, a 25-kW wireless charger is built using three half-bridge phases paralleled through coupled inductors to suppress the circulating currents [47], as shown in Fig. 21 (b). In [201], the prototyping and control of a six-phase paralleled wireless charger is expanded upon. By means of multiphase topologies, the loss dissipation is distributed into each phase to alleviate the thermal burden, and the control flexibility is also enhanced by adjusting the duty cycle of each phase and the phase-shift between them. However, the interaction between phases demands more investigation to simultaneously maintain the inductive impedance of each phase and achieve an output regulation.

C. Multi-cell Modular System

To avoid a dedicated design for paralleling devices, modules can be paralleled to supply a single coil to accommodate higher power, as illustrated in Fig. 22. As a result, conventional half- and full-bridges are readily used, where the power rating requirements for each module are reduced; this allows to use lower rating devices to improve the converter performances. In [202], a parallel topology is presented to minimize the uneven power-sharing via parameter tolerance. The reliability is also improved owing to modular redundancy. Authors in [203] investigated a method to suppress the circulating current among different modules.

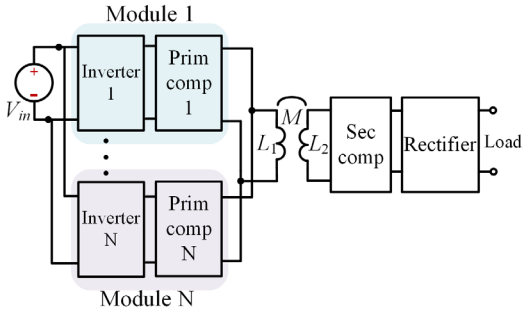

Fig. 22. Diagram of multiple inverters supplying one coil to enlarge the power capacity.

Some studies suggest that the high-power systems raise the thermal issues for power devices, coils and auxiliary components [204]. Correspondingly, some solutions proposed multi-cell systems where multiple wireless charging stages are paralleled at input and output ports simultaneously, as indicated in Fig. 23. In [205], an input-parallel-output-series (IPOS) system is built using dual primary-side coils and secondary-side coils. Cross-coupling of coils is considered to tune the input impedance of the resonant tank. In [46], a 44-kW wireless charging system for a transit bus is reported, two 22 kW modules are paralleled on both the input and output sides. To reduce the effect of cross-coupling, primary and secondary on each side are separated at a considerable distance, making the integration into a vehicle chassis more difficult and costly. In [206], the authors improve the cumbersome structure by stacking a non-polarized coil and a polarized coil on both primary and secondary sides, which minimizes the coils' footprint. Moreover, since effective coupling only happens between a specific pair of coils, the effect of cross-coupling is mostly avoided. The drawback is that the cross-coupling emerges again when the coils are misaligned in some directions. In general, the primary issue that needs to be addressed in this type of system is the cross-coupling that affects the power transfer capacity and ZVS operation.

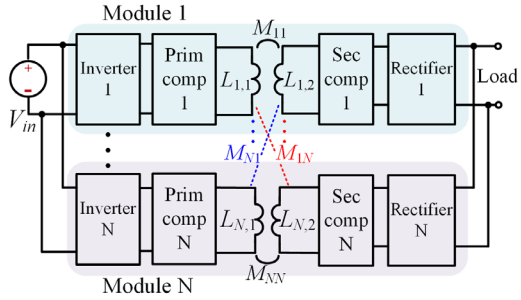

Fig. 23. Diagram of multiple WPT modules with their input and output both paralleled.

In other cases, only the primary side is paralleled to feed multiple windings, while a single coil is applied on the secondary side. In [87], flux orientation is performed by adjusting the current amplitude and phase in each coil to adapt to varied vehicle positions, as shown in Fig. 24.

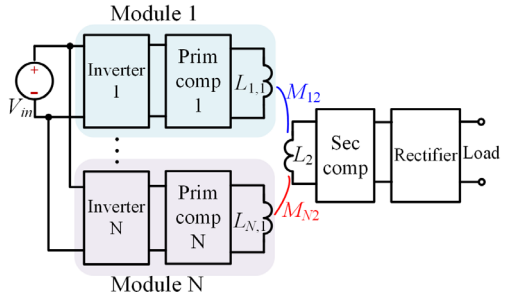

Fig. 24. Multiple coils connected to inverters supplying a single secondary coil.

Although the thermal stress on the primary side is shared among multiple coils, the single secondary has to withstand total losses, thus counteracting the idea of using modular designs to alleviate the losses and thermal issues. Therefore, this type of configuration is mainly set to enhance the flexibility of the primary regulation, instead of raising the power level. Another reason for a single secondary-side coil is based on the consideration of reducing the number of coils to minimize cross-coupling. Moreover, it is relatively easier to design a single high-voltage bridge rectifier for the secondary-side, while multiple relatively lower power primary-side inverters can share the total power.

Multiple secondary side power units are also found in literature, in which they are built up to interface multiple receivers, as shown in Fig. 25. In [86], two rectifiers are required to make a DDQ coil receiver function properly. In [125] and [207], the power fluctuation introduced by varied coupling is also reduced by a multiphase receiver.

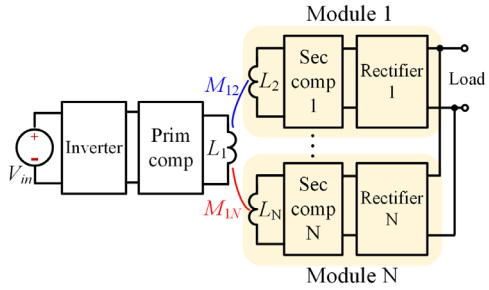

Fig. 25. One primary coil supplies multiple secondary side coils.

D. Power Conversion Architecture for Dynamic Wireless Charging Systems

The conversion architecture of DWPT systems requires careful design considerations. Compared to conventional stationary chargers, the dynamic charging system behaves as a distributed system where the operation of power electronics and coil arrays needs to be coordinated to enhance the system efficiency and maximize the utilization of charging facilities. Depending on the bus architecture and connections, power electronics can be categorized into two types.

One kind of system applies AC-DC-AC conversion units to each coil, as shown in Fig. 26.

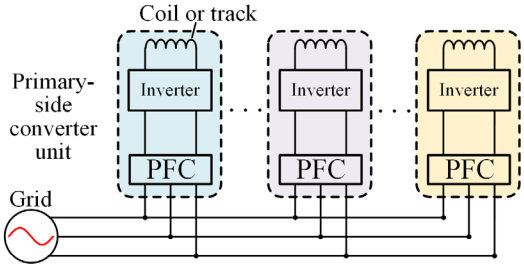

Fig. 26. Sectional power supply scheme that shares a common AC line.

Since each local coil is equipped with an independent power supply, this system configuration has the highest redundancy, and the converter fault has the least impact on the power supply coil chain. Another advantage lies in that each converter only powers the local coil so that a long cable is avoided, which accounts for a large portion of the total cost, complexity, and losses [208]. However, this configuration also significantly increases the costs and complexity of power converters [212]. Another widely adopted approach is a centralized power converter that supplies an extended rail to multiple moving pickups simultaneously [208]. Although this option may reduce the overall number of components, the centralized power converter should be sized based on the maximum power, which depends on the number of vehicles on top of the coil array or tracks. Moreover, the uncoupled area of the transmitter

increases the level of magnetic field exposure to the surroundings.

Based on the above considerations, a common DC bus can be shared between different power units, so that a cluster of coils is supplied through a single primary power source to reduce the number of converters, as shown in Fig. 27. Due to the limited capacity of a DC bus and in order to reduce high losses and costs caused by excessively long cables, the DC bus should be designed to drive a reasonable number of converters in a local area. Particularly, the power rating of the PFC stage should be designed for the maximum power that can be transferred at the total output of all the inverters.

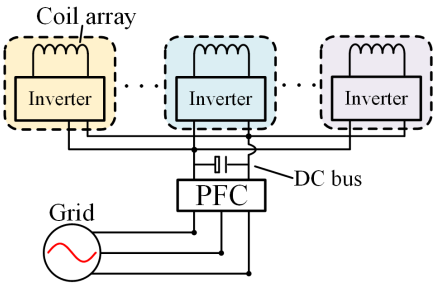

Fig. 27. Sectional power supply scheme that shares a common DC bus.

The above architecture can be further divided into the following subcategories according to the coil layout and the connection method. Fig. 28 (a) shows a scheme in which a single inverter drives a cluster of continuous transmitting coils. The drawback is that the switchgear of these continuous coils may not be able to respond to the vehicle position signal in the short time associated with the vehicle driving at high speed, which degrades the effectiveness of power transfer [213]. On the other hand, this would depend on the vehicle speed as well as the spacing between the transmitters. The above problem can be alleviated by the split power supply mode, as shown in Fig. 28 (b), where the coils driven by a single inverter are spaced apart, which creates a time gap for switching between coils [213]. However, this approach increases the length of the high-frequency AC wiring. In practice, power electronic architectures should be determined considering the design trade-offs between the vehicle speed, size of charging zone, energy efficiency, and overall cost.

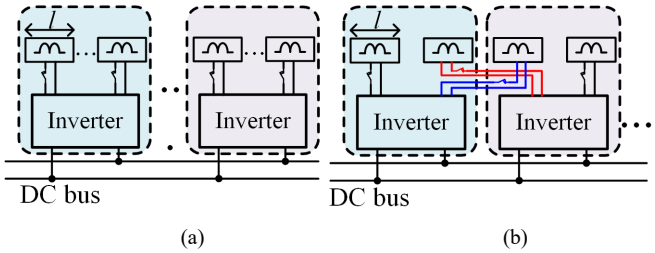

Fig. 28. (a) Single inverter supplying multiple continuously placed coils. (b) Single inverter supplying multiple separated coils.

E. The Application of WBG Devices

Recent practices of wireless charging have witnessed a widespread application of wide bandgap devices. To comply with the switching frequency for WPT1 to WPT3 specified by J2954, while reducing the losses and thermal stress in the power stage under the high power operation, the WBG devices represented by SiC have been introduced to achieve higher performance.

Owing to the high blocking voltage of SiC (1.2 kV and 1.7 kV readily available) compared to regular MOSFET, it enables higher DC bus voltage to be applied to improve the overall system efficiency. The WPT system supplied by a three-phase grid with 700 V to 800 V DC bus voltages is then achievable without resorting to a three-level topology. Furthermore, the lower turn-on and turn-off energy allows the high switching frequency to be used without causing excessive switching losses. Finally, SiC is able to withstand high junction temperatures, which reduces the thermal management requirements. In [41], a single-phase WPT charger is built with SiC MOSFETs and SiC diodes to provide 11 kW at a 91-93% grid to battery efficiency. In [192], a 7-kW wireless charger based on a semi-active bridge is operated at 85 kHz under hard-switching conditions. The reported efficiency is still able to reach 93.4% owing to the supreme switching characteristic of SiC devices. In [43], the single-stage 100-kW wireless charger demonstrated efficiency over 97%, even though the hard-switching occurred during phase-shift control. The SiC module rated at 1.2 kV/325 A plays a critical role in achieving high efficiency.

For WPT4 or higher power levels, it is expected that WBG devices play a more important role than in lower power, by providing an alternative solution using simple converter topology instead of parallel modular design options. The switching frequency was a major discussion topic in standard development as there were four frequency bands (22, 48, 85, and 140 kHz) available in vehicles without interfering other systems in the vehicle such as the keyless entry systems, tire pressure sensors, clock adjustment frequencies, infotainments systems, and other vehicles-side electronic subsystems and components. According to [209], two competing frequencies, 22 kHz and 85 kHz, are compared as the switching frequency for a 50 kW wireless charger. It is reported that the losses, EMI, and material usage are all largely reduced by pushing the frequency to 85 kHz via SiC power devices. On the other hand, WBG devices also bring in circuit-level design issues, such as the sensitivity of gate drivers and controllers due to fast switching noise (because of high dv/dt and di/dt), voltage spikes caused by commutation loop inductances, and a relatively lower thermal time constant, which requires ultrafast protection. All the above factors all add up to the complexity of circuit design.

With regards to the GaN devices, recent research focuses on pushing to the megahertz level frequencies while achieving kilowatt-level power transfer. Reference [210] describes a 1.3-kW WPT system using GaN FETs, working at 13.56 MHz. In [28], the prototype operating at 13.56-MHz achieves an efficiency of 95% at 348 W and transfers 884 W at an efficiency of 91.3% for a CPT system. Reference [211] compared the SiC and GaN using a 6.78 MHz 2.2 kW WPT system. Generally, the power rating of GaN devices is the main obstacle to its high-power operation. The other challenge of GaN devices is the difficulty in assembly of the inverters since screw terminal type device packages are not available for GaN devices.

In conclusion, the utilization of WBG devices enables a more efficient, compact, and flexible design. Among all the emerging issues brought by the WBG devices, the gate driver design and EMI suppression require special consideration to fully exploit

the advantage. More specifically, the gate driver should be carefully designed to both prevent the overvoltage breakdown of devices as well as reduce the associated EMI. The gate-driver level diagnosis and protection are also highly recommended to shut down the gating pulses in case of overcurrent or shoot-through. Moreover, the gate driver auxiliary power should be improved for immunity to high dv/dt generated by the fast switching of WBG devices.

VI. Control of WPT Systems

A. Power Control

In practical applications, WPT systems are usually operated with a closed-loop controller that tracks the reference (set point) output voltage or current [215]. Many researchers have developed control techniques for WPT systems to regulate the battery charge profiles. These techniques can be classified as primary-side control, secondary-side control, and dual-sided control [18]. In the primary-side control, the power flow is adjusted through controlling the primary pad current. The primary-side full-bridge inverter is commonly controlled using varied dc bus voltage, phase shift control, or frequency control. In [214], a primary-side power flow control is investigated and implemented. In the case of primary-side control, the battery voltage, current, and SOC information should be delivered to the primary side, which can be accomplished with a wireless communication system. Moreover, the start and stop of the charging process, as well as vehicle detection and regulating the battery charging profile, are also achieved through a wireless communication system. This can be based on Wi-Fi, Bluetooth, DSRC (Dedicated Short-Range Communication), or another wireless communication protocol. These communication systems typically have tens of milliseconds to hundreds of milliseconds of latencies, which should be taken into account in the control system design. In most cases, these latencies prevent implementing cycle-by-cycle control from the primary side. Therefore, these systems can be used for start, stop, and monitoring purposes as well as to control slowly varying variables, such as the battery current, SOC, etc. on the vehicle side. In many cases, LCL or LCC type compensation networks are used at the primary-side due to constant current characteristics on the primary coil, by which the high communication system latencies can be tolerated.

In secondary-side control, the battery current is controlled at the receiver through active rectification or adding a dc/dc converter. In dual-sided control, the primary full-bridge inverter and the secondary converter should be controlled simultaneously. This requires a fast and reliable communication link between two sides. In [215], dual-sided control has been implemented for a stationary WPT. However, communication speed and security related to the communication channel are the bottlenecks in dynamic applications [18]. One can infer that the independent control of primary and secondary sides offers several advantages in DWPT. Nevertheless, stability issues should be considered carefully while using two independent controllers [18].

In [216], a controller is proposed that measures active and reactive power in the resonant network to regulate the power flow of a bidirectional WPT system. This controller is located at the pick-up (secondary/receiver) side and minimizes the resonant tank reactive power. Song *et al.* demonstrated in [217] a constant current (CC) constant voltage (CV) battery charging profile by only employing primary-side control. This reduces the requirement for the performance of dual-side wireless communication. Most of the controllers are realized using conventional discrete Proportional-Integral (PI) control. However, in [218], discrete sliding mode control is utilized to improve the dynamic voltage regulation of a series-series compensated WPT system.

Some WPT systems use two dc/dc converters at the front side before the high-frequency inverter and one at the load side after the rectifier. Using the perturbation and observation method, these two converters can be controlled cooperatively to maximize efficiency [219]. On the other hand, Huang *et al.* proposed a decoupled controlling structure where the load side DC/DC converter only regulates the output voltage, while the front side converter is in charge of impedance matching [219].

B. Maximum Efficiency Tracking

Maximum efficiency tracking is related to an attempt to design a WPT system so that it maintains high operation efficiency despite the variation of load and coupling coefficient (misalignment or change in airgap), etc. Maximum efficiency tracking can be categorized into three groups [220]: i) the first group mainly focuses on load variation and uses impedance matching networks to dynamically convert the load impedance to an optimal impedance. This can be accomplished by using passive impedance matching networks (capacitors and inductors), as shown in [172]. Alternatively, one can realize active impedance matching by employing a dc-dc converter to dynamically match the load impedance [221]; ii) the second group integrates output control and load variation, including frequency control. For example, in [222], two dc-dc converters are used such that the primary-side converter regulates the voltage, and the secondary side converter matches the load impedance; iii) the third group applies input power control and tries to minimize the input reactive power to maximize efficiency. In this approach, the output voltage is kept constant [223].

Furthermore, Dai *et al.* studied the effect of the coupling coefficient on the system efficiency and propose a method to integrate that with the load variation and output voltage control in maximum efficiency tracking [220]. A similar approach is considered in [224] to dynamically identify the coupling coefficient. In [225], WPT systems with multiple primary-side pads are considered, and a two-step tracking method is proposed that first optimizes the primary current ratios and then optimizes the secondary load impedance. Similarly, Liu *et al.* proposed a control method to adjust the current in two primary pads [143]. As the EV moves, the direction and the ratio of the two primary-side coil currents will be adjusted to maximize the system efficiency.

Many researchers of DWPT systems have focused on the pad design [226], control strategies [227], and compensation networks [228] to increase WPT efficiency. However, one should differentiate power efficiency from energy efficiency while analyzing DWPT systems. Power efficiency is calculated at any given time typically when the transmitter and receiver are fully aligned, while energy efficiency is defined for a specified period; i.e., energy efficiency is the ratio of the

primary and secondary power-time integrals in a given period. In segmented DWPT systems, primary pads will only be energized during a limited time. Therefore, the WPT efficiency should be calculated over that time window.

Timely activation and deactivation of primary pads can improve energy efficiency significantly [229]. It is desired to energize the primary pad when there is enough mutual inductance between primary and secondary pads or when the vehicle-side coupler starts getting aligned with the transmitter. This maximizes the amount of transferred energy and reduces no-load losses. However, the power transfer efficiency varies as the EV moves along the primary pad. Hasan *et al.* analyzed energy efficiency vs. normalized DWPT time interval for a circular primary pad [230]. It has been shown that energy efficiency decreases when a higher portion of the DWPT window is energized. Using advanced control algorithms and segmented transmitters, one can energize the primary pad during a portion of the DWPT window to increase the system energy efficiency.

C. FOD and Vehicle Detection

Magnetic fields generated in a WPT system may heat up metal objects or may have some effects in living bodies, which urged many researchers to focus on Foreign Object Detection (FOD) approaches. As shown in Fig. 29, FOD methods can be categorized into three groups, including system parameters-based, wave-based, and field-based detections [231]. The effect of a foreign object on the system parameters can be detected and used. However, this effect is not significant in high-power systems, making it suitable for low power applications only. While it is relatively easy to detect the effect of metallic objects in between the couplers, it is more difficult to detect the effect of non-metallic and organic objects on the system. In wave-based detection methods, additional sensors such as imaging and thermal cameras or ultrasonic and radar sensors are required to detect foreign objects. Field-based methods detect the changes in the magnetic field distribution. In some cases, an additional coil is employed, and by monitoring its inductance and quality factor, the FOD is achieved [232].

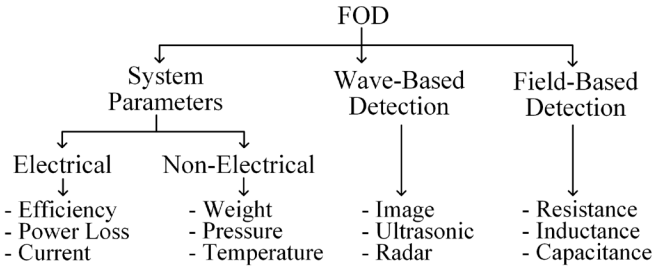

Fig. 29. Categories of FOD methods [231].

An FOD system based on secondary-side quality factor has been investigated in [236] to detect metallic objects. In [237], living object detection is discussed based on a comb pattern capacitive sensor, and in [238], a dual-purpose FOD system is developed to detect both metallic objects and approaching vehicles. In [235], a symmetric sensing coil is designed which eliminates blind zones in conventional designs.

In DWPT applications, ideally, a primary pad should only be energized when the EV is approaching. This is to eliminate the standby losses in the primary coil and avoid excessive EMF in the environment. To this aim, various vehicle detection methods are proposed in the literature. In [233], a three-coil independent detection system is presented to allow the power supply to detect an approaching EV. Furthermore, in [234], a sensorless scheme is discussed, which utilizes free resonant currents in the primary coil to detect the vehicle. The phase-angle variation between voltage and current is employed in [229] to determine the primary pad energizing time.

D. Misalignment

Mutual inductance between primary and secondary pads determines how much power can be transferred in a WPT system [158]. The mutual inductance will decrease significantly by an increase in lateral misalignment. This reduces system power transfer capability and efficiency. In [239], the authors investigated the lateral position of vehicles in a targeted lane for different driving conditions. It has been shown that the lateral vehicle misalignment is a random variable with a normal distribution. The standard deviation is 26 cm when the drivers are aware of testing, and the vehicle speed is 50 km/h [239].

According to the SAE J2954 Recommended Practice, stationary WPT systems should be tolerant of x-, y-, and z-directional misalignments [240] to some extent. Similarly, in a DWPT system, the x-misalignment is a natural vehicle movement, y-misalignment is a lateral vehicle position with respect to the primary pad center, and z-misalignment is the magnetic airgap which is defined by the distance between the surface of the receiver pad and the ground surface. The driver's driving skills will affect the y–misalignment, while the vehicle type and the payload changes the z-misalignment or vertical offset. J2954 Recommended Practice mandates an overall efficiency of no less than 80% during misalignments for stationary WPT systems [240].

Fotopoulou and Flynn [241] developed an analytical model to address the effects of misalignment in a WPT system. In [242], an adaptive impedance matching circuit is introduced to increase the system efficiency in highly misaligned conditions. In [80], [97], and [243], pad structures are proposed to improve the system misalignment tolerance. Furthermore, it has been shown that other control techniques, such as frequency control, can improve efficiency [244].

Some researchers have focused on lateral misalignment detection. Azad *et al.* [245] demonstrated a three-coil detection system that informs the driver on the lateral misalignment value. The concept of using sensing coils has been investigated in [246] to reduce lateral misalignment using two-dimensional coil positioners.

E. Communication

Communication between a roadside controller and a vehicle is a critical part of a WPT system. The secure and reliable operation of a system is dependent on a timely exchange of data between primary and secondary sides. Some of the criteria for the optimum communication protocol are low latency, the need for supporting multiple vehicles, and at least a medium-range coverage [18]. A few communication platforms have been discussed in the literature so far [247], [248]. Gil *et al*. [247] compared different wireless technologies for DWPT,

considering maximum range, data rate, latency, and mobile connectivity. Echols *et al*. employed Dedicated Short-Range Communication (DSRC) for Vehicle-to-Infrastructure communication [248]. Other communication options include Wi-Fi (IEEE 802.11), Bluetooth (IEEE 802.15.1), ZigBee (EEE 802.15.4), etc.

VII. Future Challenges and Prospects

A. Applications of Advanced Materials

Generally, the ultimate objective of a high-power wireless charger design cover the following aspects: high power rating, high efficiency, high power density, large air-gap distance, high misalignment tolerance, and safe operation. So far, various power electronics topologies, coupler designs, and control strategies are presented to realize these design targets. The designs reported so far mostly represent tradeoffs of selected design requirements. The introduction of an advanced material or an unconventional coupler geometry can be a path to fundamentally remove the design restrictions and improve the overall performance.

One major dilemma is how to account for high frequency and high power at the same time. To improve efficiency, the most straightforward approach is to increase the operating frequency in order to maximize the coil quality factor while this approach may slightly reduce the inverter efficiency with increased switching losses. Furthermore, higher frequency helps to reduce the coil current and the number of turns for the same amount of magnetic field generation or power delivery. On the other hand, high-frequency semiconductor devices can rarely support high power ratings. Recently, with the development of wide bandgap devices that feature low conduction and switching losses and high junction temperature limit, high-frequency operation is enabled to maximize the power capacity and energy efficiency. A recent example is the design of a 100-kW single-phase prototype using 1200 V/325 A SiC module that employs the designed switching frequency of 22 kHz and reaches an efficiency of 97%, which would not be possible using conventional Si devices in a single module [43]. Another example is the GaN-driven CPT systems pushing the operating frequency to tens of megahertz levels to enable kW-level operation with a large air gap [28].

Another concern regarding high-power wireless chargers is the physical limitations set by their magnetic couplers. The optimization of the couplers deals with complex interactions among efficiency, power density, leakage field, and misalignment tolerance [249]. One can notice that the bottleneck is still dependent on the material and engineering of the hardware developments. To remove the performance restriction on magnetic coils, advanced materials such as low-loss magnetic cores, ideally twisted Litz-wires with transposed wire strands and bundles, low-loss and highly compact film or ceramic capacitors, and even metamaterials used for flux guidance [249]-[250] represent future trends towards higher power, more efficient, safer, and more flexible wireless charging systems.

B. Standardization

Another challenge arises from the adaption of power supplies and magnetic couplers provided by different manufacturers. Regarding primary sides with different flux patterns, the secondary sides have to be reconfigured accordingly to effectively couple to the primary side. Moreover, compensation parameters and power electronics are required to match the coil geometry to achieve the rated power level under a wide operating range. Consequently, the interoperability needs to be defined among the power electronics, compensation topology parameters, coil types (i.e., circular, DD, etc.) and geometries to ensure their compatibility [252].

Although SAE J2954 Recommended Practice has already covered WPT1 to WPT3 vehicular wireless chargers, specifications for high-power wireless charging systems rated higher than 22 kVA (from the input side) have not been defined with regards to the allowable stray field level, operating frequency, power electronics, compensation topology, and coil geometry [240]. Therefore, standardization needs to be further advanced to promote the application of high-power wireless chargers. A similar effort is expected in the field of dynamic charging systems where the lack of technical guidance forces the researchers to define their own boundaries and compatibility requirements. As an example, different DWPT operation frequencies are still in use, some of them not matching the standardized frequency range specified in J2954 for stationary EV charging [52], [253]. While it is expected that the vehicles would have interoperability and compatibility between stationary and dynamic WPT transmitters, interoperability between different vehicle classes (i.e., light, medium, and heavy-duty) is also desirable to reduce the infrastructure and installation costs. This would also simplify the vehicle-side coupler and the electronics since a single system would be able to operate in both cases.

C. Electromagnetic Measurements and Safety Evaluation

Despite the fact that SAE J2954 has not defined shielding solutions for power levels higher than WPT3, electromagnetic and electric field emissions inevitably becomes a major threat to safety in high-power WPT systems and thus requires dedicated design. Moreover, when the future power ratings increase to foreseeable hundreds of kilowatts, coil misalignments will further add to the magnetic field emissions and lead to greater difficulty in the shielding design. Therefore, the worst misalignment case should be considered jointly with the stray field limitations and safety margins.

Steadily increasing power levels raise the question of the accuracy of the field exposure measurement. An inspection of the stray field guideline regarding human exposure is performed by an EU collaborative project [251]. The measurement accuracy and limitations of existing instruments are evaluated. Using the newly developed measurement tools, detailed dosimetric models have been set up to reproduce the human exposure in real charging stations. It is found that the developed calibration facilities help the assessment of human exposure to electromagnetic fields achieve higher accuracy. A set of open questions to be explored includes the stray field measurement and mitigation in wireless charging for heavy-duty vehicles and the electromagnetic safety of dynamic charging systems.

D. Customized Design

Recently, wireless charging technology has received substantial attention in special applications such as underwater charging [254], powering unmanned aerial vehicles [255], autonomous vehicle charging [194], power supplies for emergency situations, and auxiliary power supplies in medium voltage power conversion [256]. In such applications, the design of magnetic couplers, compensation networks, and control strategy should be customized to address various demands. Depending on the environment, a wireless charging based on the magnetic coupling may not be able to perform equally well in all conditions. Consequently, high-power wireless charging system based on capacitive coupling, supersonic vibration, laser beams, or any other medium is a potential substitution for traditional magnetic-field-based wireless chargers [257], [258].

E. Economic Evaluation and New Integration Approaches

The economic evaluation of DWPT charging is the basis for its promotion. The establishment of a wireless charging system can significantly reduce the vehicle energy storage capacity and reduce vehicle costs. However, it is also necessary to consider the cost of battery depreciation, road facilities, distribution network transformer, and power quality and grid impact management. Following this, one can perform a comprehensive evaluation under different optimization objective functions. In [152], researchers studied the economic viability of DWPT systems and their environmental impact. Their results depend on upfront capital costs and technology adoption. However, they prove that DWPT systems can provide both economic and environmental benefits when compared to conventional internal combustion engine transportation. Mi *et al.* studied the economic feasibility of the OLEV in Seoul South Korea, assuming each vehicle runs 20,000 km each year, and all major roads in the city are equipped with DWPT systems. They showed that the benefit-to-cost ratio for commercializing OLEVs will be more than one by 2024 [153].

The integration of WPT systems into the zonal distribution network can promote the higher penetration of renewable energy. Based on the fluctuation of the energy consumption of a DWPT system, it is possible to configure an operation mode in which the DWPT system serves as a local, controllable load on a microgrid. Moreover, integrating DWPT systems with energy storage and renewables may reduce the dependency on the grid and reduce or eliminate the grid impact. It can also eliminate the need for deploying new transmission and distribution lines along the roadways since the electrified roadways can be powered by renewable energy sources buffered by stationary energy storage systems.

F. Power Metering

For fair and trustworthy billing, an accurate, reliable, and safe method for power metering in WPT systems is needed. In [251], the authors discussed the accuracy of measuring power in a WPT system, mainly focused on metering AC high-frequency power (20-150 kHz). Due to total harmonic distortion of the AC current (up to 2%) and voltage (up to 45%), the modern current and voltage transducers and power analyzers can experience a power measuring error up to 10% at 100 kHz. That is enough to generate a significant error in efficiency measurement and subsequent billing. As illustrated in [266], even a 1% error can cause billions of dollars of inaccurate billing if EV consumption reaches 1,900 TWh, as expected by 2040. Without proper measurement tools and methods to deal with the increasing power level, the accumulated measurement error may result in misjudgment of WPT performance and cause substantial economic losses. Through the Metrology for Inductive Charging of Electric (MICEV) project, a group of institutions and universities in Europe is working on developing a high-accuracy power measurement unit for on-board power measurement for static WPT charging [251]. They propose the use of coaxial shunts as current transformers, and to correct the ratio and phase error of existing voltage transducers, with the expected accuracy better than 0.1%.

To measure power, the authors in [266] propose a non-contact method based on sensing magnetic field in the zone between coils, as illustrated in Fig. 30. The proposed sensing method guarantees accuracy while charging for the electricity since it excludes the individual losses of primary and secondary from the measurements. They propose two sensing coils positioned in the transfer-space to measure real power. The estimated power is first calculated in the frequency domain to be converted in the time domain by means of Parseval's theorem. The reported experimental accuracy of the apparatus is 0.06% after calibration, which is well within the energy metering standards (±0.2%, ANSI C12.20). In [267], the authors evaluate the calibration methods for the sensing coils proposed in [266], particularly focusing on the mobile calibration equipment and systems that can be used in future energy service stations. The proposed solution is based on calibrated open-circuited sensing coils, and it is expected to be compatible with J2954. It should be noted that most of these efforts to calculate the power received by the vehicle are based on the belief that the users should be billed for the energy delivery to the vehicle. However, in plug-in chargers, like in all other devices and appliances, the energy is measured at the input of the front-end converters, which involves reading the voltage and current of the 60 Hz AC grid. The energy consumption of the wireless chargers can also be measured on the input (AC grid) side, which simplifies the entire measurement and billing process. Therefore, measuring the high-frequency AC voltage and current or the magnetic field is not necessarily needed since the customers will be responsible for the energy that comes from the grid and not necessarily the energy that is delivered to their vehicle.

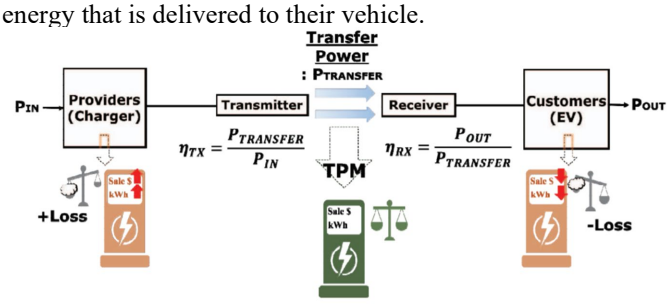

Fig. 30. Transfer-power metering system proposed in [266].

G. Impact of DWPT on Power Grid Stability and Quality

It is evident that a massive deployment of EVs would impact power distribution networks. Putrus *et al.* studied how to

schedule residential EV charging to improve the load profile [259]. They suggested having some sort of incentive for customers to distribute charging throughout the day. That way, EV load does not add to pre-existing peak load since it will be scheduled for off-peak hours. In [260], another EV charging coordination scheme is investigated, such that the EV demand is allocated during the valley period of the load profile. It is also considered to charge EVs when there are the maximum number of renewable sources in the network. Furthermore, vehicle-to-grid (V2G) EV capability is employed to minimize the network load variance.

He *et al*. investigated an optimal deployment of public charging stations for EVs [261]. The optimal number of charging stations allocated to each metropolitan area is a strategic decision that should be determined based on the network load profile. Similarly, in [262], the authors investigated which lanes in a regional road network should be deployed with dynamic charging infrastructure. Their model optimizes the travel time and EV speed such that the driver can reach the destination without running out of charge. However, in the model, the power network load profile and the load peak hours are not considered. For future research, an optimization algorithm can encourage EVs to choose dynamic charging routes that help improve load profile. In [263], three different cases are studied, showing that the grid voltages vary significantly due to the implementation of DWPT systems. The paper suggests a combination of smart control and energy storage or DC distribution infrastructure to maintain grid stability.

Fig. 31 illustrates a grid-side power profile for a segmented DWPT system. One can see that the average power transfer P_{avg} is much less than the maximum power P_{max}. The power pulsation will significantly affect the grid-side power quality. This problem tends to be more severe as the length of primary pads reduces. Ruddell *et al*. proposed a solution to combine a WPT system with a SuperCapacitor (SC) energy storage. This system is implemented at the vehicle side to smoothen high-power pulses to the battery [264].

Fig. 32(a) shows how the primary inverter current I_{in} is equalized at the battery side I_{out}. Furthermore, Azad *et al*. proposed a novel topology at the primary side to reduce power fluctuations at the input of a DWPT system [265], which utilizes the existing power converter to smoothen the input power profile, as shown in Fig. 32(b).

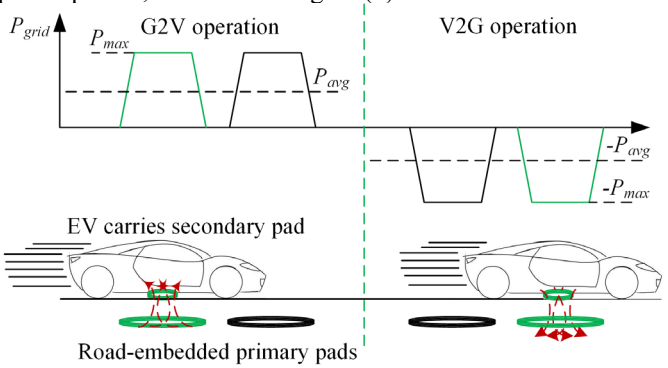

Fig. 31. Grid-side DWPT power profile in segmented DWPT systems.

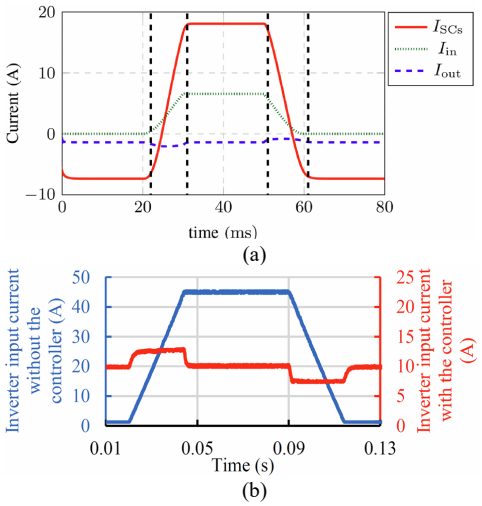

Fig. 32. Use of supercapacitors to smoothen the power profile in segmented DWPT systems. (a) SCs at the vehicle side, I_{in} is the inverter input current, I_{out} is the battery current, and I_{SC} is the SC current [264]. (b) Power smoothening SC located at the primary [265].

The impact of massive deployment of DWPT on the utility side can be predicted using load and source profiles. However, the precise pattern of stochastic charging via DWPT requires abundant data collection, based on which the negative effect can be mitigated through dedicated planning on charging and discharging behavior of DWPT systems.

H. Issues Related to System Construction and Installation

The integration of a WPT system into existing infrastructure is a complicated task, particularly for the road embedded static and dynamic WPT systems. This complexity is reflected in several aspects: i) the mechanical structure may alter the coil's magnetic characteristics; ii) the construction material itself may generate losses, and iii) the coil integration should not jeopardize the mechanical integrity of the roadway, namely the compatibility. Meanwhile, the mechanical strength of the coil must withstand the weight posed on the path. To evaluate the losses in construction material, concrete magnetic characteristics are identified in [268], and the effect on coil electrical performances are elaborated, which provides guidelines for designing the coil geometry. However, the integration of shielding structures (ferrite and aluminum) has not been discussed. Dielectric losses induced in pavement surfacing material are analyzed in [269]. The results indicate that the losses in surfacing material are minor compared to other sources. Besides, the high moisture-sensitivity of the losses demands a waterproof design of the mechanical structure. To resolve the fragility of ferrite, magnetizable concrete is fabricated by mixing magnetic material with cement in [270]. This approach is expected to reduce the cost of construction and provide higher mechanical strength for coils.

Regarding the road compatibility study, in [271], the durability of pavement after integrating the wireless charging equipment is examined by studying the case in Belgium. The implementation of the inductive charging system showed that it is feasible to introduce components in the road that are foreign to the conventional pavement. On the contrary, another similar study assessed the life cycle of an electrified road (e-road) using the data collected from a test site in Italy [272]. The research raised a warning regarding the integration of charging

facilities into the road. The authors claimed that embedded pads account for only 1% of the total pavement weight but more than 30% of the reduced durability of an e-road.

Based on the research presented so far, one can conclude that more investigation is needed to understand and quantify the influence of road-embedded coils on mechanical integrity and loss generation inside the road material. From the design perspective, the deviation of electromagnetic and mechanical performances of couplers after being embedded into an asphalt or concrete road needs to be taken into account. Finally, the issues of shielding, packaging, material selection, and coil integration should be assessed at an early design stage.

I. Cybersecurity of Wireless Charging Systems

The cybersecurity of wireless charging stations is an emerging challenge related to both the energy and information safety of WPT systems. With wireless charging infrastructure moving towards higher power levels, the systematic cybersecurity vulnerability of the charging network is also increasing. In [273], multiple federal agencies in the US agreed that there is a lack of even some basic cybersecurity guidelines for wireless charging systems. According to [273], a wireless charging system faces the same cybersecurity challenges as a wired one, but due to a lack of physical connection between the EV and a charger, some unique threats need to be considered. The central issue is that the EV and Electric Vehicle Supply Equipment (EVSE) utilize over-the-air communication for all handshaking aspects, including the start & stop and control of the charging process. This makes the two-way communication exposed to eavesdroppers and vulnerable to denial of service, message injection, and Man-in-the-middle (MITM) over the air. That way, a malicious actor could potentially compromise the safety, privacy, or operation of not only the charging process but also the other aspects of an EV or EVSE. Since the power is transferred wirelessly, there is a possibility that the energy is picked up by uncensored clients mimicking a legit customer causing economic loss. Moreover, WPT communication protocols can be used to steal the identity of customers, vehicles, or even jeopardize the public charging facilities. To reduce the risk of security incidents, cybersecurity is required to be considered at an early design stage, by deploying modern diagnostic and prevention tools. In [274], potential losses and damages are evaluated on a 100-kW WPT system considering the worst cases, where the control of the charging stations and the vehicle-side BMS is taken by hackers. The analysis shows that the fault energy losses can be high enough to damage the main components in charging stations and vehicles.

VIII. CONCLUSION

Wireless charging systems are envisaged to provide a reliable, convenient, and efficient charging in a safe environment with minimum human engagement. Wireless charging towards high power can largely shorten the equivalent recharging time, enhance the charging experience, and reduce the range anxiety. High-power wireless chargers operating at hundreds of kilowatts can provide a fast charging experience commensurate to that of the existing refueling stations. This paper presents a review of some recent advances in high-power wireless charger designs. The essential design considerations in terms of magnetic design, compensation network, power electronics, control, and communication are given for both stationary and dynamic wireless charging systems. The paper also describes some major limitations of wireless charging and suggests directions for future development. The ever-growing application of high-power wireless chargers is expected to serve as an important supplement to existing conductive chargers and accelerate the mass market penetration of EVs and other electrically driven means of transportation.

ACKNOWLEDGMENT

This research is supported by the U.S. Department of Energy, Vehicle Technologies Office funded projects under the “Batteries and Electrification to Enable Extreme Fast Charging (XFC)” Funding Opportunity Announcement, DE-FOA-0001808. Both NCSU and ORNL are the recipients of this award and collaborated for this publication. The authors would like to thank Mr. Lee Slezak (US Department of Energy) for his support of this work which is greatly appreciated. Authors also would like to acknowledge the support and guidance of Dr. Srdjan Lukic (NCSU) and Dr. David E. Smith (ORNL) on this publication.

REFERENCES

[1] V. Etacheri, R. Marom, R. Elazari, G. Salitra, and D. Aurbach, “Challenges in the development of advanced Li-ion batteries: A review,” Energy Environ. Sci., vol. 4, no. 9, pp. 3243–3262, 2011.

[2] S. Li and C. C. Mi, "Wireless Power Transfer for Electric Vehicle Applications," IEEE J. Emerg. Sel. Top. Power Electron., vol. 3, no. 1, pp. 4-17, March 2015.

[3] S. Lukic and Z. Pantic, "Cutting the Cord: Static and Dynamic Inductive Wireless Charging of Electric Vehicles," IEEE Electrification Magazine, vol. 1, no. 1, pp. 57-64, Sept. 2013.

[4] S.Y.R. Hui, W. Zhong, and C.K. Lee, "A Critical Review of Recent Progress in Mid-Range Wireless Power Transfer," IEEE Trans. Power Electron., vol. 29, no. 9, pp. 4500-4511, Sept. 2014.

[5] T. Kan, Y. Zhang, Z. Yan, P. Mercier, and C. C. Mi, “A Rotation-Resilient Wireless Charging System for Lightweight Autonomous Underwater Vehicles,” IEEE Trans. Veh. Technol., pp. 1–1, 2018.

[6] M. Lu, M. Bagheri, A. P. James, and T. Phung, "Wireless Charging Techniques for UAVs: A Review, Reconceptualization, and Extension," IEEE Access, vol. 6, pp. 29865-29884, 2018.

[7] J. Shin et al., "Design and Implementation of Shaped Magnetic-Resonance-Based Wireless Power Transfer System for Roadway-Powered Moving Electric Vehicles," IEEE Trans. Ind. Electron, vol. 61, no. 3, pp. 1179-1192, March 2014.

[8] S. Chopra and P. Bauer, "Driving Range Extension of EV With On-Road Contactless Power Transfer — A Case Study," IEEE Trans. Ind. Electron., vol. 60, no. 1, pp. 329-338, Jan. 2013.

[9] A. Caillierez, D. Sadarnac, A. Jaafari, A. Caillierez, and S. Loudot, "Unlimited range for electric vehicles," in Proc. Int Symposium on Power Electron, Electrical Drives, Automation and Motion, Ischia, 2014, pp. 941-946.

[10] A. A. S. Mohamed, C. R. Lashway, and O. Mohammed, "Modeling and Feasibility Analysis of Quasi-Dynamic WPT System for EV Applications," *IEEE Trans. Transp. Electrification*, vol. 3, no. 2, pp. 343-353, June 2017.

[11] Neubauer, Jeremy, and Eric Wood. "The impact of range anxiety and home, workplace, and public charging infrastructure on simulated battery electric vehicle lifetime utility," *Journal of power sources* 257 (2014): 12-20.

[12] S. Jeong, Y. J. Jang, and D. Kum, "Economic Analysis of the Dynamic Charging Electric Vehicle," *IEEE Trans. Power Electron.*, vol. 30, no. 11, pp. 6368-6377, Nov. 2015.

[13] J. Dai and D. C. Ludois, "A Survey of Wireless Power Transfer and a Critical Comparison of Inductive and Capacitive Coupling for Small Gap Applications," *IEEE Trans. Power Electron.*, vol. 30, no. 11, pp. 6017-6029, Nov. 2015.

[14] S. Sasaki, K. Tanaka, and K. Maki, "Microwave Power Transmission Technologies for Solar Power Satellites," *Proceedings of the IEEE*, vol. 101, no. 6, pp. 1438-1447, June 2013.

[15] I. Mayordomo, T. Dräger, P. Spies, J. Bernhard, and A. Pflaum, "An Overview of Technical Challenges and Advances of Inductive Wireless Power Transmission," *Proceedings of the IEEE*, vol. 101, no. 6, pp. 1302-1311, June 2013.

[16] J. O. McSpadden and J. C. Mankins, "Space solar power programs and microwave wireless power transmission technology," *IEEE Microwave Magazine*, vol. 3, no. 4, pp. 46-57, Dec. 2002.

[17] N. Shinohara, "Beam Control Technologies With a High-Efficiency Phased Array for Microwave Power Transmission in Japan," *Proceedings of the IEEE*, vol. 101, no. 6, pp. 1448-1463, June 2013.

[18] D. Patil, M. K. McDonough, J. M. Miller, B. Fahimi, and P. T. Balsara, "Wireless Power Transfer for Vehicular Applications: Overview and Challenges," *IEEE Trans. Transp. Electrification*, vol. 4, no. 1, pp. 3-37, March 2018.

[19] Z. Zhang, H. Pang, A. Georgiadis, and C. Cecati, "Wireless Power Transfer—An Overview," *IEEE Transactions on Industrial Electronics*, vol. 66, no. 2, pp. 1044-1058, Feb. 2019.

[20] V. Cirimele, M. Diana, F. Freschi, and M. Mitolo, "Inductive Power Transfer for Automotive Applications: State-of-the-Art and Future Trends," *IEEE Transactions on Industry Applications*, vol. 54, no. 5, pp. 4069-4079, Sept.-Oct. 2018.

[21] M. Yilmaz and P. T. Krein, "Review of Battery Charger Topologies, Charging Power Levels, and Infrastructure for Plug-In Electric and Hybrid Vehicles," *IEEE Trans. Power Electron.*, vol. 28, no. 5, pp. 2151-2169, May 2013.

[22] E. Waffenschmidt, and T. Staring, "Limitation of inductive power transfer for consumer applications," in *Proc. 13th European Conf. Power Electron. Appl. (EPE-ECCE Europe),* 2009, pp.3538.

[23] J. H. Kim *et al*., "Development of 1-MW Inductive Power Transfer System for a High-Speed Train," *IEEE Trans. Ind. Electron.*, vol. 62, no. 10, pp. 6242-6250, Oct. 2015.

[24] A. Kurs, A. Karalis, R. Moffatt, J.D. Joannopoulos, P. Fisher, and M. Soljacic, "Wireless Power Transfer via Strongly Coupled Magnetic Resonances," *SCIENCE*, vol. 317, no. 5834, pp. 83-86, 2007.

[25] S. L. Ho, J. Wang, W. N. Fu, and M. Sun, "A Comparative Study Between Novel WiTricity and Traditional Inductive Magnetic Coupling in Wireless Charging," *IEEE Trans. Mag*, vol. 47, no. 5, pp. 1522-1525, May 2011.

[26] M. P. Theodoridis, "Effective Capacitive Power Transfer," *IEEE Trans. Power Electron.*, vol. 27, no. 12, pp. 4906-4913, Dec. 2012.

[27] S. Sinha, B. Regensburger, K. Doubleday, A. Kumar, S. Pervaiz, and K. K. Afridi, "High-power-transfer-density capacitive wireless power transfer system for electric vehicle charging," in *Proc. IEEE Energy Conversion Congress. Exposition (ECCE)*, Cincinnati, OH, 2017, pp. 967-974.

[28] B. Regensburger, A. Kumar, S. Sinha, and K. Afridi, "High-Performance 13.56-MHz Large Air-Gap Capacitive Wireless Power Transfer System for Electric Vehicle Charging," *2018 IEEE 19th Workshop on Control and Modeling for Power Electronics (COMPEL)*, Padua, 2018, pp. 1-4.

[29] H. Zhang, F. Lu, H. Hofmann, W. Liu, and C. C. Mi, "A Four-Plate Compact Capacitive Coupler Design and LCL-Compensated Topology for Capacitive Power Transfer in Electric Vehicle Charging Application," *IEEE Transactions on Power Electronics*, vol. 31, no. 12, pp. 8541-8551, Dec. 2016.

[30] H. Zhang, F. Lu, H. Hofmann, W. Liu, and C. C. Mi, "Six-Plate Capacitive Coupler to Reduce Electric Field Emission in Large Air-Gap Capacitive Power Transfer," *IEEE Transactions on Power Electronics*, vol. 33, no. 1, pp. 665-675, Jan. 2018.

[31] F. Lu, H. Zhang, H. Hofmann, and C. Mi, "A Double-Sided LCLC-Compensated Capacitive Power Transfer System for Electric Vehicle Charging," *IEEE Trans. Power Electron.*, vol. 30, no. 11, pp. 6011-6014, Nov. 2015.

[32] M. Antivachis, M. Kasper, D. Bortis, and J. W. Kolar, "Analysis of capacitive power transfer GaN ISOP multi-cell DC/DC converter systems for single-phase telecom power supply modules," *IECON-42nd Annual Conference of the IEEE Industrial Electronics Society*, Florence, 2016, pp. 1280-1287.

[33] *7 kW Wireless Power Transmissioin Technology for EV Charging.* [Online]. Available:https://www.toshiba.co.jp/rdc/rd/fields/14_e01_e.html

[34] *WiT-3300™ FOD System.* [Online]. Available:http://www.terraelectronica.ru/pdf/WITRCITY/WiT-3300DS.pdf

[35] *BOMBARDIER PRIMOVE to Provide Wireless Charging and Battery Technology to Berlin*. [Online]. Available: https://www.bombardier.com/en/media/newsList/details.bombardiertransportation20150318ebusberlinabsommerfaehrtdielini.bombardiercom.html?filter-bu=tran

[36] *Momentum Dynamics*. [Online]. Available: http://www.momentumdynamics.com

[37] G. Guidi, J. A. Suul, F. Jenset, and I. Sorfonn, "Wireless Charging for Ships: High-Power Inductive Charging for Battery Electric and Plug-In Hybrid Vessels," *IEEE Electrification Magazine*, vol. 5, no. 3, pp. 22-32, Sept. 2017.

[38] R. Bosshard and J. W. Kolar, "Multi-Objective Optimization of 50 kW/85 kHz IPT System for Public Transport," *IEEE J. Emerg. Sel. Top. Power Electron.*, vol. 4, no. 4, pp. 1370-1382, Dec. 2016.

[39] *Inductive Power Transfer IPT®-Charge*. [Online]. Available: https://www.conductix.us/en/products/inductive-power-transfer-iptr/inductive-power-transfer-iptr-charge?parent_id=5798

[40] *Wave IPT - Wirelessly charging electric vehicles.* [Online]. Available: www.waveipt.com.

[41] *WiTricity Electric Vehicle Charger*, [Online]. Available: https://www.st.com/content/ccc/resource/sales_and_marketing/presentation/product_presentation/group0/5a/b1/8e/6c/2b/0d/46/3c/Apec/files/APEC_2016_SiC_%20Wtricity_Wireless_Charging.pdf/_jcr_content/translations/en.APEC_2016_SiC_%20Wtricity_Wireless_Charging.pdf

[42] J. Tritschler, S. Reichert, and B. Goeldi, "A practical investigation of a high power, bidirectional charging system for electric vehicles," in *Proc. 16th European Conf. Power Electron. Appl*, Lappeenranta, 2014, pp. 1-7.

[43] V. P. Galigekere *et al*., "Design and Implementation of an Optimized 100 kW Stationary Wireless Charging System for EV Battery Recharging," in *Proc. IEEE Energy Conversion Congress and Exposition (ECCE)*, Portland, OR, 2018, pp. 3587-3592.

[44] [Online]. Available: http://www.intis.de/wireless-power-transfer.html#projects

[45] [Online]. Available: https://www.ornl.gov/news/ornl-demonstrates-120-kilowatt-wireless-charging-vehicles

[46] M. Suzuki, K. Ogawa, F. Moritsuka, T. Shijo, H. Ishihara, Y. Kanekiyo, K. Ogura, S. Obayashi, and M. Ishida,"Design Method for Low Radiated Emission of 85 kHz Band 44 kW Rapid Charger for Electric Bus," in *Proc. Annual IEEE Applied Power Electronics Conference and Exposition (APEC).,* 2017, pp.3695-3701.

[47] M. Bojarski, E. Asa, K. Colak, and D. Czarkowski, "Analysis and Control of Multiphase Inductively Coupled Resonant Converter for Wireless Electric Vehicle Charger Applications," *IEEE Trans. Transp. Electrification*, vol. 3, no. 2, pp. 312-320, June 2017.

[48] S. Y. Choi, B. W. Gu, S. Y. Jeong, and C. T. Rim, "Advances in Wireless Power Transfer Systems for Roadway-Powered Electric Vehicles," *IEEE J. Emerg. Sel. Top. Power Electron.*, vol. 3, no. 1, pp. 18-36, March 2015.

[49] [Online]. Available: https://www.dcstreetcar.com/wp-content/uploads/2014/08/Section-D-Part-6-723-830-pagesred.pdf

[50] [Online]. Available:http://www.intis.de/intis/mobility.html

[51] *INTIS inductive energy transfer systems at a glance,* [Online]. Available: http://www.intis.de/wireless-power-transfer.html#applications

[52] R. Tavakoli and Z. Pantic, "Analysis, Design, and Demonstration of a 25-kW Dynamic Wireless Charging System for Roadway Electric Vehicles," *IEEE J. Emerg. Sel. Top. Power Electron.*, vol. 6, no. 3, pp. 1378-1393, Sept. 2018.

[53] I. Villar, A. Garcia-Bediaga, U. Iruretagoyena, R. Arregi, and P. Estevez, "Design and experimental validation of a 50kW IPT for Railway Traction Applications," in *Proc. IEEE Energy Conversion Congress and Exposition (ECCE)*, Portland, OR, 2018, pp. 1177-1183.

[54] Chwei-Sen Wang, O. H. Stielau, and G. A. Covic, "Design considerations for a contactless electric vehicle battery charger," *IEEE Trans. Ind. Electron.*, vol. 52, no. 5, pp. 1308-1314, Oct. 2005.

[55] D. Howell, S. Boyd, B. Cunningham, S. Gillard, L. Slezak, S. Ahmed, I. Bloom, A. Burnham, K. Hardy, A. N. Jansen, P. A. Nelson. "*Enabling*

fast charging: A technology gap assessment," U.S. Department of Energy; October 2017, [online] available:https://www.energy.gov/eere/vehicles/downloads/enabling-extreme-fast-charging-technology-gap-assessment

[56] I. Nam, R. Dougal, and E. Santi, "General optimal design method for series-series resonant tank in loosely-coupled wireless power transfer applications," in *Proc. IEEE Applied Power Electronics Conference and Exposition (APEC)*, Fort Worth, TX, 2014, pp. 857-866.

[57] C. Zheng, B. Chen, L. Zhang, R. Chen, and J. Lai, "Design considerations of LLC resonant converter for contactless laptop charger," in *Proc. IEEE Applied Power Electronics Conference and Exposition (APEC)*, Charlotte, NC, 2015, pp. 3341-3347.

[58] S. Lee, B. Choi, and C. T. Rim, "Dynamics Characterization of the Inductive Power Transfer System for Online Electric Vehicles by Laplace Phasor Transform," *IEEE Trans. Power Electron.*, vol. 28, no. 12, pp. 5902-5909, Dec. 2013.

[59] H. Li, K. Wang, L. Huang, W. Chen, and X. Yang, "Dynamic Modeling Based on Coupled Modes for Wireless Power Transfer Systems," *IEEE Trans. Power Electron.*, vol. 30, no. 11, pp. 6245-6253, Nov. 2015.

[60] S. Wang *et al.*, "Modeling and control methods of dynamic wireless power transfer system," in *2017 IEEE Transportation Electrification Conference and Expo, Asia-Pacific (ITEC Asia-Pacific)*, 2017, pp. 1–4.

[61] Y. Guo, L. Wang, Q. Zhu, C. Liao, and F. Li, "Switch-On Modeling and Analysis of Dynamic Wireless Charging System Used for Electric Vehicles," *IEEE Trans. Ind. Electron.*, vol. 63, no. 10, pp. 6568–6579, Oct. 2016.

[62] N. Teerakawanich, "Dynamic Modeling of Wireless Power Transfer Systems with a Moving Coil Receiver," in *2018 IEEE Transportation Electrification Conference and Expo, Asia-Pacific (ITEC Asia-Pacific)*, 2018, pp. 1–5.

[63] C. Cui, K. Song, C. Zhu, Q. Zhang, Y. Liu, and S. Dong, "State Feedback Controller Design of Dynamic Wireless Power Transfer System," in *2018 IEEE PELS Workshop on Emerging Technologies: Wireless Power Transfer (Wow)*, 2018, pp. 1–5.

[64] Z. Chen, F. He, and Y. Yin, "Optimal deployment of charging lanes for electric vehicles in transportation networks," *Transp. Res. Part B Methodol.*, vol. 91, pp. 344–365, 2016.

[65] Z. Liu and Z. Song, "Robust planning of dynamic wireless charging infrastructure for battery electric buses," *Transp. Res. Part C, Emerg. Technol.*, vol. 83, pp. 77–103, 2017.

[66] D. Kobayashi, T. Imura, and Y. Hori, "Real-time coupling coefficient estimation and maximum efficiency control on dynamic wireless power transfer for electric vehicles," in *2015 IEEE PELS Workshop on Emerging Technologies: Wireless Power (2015 WoW)*, 2015, pp. 1–6.

[67] Y. Dai, L. Ma, M. Huang, and H. Su, "Modeling and Analysis Methods for the DWPT System Applicated in EVs Charging," in *2018 IEEE PELS Workshop on Emerging Technologies: Wireless Power Transfer (Wow)*, 2018, pp. 1–6.

[68] R. Tavakoli and Z. Pantic, "DC Modeling of an LCC Resonant Compensation Network in Wireless Power Transfer Systems," in *2018 IEEE Energy Conversion Congress and Exposition (ECCE)*, 2018, pp. 6187–6193.

[69] J. M. Arteaga, S. Aldhaher, G. Kkelis, D. C. Yates, and P. D. Mitcheson, "Multi-MHz IPT Systems for Variable Coupling," *IEEE Trans. Power Electron.*, vol. 33, no. 9, pp. 7744–7758, Sep. 2018.

[70] S. Y. Hui, "Planar Wireless Charging Technology for Portable Electronic Products and Qi," in *Proceedings of the IEEE*, vol. 101, no. 6, pp. 1290-1301, June 2013.

[71] AirFuel Resonant, [Online]. Available: https://airfuel.org/wireless-power/electromagnetic-coupling/

[72] SAE J2954 Recommended Practice, "Wireless Power Transfer for Light-Duty Plug-In / Electric Vehicles and Alignment Methodology," [Online]. Available: https://saemobilus.sae.org/content/j2954_201904. [Accessed: 23-Apr-2019].

[73] Schneider, J., Carlson, R., Sirota, J., Sutton, R. et al., "Validation of Wireless Power Transfer up to 11kW Based on SAE J2954 with Bench and Vehicle Testing," SAE Technical Paper, 2019-01-0868, 2019.

[74] Electric vehicle wireless power transfer (WPT) systems - Part 3: Specific requirements for the magnetic field wireless power transfer systems, IEC 61980-3/Ed.1.

[75] K. V. Schuylenbergh and R. Puers, *Inductive Powering—Basic Theory and Application to Biomedical Systems*. New York, NY, USA: Springer-Verlag, 2009.

[76] R. Bosshard, J. Mühlethaler, J. W. Kolar, and I. Stevanović, "The η-α-Pareto front of inductive power transfer coils," *IECON 2012 - 38th Annual Conference on IEEE Industrial Electronics Society*, Montreal, QC, 2012, pp. 4270-4277.

[77] G. A. Covic and J. T. Boys, "Modern Trends in Inductive Power Transfer for Transportation Applications," *IEEE J. Emerg. Sel. Top. Power Electron.*, vol. 1, no. 1, pp. 28–41, Mar. 2013.

[78] M. Budhia, J. T. Boys, G. A. Covic, and C. Y. Huang, "Development of a Single-Sided Flux Magnetic Coupler for Electric Vehicle IPT Charging Systems," *IEEE Trans. Ind. Electron.*, vol. 60, no. 1, pp. 318–328, Jan. 2013.

[79] Y. Nagatsuka, N. Ehara, Y. Kaneko, S. Abe, and T. Yasuda, "Compact contactless power transfer system for electric vehicles," in *Proc. The International Power Electronics Conference (ECCE ASIA)*, 2010, pp. 807–813.

[80] G. A. J. Elliott, S. Raabe, G. A. Covic, and J. T. Boys, "Multiphase Pickups for Large Lateral Tolerance Contactless Power-Transfer Systems," *IEEE Trans. Ind. Electron.*, vol. 57, no. 5, pp. 1590–1598, May 2010.

[81] M. Budhia, G. A. Covic, and J. T. Boys, "Design and Optimization of Circular Magnetic Structures for Lumped Inductive Power Transfer Systems," *IEEE Trans. Power Electron.*, vol. 26, no. 11, pp. 3096–3108, Nov. 2011.

[82] G. Buja, M. Bertoluzzo, and K. N. Mude, "Design and Experimentation of WPT Charger for Electric City Car," *IEEE Trans. Ind. Electron.*, vol. 62, no. 12, pp. 7436–7447, Dec. 2015.

[83] S. Y. Jeong, S. Y. Choi, M. R. Sonapreetha, and C. T. Rim, "DQ-quadrature power supply coil sets with large tolerances for wireless stationary EV chargers," in *Proc. IEEE PELS Workshop on Emerging Technologies: Wireless Power (WoW)*, 2015, pp. 1–6.

[84] G. A. Covic, M. L. G. Kissin, D. Kacprzak, N. Clausen, and H. Hao, "A bipolar primary pad topology for EV stationary charging and highway power by inductive coupling," in *Proc. IEEE Energy Conversion Congress and Exposition (ECCE)*, 2011, pp. 1832–1838.

[85] A. Zaheer, G. A. Covic, and D. Kacprzak, "A bipolar pad in a 10-kHz 300-W distributed IPT system for AGV applications," *IEEE Trans. Ind. Electron.*, vol. 61, no. 7, pp. 3288–3301, 2014.

[86] A. Zaheer, D. Kacprzak, and G. A. Covic, "A bipolar receiver pad in a lumped IPT system for electric vehicle charging applications," in *Proc. IEEE Energy Conversion Congress and Exposition (ECCE)*, 2012, pp. 283–290.

[87] S. Kim, G. A. Covic, and J. T. Boys, "Tripolar Pad for Inductive Power Transfer Systems for EV Charging," *IEEE Trans. Power Electron.*, vol. 32, no. 7, pp. 5045–5057, Jul. 2017.

[88] S. Bandyopadhyay, P. Venugopal, J. Dong, and P. Bauer, "Comparison of Magnetic Couplers for IPT based EV Charging using Multi-Objective Optimization," *IEEE Trans. Veh. Technol.*, 2019.

[89] A. Ahmad, M. S. Alam, and R. Chabaan, "A comprehensive review of wireless charging technologies for electric vehicles," *IEEE Trans. Transp. Electrification*, vol. 4, no. 1, pp. 38–63, 2018.

[90] S. Kim, G. A. Covic, and J. T. Boys, "Comparison of Tripolar and Circular Pads for IPT Charging Systems," *IEEE Trans. Power Electron.*, vol. 33, no. 7, pp. 6093–6103, Jul. 2018.

[91] S. Moon, B. Kim, S. Cho, C. Ahn, and G. Moon, "Analysis and Design of a Wireless Power Transfer System With an Intermediate Coil for High Efficiency," *IEEE Trans. Ind. Electron.*, vol. 61, no. 11, pp. 5861–5870, Nov. 2014.

[92] J. Kim, H. Son, K. Kim, and Y. Park, "Efficiency Analysis of Magnetic Resonance Wireless Power Transfer With Intermediate Resonant Coil," *IEEE Antennas Wirel. Propag. Lett.*, vol. 10, pp. 389–392, 2011.

[93] F. Zhang, S. A. Hackworth, W. Fu, C. Li, Z. Mao, and M. Sun, "Relay Effect of Wireless Power Transfer Using Strongly Coupled Magnetic Resonances," *IEEE Trans. Magn.*, vol. 47, no. 5, pp. 1478–1481, May 2011.

[94] M. Kiani, U. M. Jow, and M. Ghovanloo, "Design and Optimization of a 3-Coil Inductive Link for Efficient Wireless Power Transmission," *IEEE Trans. Biomed. Circuits Syst.*, vol. 5, no. 6, pp. 579–591, Dec. 2011.

[95] D. Ahn and S. Hong, "A Study on Magnetic Field Repeater in Wireless Power Transfer," *IEEE Trans. Ind. Electron.*, vol. 60, no. 1, pp. 360–371, Jan. 2013.

[96] A. Kamineni, G. A. Covic, and J. T. Boys, "Analysis of Coplanar Intermediate Coil Structures in Inductive Power Transfer Systems," *IEEE Trans. Power Electron.*, vol. 30, no. 11, pp. 6141–6154, Nov. 2015.

[97] R. Mai, B. Yang, Y. Chen, N. Yang, Z. He, and S. Gao, "A Misalignment Tolerant IPT System With Intermediate Coils for Constant-Current

Output," *IEEE Trans. Power Electron.*, vol. 34, no. 8, pp. 7151–7155, Aug. 2019.

[98] T. Kan, T. Nguyen, J. C. White, R. K. Malhan, and C. C. Mi, "A New Integration Method for an Electric Vehicle Wireless Charging System Using LCC Compensation Topology: Analysis and Design," *IEEE Trans. Power Electron.*, vol. 32, no. 2, pp. 1638–1650, Feb. 2017.

[99] W. Li, H. Zhao, S. Li, J. Deng, T. Kan, and C. C. Mi, "Integrated LCC Compensation Topology for Wireless Charger in Electric and Plug-in Electric Vehicles," *IEEE Trans. Ind. Electron.*, vol. 62, no. 7, pp. 4215–4225, Jul. 2015.

[100] N. Rasekh, J. Kavianpour, and M. Mirsalim, "A Novel Integration Method for a Bipolar Receiver Pad UsingLCCCompensation Topology for Wireless Power Transfer," *IEEE Trans. Veh. Technol.*, vol. 67, no. 8, pp. 7419–7428, Aug. 2018.

[101] F. Lu, H. Zhang, H. Hofmann, W. Su, and C. C. Mi, "A Dual-Coupled LCC-Compensated IPT System With a Compact Magnetic Coupler," *IEEE Trans. Power Electron.*, vol. 33, no. 7, pp. 6391–6402, Jul. 2018.

[102] T. Kan, F. Lu, T. Nguyen, P. P. Mercier, and C. C. Mi, "Integrated Coil Design for EV Wireless Charging Systems Using LCC Compensation Topology," *IEEE Trans. Power Electron.*, vol. 33, no. 11, pp. 9231–9241, Nov. 2018.

[103] J. Deng, W. Li, T. D. Nguyen, S. Li, and C. C. Mi, "Compact and Efficient Bipolar Coupler for Wireless Power Chargers: Design and Analysis," *IEEE Trans. Power Electron.*, vol. 30, no. 11, pp. 6130–6140, Nov. 2015.

[104] A. Tejeda, S. Kim, F. Y. Lin, G. A. Covic, and J. T. Boys, "A Hybrid Solenoid Coupler for Wireless Charging Applications," *IEEE Trans. Power Electron.*, vol. 34, no. 6, pp. 5632–5645, Jun. 2019.

[105] Y. Yao, Y. Wang, X. Liu, Y. Pei, and D. Xu, "A Novel Unsymmetrical Coupling Structure Based on Concentrated Magnetic Flux for High-Misalignment IPT Applications," *IEEE Trans. Power Electron.*, vol. 34, no. 4, pp. 3110–3123, Apr. 2019.

[106] M. G. S. Pearce, G. A. Covic, and J. T. Boys, "Robust Ferrite-Less Double D Topology for Roadway IPT Applications," *IEEE Trans. Power Electron.*, vol. 34, no. 7, pp. 6062–6075, Jul. 2019.

[107] D. Ongayo and M. Hanif, "Comparison of circular and rectangular coil transformer parameters for wireless Power Transfer based on Finite Element Analysis," in *Proc. IEEE 13th Brazilian Power Electronics Conference and 1st Southern Power Electronics Conference (COBEP/SPEC)*, 2015, pp. 1–6.

[108] N. Liu and T. G. Habetler, "Design of a Universal Inductive Charger for Multiple Electric Vehicle Models," *IEEE Trans. Power Electron.*, vol. 30, no. 11, pp. 6378–6390, Nov. 2015.

[109] R. Bosshard, J. Mühlethaler, J. W. Kolar, and I. Stevanović, "Optimized magnetic design for inductive power transfer coils," in *Proc. IEEE Applied Power Electronics Conference and Exposition (APEC)*, Long Beach, CA, 2013, pp. 1812-1819.

[110] Z. Zhang, B. Jia, H. Pang, and C. Liu, "Comparative analysis and optimization of dynamic charging coils for roadway-powered electric vehicles," in *Proc. IEEE International Magnetics Conference (INTERMAG)*, 2017, pp. 1–1.

[111] R. Bosshard, U. Iruretagoyena, and J. W. Kolar, "Comprehensive Evaluation of Rectangular and Double-D Coil Geometry for 50 kW/85 kHz IPT System," *IEEE J. Emerg. Sel. Top. Power Electron.*, vol. 4, no. 4, pp. 1406–1415, Dec. 2016.

[112] Z. Luo and X. Wei, "Analysis of Square and Circular Planar Spiral Coils in Wireless Power Transfer System for Electric Vehicles," *IEEE Trans. Ind. Electron.*, vol. 65, no. 1, pp. 331–341, Jan. 2018.

[113] D. Kurschner, C. Rathge, and U. Jumar, "Design Methodology for High Efficient Inductive Power Transfer Systems With High Coil Positioning Flexibility," *IEEE Trans. Ind. Electron.*, vol. 60, no. 1, pp. 372–381, Jan. 2013.

[114] B. Klaus, D. Barth, B. Sillmann, and T. Leibfried, "Design and implementation of a transmission system for high-performance contactless electric vehicle charging," in *Proc. IEEE Transportation Electrification Conference and Expo (ITEC)*, 2017, pp. 39–44.

[115] Z. Wang, X. Wei, and H. Dai, "Nested three-layer optimisation method for magnetic coils used in 3 kW vehicle-mounted wireless power transfer system," *IET Power Electron.*, vol. 9, no. 13, pp. 2562–2570, 2016.

[116] R. Bosshard, J. W. Kolar, J. Mühlethaler, I. Stevanović, B. Wunsch, and F. Canales, "Modeling and η - α - Pareto Optimization of Inductive Power Transfer Coils for Electric Vehicles," *IEEE J. Emerg. Sel. Top. Power Electron.*, vol. 3, no. 1, pp. 50–64, Mar. 2015.

[117] P. Ning, O. Onar, and J. Miller, "Genetic algorithm based coil system optimization for wireless power charging of electric vehicles," in *Proc. IEEE Transportation Electrification Conference and Expo (ITEC)*, 2013, pp. 1–5.

[118] T. Yilmaz, N. Hasan, R. Zane, and Z. Pantic, "Multi-Objective Optimization of Circular Magnetic Couplers for Wireless Power Transfer Applications," *IEEE Trans. Magn.*, vol. 53, no. 8, pp. 1–12, Aug. 2017.

[119] A. Hariri, A. Elsayed, and O. A. Mohammed, "An Integrated Characterization Model and Multiobjective Optimization for the Design of an EV Charger's Circular Wireless Power Transfer Pads," *IEEE Trans. Magn.*, vol. 53, no. 6, pp. 1–4, Jun. 2017.

[120] P. Meyer, "Modeling of Inductive Contactless Energy Transfer Systems," Ph.D. dissertation, ÉCOLE POLYTECHNIQUE FÉDÉRALE DE LAUSANNE, Switzerland 2012.

[121] S. Bandyopadhyay, V. Prasanth, P. Bauer, and J. A. Ferreira, "Multi-objective optimization of a 1-kW wireless IPT systems for charging of electric vehicles," in *Proc. IEEE Transportation Electrification Conference and Expo (ITEC)*, 2016, pp. 1–7.

[122] R. Besuchet, C. Auvigne, D. Shi, C. Winter, Y. Civet, and Y. Perriard, "Optimisation of an inductive power transfer structure," *J. Int. Conf. Electr. Mach. Syst.*, vol. 2, no. 3, pp. 349–355, 2013.

[123] M. Pathmanathan, S. Nie, N. Yakop, and P. W. Lehn, "Field-oriented control of a three-phase wireless power transfer system transmitter," *IEEE Trans. Transp. Electrification*, 2019.

[124] F. Liu, Z. Ding, X. Fu, and R. Kennel, "Parametric Optimization of a Three-Phase MCR WPT System with Cylinder-Shaped Coils Oriented by Soft-Switching Range and Stable Output Power," *IEEE Trans. Power Electron.*, 2019.

[125] H. Li, Y. Liu, K. Zhou, Z. He, W. Li, and R. Mai, "Uniform power IPT system with three-phase transmitter and bipolar receiver for dynamic charging," *IEEE Trans. Power Electron.*, vol. 34, no. 3, pp. 2013–2017, 2018.

[126] G. A. Covic, J. T. Boys, M. L. G. Kissin, and H. G. Lu, "A Three-Phase Inductive Power Transfer System for Roadway-Powered Vehicles," *IEEE Trans. Ind. Electron.*, vol. 54, no. 6, pp. 3370–3378, Dec. 2007.

[127] D. J. Thrimawithana and U. K. Madawala, "A three-phase bi-directional IPT system for contactless charging of electric vehicles," in *Proc. IEEE International Symposium on Industrial Electronics (ISIE)*, 2011, pp. 1957–1962.

[128] H. Matsumoto, Y. Neba, H. Iura, D. Tsutsumi, K. Ishizaka, and R. Itoh, "Trifoliate Three-Phase Contactless Power Transformer in Case of Winding-Alignment," *IEEE Trans. Ind. Electron.*, vol. 61, no. 1, pp. 53–62, Jan. 2014.

[129] H. Matsumoto, Y. Neba, K. Ishizaka, and R. Itoh, "Model for a Three-Phase Contactless Power Transfer System," *IEEE Trans. Power Electron.*, vol. 26, no. 9, pp. 2676–2687, Sep. 2011.

[130] H. Matsumoto, Y. Neba, K. Ishizaka, and R. Itoh, "Comparison of Characteristics on Planar Contactless Power Transfer Systems," *IEEE Trans. Power Electron.*, vol. 27, no. 6, pp. 2980–2993, Jun. 2012.

[131] G. Su, O. C. Onar, J. Pries, and V. P. Galigekere, "Variable Duty Control of Three-Phase Voltage Source Inverter for Wireless Power Transfer Systems," in *Proc. IEEE Energy Conversion Congress and Exposition (ECCE)*, 2019, pp. 2118–2124.

[132] K. Throngnumchai, A. Hanamura, Y. Naruse, and K. Takeda, "Design and evaluation of a wireless power transfer system with road embedded transmitter coils for dynamic charging of electric vehicles," in *Proc. World Electric Vehicle Symposium and Exhibition (EVS27)*, 2013, pp. 1–10.

[133] Z. Chen, W. Jing, X. Huang, L. Tan, C. Chen, and W. Wang, "A Promoted Design for Primary Coil in Roadway-Powered System," *IEEE Trans. Magn.*, vol. 51, no. 11, pp. 1–4, Nov. 2015.

[134] W. Zhang, S. C. Wong, C. K. Tse, and Q. Chen, "An Optimized Track Length in Roadway Inductive Power Transfer Systems," *IEEE J. Emerg. Sel. Top. Power Electron.*, vol. 2, no. 3, pp. 598–608, Sep. 2014.

[135] G. Buja, M. Bertoluzzo, and H. K. Dashora, "Lumped Track Layout Design for Dynamic Wireless Charging of Electric Vehicles," *IEEE Trans. Ind. Electron.*, vol. 63, no. 10, pp. 6631–6640, Oct. 2016.

[136] X. Zhang, Z. Yuan, Q. Yang, Y. Li, J. Zhu, and Y. Li, "Coil Design and Efficiency Analysis for Dynamic Wireless Charging System for Electric Vehicles," *IEEE Trans. Magn.*, vol. 52, no. 7, pp. 1–4, Jul. 2016.

[137] F. Lu, H. Zhang, H. Hofmann, and C. C. Mi, "A Dynamic Charging System With Reduced Output Power Pulsation for Electric Vehicles," *IEEE Trans. Ind. Electron.*, vol. 63, no. 10, pp. 6580–6590, Oct. 2016.

[138] M. Bertoluzzo, G. Buja, and H. K. Dashora, "Design of DWC System Track with Unequal DD Coil Set," *IEEE Trans. Transp. Electrification*, vol. 3, no. 2, pp. 380–391, Jun. 2017.

[139] L. Xiang, Y. Sun, C. Tang, X. Dai, and C. Jiang, "Design of crossed DD coil for dynamic wireless charging of electric vehicles," in *Proc. IEEE PELS Workshop on Emerging Technologies: Wireless Power Transfer (WoW)*, 2017, pp. 1–5.

[140] W. Chen, C. Liu, C. H. Lee, and Z. Shan, "Cost-effectiveness comparison of coupler designs of wireless power transfer for electric vehicle dynamic charging," *Energies*, vol. 9, no. 11, p. 906, 2016.

[141] Y. SU, S. ZHANG, Y. XU, and C. TANG, "Design and Switching Control of Power Supply Coils Applied to ICPT-Based Electric Vehicles," *J. Southwest Jiaotong Univ.*, vol. 1, p. 024, 2016.

[142] L. Jiang, L. Shi, M. Fan, F. Zhang, and Y. Li, "Segment Control Scheme of Inductive Power Transfer System for Rail Transit," *IEEE Trans. Ind. Appl.*, vol. 54, no. 4, pp. 3271–3280, Jul. 2018.

[143] Y. Liu, R. Mai, D. Liu, Y. Li, and Z. He, "Efficiency Optimization for Wireless Dynamic Charging System With Overlapped DD Coil Arrays," *IEEE Trans. Power Electron.*, vol. 33, no. 4, pp. 2832–2846, Apr. 2018.

[144] International Commission on Non-Ionizing Radiation Protection, "Guidelines for limiting exposure to time-varying electric and magnetic fields (1 Hz to 100 kHz)," *Health Phys.*, vol. 99, no. 6, pp. 818–836, 2010.

[145] J. Kim *et al.*, "Coil Design and Shielding Methods for a Magnetic Resonant Wireless Power Transfer System," *Proc. IEEE*, vol. 101, no. 6, pp. 1332–1342, Jun. 2013.

[146] Mohammad, Mostak, Jason Pries, Omer Onar, Veda P. Galigekere, Gui-Jia Su, Saeed Anwar, Jonathan Wilkins, Utkarsh D. Kavimandan, and Devendra Patil, "Design of an EMF Suppressing Magnetic Shield for a 100-kW DD-Coil Wireless Charging System for Electric Vehicles," *2019 IEEE Applied Power Electronics Conference and Exposition (APEC)*, Anaheim, CA, 2019, pp. 1521-1527.

[147] Mohammad, Mostak, Jason Pries, Omer Onar, Saeed Anwar, Veda P. Galigekere, Gui-Jia Su, and Jonathan Wilkins, "Comparison of Leakage Magnetic Field from Matched and Mismatched Double-D Coil based Wireless Charging System for Electric Vehicles," in *2019 IEEE Energy Conversion Congress and Exposition (ECCE)*, Baltimore, MD, pp. 5733-5739.

[148] I. Ramos, K. Afridi, J. A. Estrada, and Z. Popović, "Near-field capacitive wireless power transfer array with external field cancellation," *2016 IEEE Wireless Power Transfer Conference (WPTC)*, Aveiro, 2016, pp. 1-4.

[149] Seungyoung Ahn and Joungho Kim, "Magnetic field design for high efficient and low EMF wireless power transfer in on-line electric vehicle," in *Proc. the 5th European Conference on Antennas and Propagation (EUCAP)*, 2011, pp. 3979–3982.

[150] J. Pries *et al*., "Coil Power Density Optimization and Trade-off Study for a 100kW Electric Vehicle IPT Wireless Charging System," *2018 IEEE Energy Conversion Congress and Exposition (ECCE)*, Portland, OR, 2018, pp. 1196-1201.

[151] Zhang, Bo, et al. "Challenges of future high power wireless power transfer for light-duty electric vehicles----technology and risk management," *eTransportation,* vol. 2, 2019): 100012.

[152] B. J. Limb *et al.*, "Economic Viability and Environmental Impact of In-Motion Wireless Power Transfer," *IEEE Trans. Transp. Electrification*, pp. 1–1, 2018.

[153] C. C. Mi, G. Buja, S. Y. Choi, and C. T. Rim, "Modern advances in wireless power transfer systems for roadway powered electric vehicles," *IEEE Trans. Ind. Electron.*, vol. 63, no. 10, pp. 6533–6545, 2016.

[154] I. Nam, R. Dougal, and E. Santi, "Optimal design method to achieve both good robustness and efficiency in loosely-coupled wireless charging system employing series-parallel resonant tank with asymmetrical magnetic coupler," in *Proc. IEEE Energy Conversion Congress and Exposition (ECCE)*, Denver, CO, 2013, pp. 3266-3276.

[155] W. Zhang, S. Wong, C. K. Tse, and Q. Chen, "Analysis and Comparison of Secondary Series- and Parallel-Compensated Inductive Power Transfer Systems Operating for Optimal Efficiency and Load-Independent Voltage-Transfer Ratio," *IEEE Trans. Power Electron.*, vol. 29, no. 6, pp. 2979-2990, June 2014.

[156] J. Deng, Fei Lu, S. Li, T. Nguyen, and C. Mi, "Development of a high efficiency primary side controlled 7kW wireless power charger," in *Proc. IEEE International Electric Vehicle Conference (IEVC)*, Florence, 2014, pp. 1-6.

[157] P. Schumann, O. Blum, J. Eckhardt, and A. Henkel, "High efficient, compact vehicle power electronics for 22kW inductive charging," in *Proc. 4th International Electric Drives Production Conference (EDPC)*, Nuremberg, 2014, pp. 1-5.

[158] Chwei-Sen Wang, G. A. Covic, and O. H. Stielau, "Power transfer capability and bifurcation phenomena of loosely coupled inductive power transfer systems," *IEEE Trans. Ind. Electron.*, vol. 51, no. 1, pp. 148-157, Feb. 2004.

[159] H. Hao, G. A. Covic, and J. T. Boys, "An Approximate Dynamic Model of LCL-T-Based Inductive Power Transfer Power Supplies," *IEEE Trans. Power Electron.*, vol. 29, no. 10, pp. 5554-5567, Oct. 2014.

[160] W. Zhang, S. Wong, C. K. Tse, and Q. Chen, "Load-Independent Duality of Current and Voltage Outputs of a Series- or Parallel-Compensated Inductive Power Transfer Converter With Optimized Efficiency," *IEEE J. Emerg. Sel. Top. Power Electron.*, vol. 3, no. 1, pp. 137-146, March 2015.

[161] W. Zhang, S. Wong, C. K. Tse, and Q. Chen, "Design for Efficiency Optimization and Voltage Controllability of Series–Series Compensated Inductive Power Transfer Systems," *IEEE Trans. Power Electron.*, vol. 29, no. 1, pp. 191-200, Jan. 2014.

[162] J. Hou, Q. Chen, Z. Zhang, S. Wong, and C. K. Tse, "Analysis of Output Current Characteristics for Higher Order Primary Compensation in Inductive Power Transfer Systems," *IEEE Trans. Power Electron.*, vol. 33, no. 8, pp. 6807-6821, Aug. 2018.

[163] J. Hou, Q. Chen, S. Wong, C. K. Tse, and X. Ruan, "Analysis and Control of Series/Series-Parallel Compensated Resonant Converter for Contactless Power Transfer," *IEEE J. Emerg. Sel. Top. Power Electron.*, vol. 3, no. 1, pp. 124-136, March 2015.

[164] B. Esteban, M. Sid-Ahmed, and N. C. Kar, "A Comparative Study of Power Supply Architectures in Wireless EV Charging Systems," *IEEE Trans. Power Electron.*, vol. 30, no. 11, pp. 6408-6422, Nov. 2015.

[165] Z. Pantic, S. Bai, and S. M. Lukic, "ZCS LCC-Compensated Resonant Inverter for Inductive-Power-Transfer Application," *IEEE Trans. Ind. Electron.*, vol. 58, no. 8, pp. 3500-3510, Aug. 2011.

[166] A. Zaheer, M. Neath, H. Z. Z. Beh, and G. A. Covic, "A Dynamic EV Charging System for Slow Moving Traffic Applications," *IEEE Trans. Transp. Electrification*, vol. 3, no. 2, pp. 354-369, June 2017.

[167] N. A. Keeling, G. A. Covic, and J. T. Boys, "A Unity-Power-Factor IPT Pickup for High-Power Applications," *IEEE Trans. Ind. Electron.*, vol. 57, no. 2, pp. 744-751, Feb. 2010.

[168] S. Li, W. Li, J. Deng, T. D. Nguyen, and C. C. Mi, "A Double-Sided LCC Compensation Network and Its Tuning Method for Wireless Power Transfer," *IEEE Trans. Veh. Technol.*, vol. 64, no. 6, pp. 2261-2273, June 2015.

[169] F. Lu, H. Hofmann, J. Deng, and C. Mi, "Output power and efficiency sensitivity to circuit parameter variations in double-sided LCC-compensated wireless power transfer system," in *Proc. IEEE Applied Power Electronics Conference and Exposition (APEC)*, Charlotte, NC, 2015, pp. 597-601.

[170] J. L. Villa, J. Sallan, J. F. Sanz Osorio, and A. Llombart, "High-Misalignment Tolerant Compensation Topology For ICPT Systems," *IEEE Trans. Ind. Electron.*, vol. 59, no. 2, pp. 945-951, Feb. 2012.

[171] Q. Zhu, Y. Guo, L. Wang, C. Liao, and F. Li, "Improving the Misalignment Tolerance of Wireless Charging System by Optimizing the Compensate Capacitor," *IEEE Trans. Ind. Electron.*, vol. 62, no. 8, pp. 4832-4836, Aug. 2015.

[172] Y. Lim, H. Tang, S. Lim, and J. Park, "An Adaptive Impedance-Matching Network Based on a Novel Capacitor Matrix for Wireless Power Transfer," *IEEE Trans. Power Electron.*, vol. 29, no. 8, pp. 4403-4413, Aug. 2014.

[173] Y. Chen, B. Yang, Z. Kou, Z. He, G. Cao, and R. Mai, "Hybrid and Reconfigurable IPT Systems With High-Misalignment Tolerance for Constant-Current and Constant-Voltage Battery Charging," *IEEE Trans. Power Electron.*, vol. 33, no. 10, pp. 8259-8269, Oct. 2018.

[174] J. Zhao, T. Cai, S. Duan, H. Feng, C. Chen, and X. Zhang, "A General Design Method of Primary Compensation Network for Dynamic WPT System Maintaining Stable Transmission Power," *IEEE Trans. Power Electron.*, vol. 31, no. 12, pp. 8343-8358, Dec. 2016.

[175] H. Feng, T. Cai, S. Duan, X. Zhang, H. Hu, and J. Niu, "A Dual-Side-Detuned Series-Series Compensated Resonant Converter for Wide Charging Region in a Wireless Power Transfer System," *IEEE Trans. Ind. Electron.*, vol. 65, no. 3, pp. 2177-2188, March 2018.

[176] H. Feng, T. Cai, S. Duan, J. Zhao, X. Zhang, and C. Chen, "An LCC-Compensated Resonant Converter Optimized for Robust Reaction to Large Coupling Variation in Dynamic Wireless Power Transfer," *IEEE Trans. Ind. Electron.*, vol. 63, no. 10, pp. 6591-6601, Oct. 2016.

[177] L. Zhao, D. J. Thrimawithana, and U. K. Madawala, "Hybrid Bidirectional Wireless EV Charging System Tolerant to Pad Misalignment," *IEEE Trans. Ind. Electron.*, vol. 64, no. 9, pp. 7079-7086, Sept. 2017.

[178] F. Lu, H. Zhang, H. Hofmann, and C. Mi, "A Double-Sided LCLC-Compensated Capacitive Power Transfer System for Electric Vehicle Charging," *IEEE Transactions on Power Electronics*, vol. 30, no. 11, pp. 6011-6014, Nov. 2015.

[179] F. Lu, H. Zhang, H. Hofmann, and C. C. Mi, "A Double-Sided LC-Compensation Circuit for Loosely Coupled Capacitive Power Transfer," in *IEEE Transactions on Power Electronics*, vol. 33, no. 2, pp. 1633-1643, Feb. 2018.

[180] F. Lu, H. Zhang, and C. Mi, "A Two-Plate Capacitive Wireless Power Transfer System for Electric Vehicle Charging Applications," *IEEE Transactions on Power Electronics*, vol. 33, no. 2, pp. 964-969, Feb. 2018.

[181] A. Pacini, A. Costanzo, S. Aldhaher, and P. D. Mitcheson, "Load- and Position-Independent Moving MHz WPT System Based on GaN-Distributed Current Sources," *IEEE Trans. Microw Theory and Tech*, vol. 65, no. 12, pp. 5367-5376, Dec. 2017.

[182] J. M. Arteaga, S. Aldhaher, G. Kkelis, C. Kwan, D. C. Yates, and P. D. Mitcheson, "Dynamic Capabilities of Multi-MHz Inductive Power Transfer Systems Demonstrated With Batteryless Drones," *IEEE Trans. Power Electron.*, vol. 34, no. 6, pp. 5093-5104, June 2019.

[183] Z. U. Zahid, Z. M. Dalala, R. Chen, B. Chen, and J. Lai, "Design of Bidirectional DC-DC Resonant Converter for Vehicle-to-Grid (V2G) Applications," *IEEE Trans. Transp. Electrification*, vol. 1, no. 3, pp. 232-244, Oct. 2015.

[184] M. Petersen and F. W. Fuchs, "Design of a Highly Efficient Inductive Power Transfer (IPT) System for Low Voltage Applications," in *Proc. Inter Exhibition. Conf Power Electron, Intelligent Motion, Renewable Energy and Energy Managemen (PCIM Europe)*, Nuremberg, Germany, 2015, pp. 1-8.

[185] X. Zhang *et al*., "A Control Strategy for Efficiency Optimization and Wide ZVS Operation Range in Bidirectional Inductive Power Transfer System," *IEEE Trans. Ind. Electron.*, vol. 66, no. 8, pp. 5958-5969, Aug. 2019.

[186] W. Li, H. Zhao, J. Deng, S. Li, and C. C. Mi, "Comparison Study on SS and Double-Sided LCC Compensation Topologies for EV/PHEV Wireless Chargers," *IEEE Trans. Veh. Technol.*, vol. 65, no. 6, pp. 4429-4439, June 2016.

[187] M. Petersen and F. W. Fuchs, "Investigation on power electronics topologies for inductive power transfer (IPT) systems in high power low voltage applications," in *Proc.17th European Conf. Power Electron. Appl (EPE ECCE-Europe)*, Geneva, 2015, pp. 1-10.

[188] K. Colak, E. Asa, M. Bojarski, and D. Czarkowski, "A novel common mode multi-phase half-wave semi-synchronous rectifier for inductive power transfer applications," in *Proc. IEEE Transportation Electrification Conference and Expo (ITEC)*, Dearborn, MI, 2015, pp. 1-6.

[189] T. Diekhans, F. Stewing, G. Engelmann, H. van Hoek, and R. W. De Doncker, "A systematic comparison of hard- and soft-switching topologies for inductive power transfer systems," in *Proc. 4th International Electric Drives Production Conference (EDPC)*, Nuremberg, 2014, pp. 1-8.

[190] K. Colak, E. Asa, M. Bojarski, D. Czarkowski, and O. C. Onar, "A Novel Phase-Shift Control of Semibridgeless Active Rectifier for Wireless Power Transfer," *IEEE Trans. Power Electron.*, vol. 30, no. 11, pp. 6288-6297, Nov. 2015.

[191] J. Tritschler, B. Goeldi, S. Reichert, and G. Griepentrog, "Comparison of different control strategies for series-series compensated inductive power transmission systems," in *Proc.17th European Conf. Power Electron. Appl (EPE ECCE-Europe)*, Geneva, 2015, pp. 1-8.

[192] P. Schumann, T. Diekhans, O. Blum, U. Brenner, and A. Henkel, "Compact 7 kW inductive charging system with circular coil design," in *Proc. 5th International Electric Drives Production Conference (EDPC)*, Nuremberg, 2015, pp. 1-5.

[193] S. Samanta and A. K. Rathore, "A New Current-Fed CLC Transmitter and LC Receiver Topology for Inductive Wireless Power Transfer Application: Analysis, Design, and Experimental Results," *IEEE Trans. Transp. Electrification*, vol. 1, no. 4, pp. 357-368, Dec. 2015.

[194] T. Kan, R. Mai, P. P. Mercier, and C. C. Mi, "Design and Analysis of a Three-Phase Wireless Charging System for Lightweight Autonomous Underwater Vehicles," *IEEE Trans. Power Electron.*, vol. 33, no. 8, pp. 6622-6632, Aug. 2018.

[195] C. Song *et al*., "EMI Reduction Methods in Wireless Power Transfer System for Drone Electrical Charger Using Tightly Coupled Three-Phase Resonant Magnetic Field," *IEEE Trans. Ind. Electron.*, vol. 65, no. 9, pp. 6839-6849, Sept. 2018.

[196] K. Kusaka, R. Kusui, J. Itoh, D. Sato, S. Obayashi, and M. Ishida, "A 22 kW-85 kHz Three-phase Wireless Power Transfer System with 12 coils," *2019 IEEE Energy Conversion Congress and Exposition (ECCE)*, Baltimore, MD, USA, 2019, pp. 3340-3347.

[197] F. Liu, Z. Ding, X. Fu, and R. M. Kennel, "Parametric Optimization of a Three-Phase MCR WPT System With Cylinder-Shaped Coils Oriented by Soft-Switching Range and Stable Output Power," *IEEE Transactions on Power Electronics*, vol. 35, no. 1, pp. 1036-1044, Jan. 2020.

[198] U. Iruretagoyena, A. Garcia-Bediaga, L. Mir, H. Camblong, and I. Villar, "Bifurcation Limits and Non-Idealities Effects in a Three-Phase Dynamic IPT System," *IEEE Transactions on Power Electronics*, vol. 35, no. 1, pp. 208-219, Jan. 2020.

[199] Y. Song, U. K. Madawala, D. J. Thrimawithana, and M. Vilathgamuwa, "Three-phase bi-directional wireless EV charging system with high tolerance to pad misalignment," *IET Power Electronics*, vol. 12, no. 10, pp. 2697-2705, 28 8 2019.

[200] J. Pries, V. P. Galigekere, O. C. Onar, and G. Su, "A 50kW Three-Phase Wireless Power Transfer System using Bipolar Windings and Series Resonant Networks for Rotating Magnetic Fields," *IEEE Transactions on Power Electronics*, Early Access.

[201] Q. Deng *et al*., "Modeling and Control of Inductive Power Transfer System Supplied by Multiphase Phase-Controlled Inverter," *IEEE Trans. Power Electron.*, vol. 34, no. 9, pp. 9303-9315, Sept. 2019.

[202] H. Hao, G. A. Covic, and J. T. Boys, "A Parallel Topology for Inductive Power Transfer Power Supplies," *IEEE Trans. Power Electron.*, vol. 29, no. 3, pp. 1140-1151, March 2014.

[203] Y. Li, R. Mai, L. Lu, and Z. He, "Active and Reactive Currents Decomposition-Based Control of Angle and Magnitude of Current for a Parallel Multiinverter IPT System," *IEEE Trans. Power Electron.*, vol. 32, no. 2, pp. 1602-1614, Feb. 2017.

[204] J. M. Miller and A. Daga, "Elements of Wireless Power Transfer Essential to High Power Charging of Heavy Duty Vehicles," *IEEE Trans. Transp. Electrification*, vol. 1, no. 1, pp. 26-39, June 2015.

[205] Hang Liu, Qianhong Chen, Guangjie Ke, Xiaoyong Ren, and Siu-Chung Wong, "Research of the input-parallel output-series inductive power transfer system," in *Proc. IEEE PELS Workshop on Emerging Technologies: Wireless Power (WoW)*, Daejeon, 2015, pp. 1-7.

[206] Y. Li, T. Lin, R. Mai, L. Huang, and Z. He, "Compact Double-Sided Decoupled Coils-Based WPT Systems for High-Power Applications: Analysis, Design, and Experimental Verification," *IEEE Trans. Transp. Electrification*, vol. 4, no. 1, pp. 64-75, March 2018.

[207] S. Cui, Z. Wang, S. Han, and C. Zhu, "Analysis and Design of Multiphase Receiver With Reduction of Output Fluctuation for EV Dynamic Wireless Charging System," *IEEE Trans. Power Electron.*, vol. 34, no. 5, pp. 4112-4124, May 2019.

[208] L. Chen, G. R. Nagendra, J. T. Boys, and G. A. Covic, "Double-Coupled Systems for IPT Roadway Applications," *IEEE J. Emerg. Sel. Top. Power Electron.*, vol. 3, no. 1, pp. 37-49, March 2015.

[209] M. S. Haque, M. Mohammad, J. L. Pries, and S. Choi, "Comparison of 22 kHz and 85 kHz 50 kW Wireless Charging System Using Si and SiC Switches for Electric Vehicle," *2018 IEEE 6th Workshop on Wide Bandgap Power Devices and Applications (WiPDA)*, Atlanta, GA, 2018, pp. 192-198.

[210] Jungwon Choi, D. Tsukiyama, Y. Tsuruda, and J. Rivas, "13.56 MHz 1.3 kW resonant converter with GaN FET for wireless power transfer," *2015 IEEE Wireless Power Transfer Conference (WPTC)*, Boulder, CO, 2015, pp. 1-4.

[211] J. Choi, D. Tsukiyama, and J. Rivas, "Comparison of SiC and eGaN devices in a 6.78 MHz 2.2 kW resonant inverter for wireless power transfer," *2016 IEEE Energy Conversion Congress and Exposition (ECCE)*, Milwaukee, WI, 2016, pp. 1-6.

[212] J. M. Miller *et al*., "Demonstrating Dynamic Wireless Charging of an Electric Vehicle: The Benefit of Electrochemical Capacitor Smoothing," *IEEE Power Electronics Magazine*, vol. 1, no. 1, pp. 12-24, March 2014.

[213] Jinbo, Zhao et al. "Relay control method for sectional track based dynamic wireless charging system," *Automation of Electric Power Systems* 40.16 (2016): 64-70.

[214] J. M. Miller, O. C. Onar, and M. Chinthavali, "Primary-Side Power Flow Control of Wireless Power Transfer for Electric Vehicle Charging," *IEEE J. Emerg. Sel. Top. Power Electron.*, vol. 3, no. 1, pp. 147–162, Mar. 2015.

[215] H. H. Wu, A. Gilchrist, K. D. Sealy, and D. Bronson, "A High Efficiency 5 kW Inductive Charger for EVs Using Dual Side Control," *IEEE Trans. Ind. Inform.*, vol. 8, no. 3, pp. 585–595, Aug. 2012.

[216] Y. Tang, Y. Chen, U. K. Madawala, D. J. Thrimawithana, and H. Ma, "A new controller for bidirectional wireless power transfer systems," *IEEE Trans. Power Electron.*, vol. 33, no. 10, pp. 9076–9087, 2017.

[217] K. Song, Z. Li, J. Jiang, and C. Zhu, "Constant current/voltage charging operation for series–series and series–parallel compensated wireless power transfer systems employing primary-side controller," *IEEE Trans. Power Electron.*, vol. 33, no. 9, pp. 8065–8080, 2017.

[218] Y. Yang, W. Zhong, S. Kiratipongvoot, S.-C. Tan, and S. Y. R. Hui, "Dynamic improvement of series–series compensated wireless power transfer systems using discrete sliding mode control," *IEEE Trans. Power Electron.*, vol. 33, no. 7, pp. 6351–6360, 2017.

[219] Z. Huang, S.-C. Wong, and K. T. Chi, "Control design for optimizing efficiency in inductive power transfer systems," *IEEE Trans. Power Electron.*, vol. 33, no. 5, pp. 4523–4534, 2017.

[220] X. Dai, X. Li, Y. Li, and A. P. Hu, "Maximum efficiency tracking for wireless power transfer systems with dynamic coupling coefficient estimation," *IEEE Trans. Power Electron.*, vol. 33, no. 6, pp. 5005–5015, 2017.

[221] M. Fu, H. Yin, X. Zhu, and C. Ma, "Analysis and Tracking of Optimal Load in Wireless Power Transfer Systems," *IEEE Trans. Power Electron.*, vol. 30, no. 7, pp. 3952–3963, Jul. 2015.

[222] H. Li, J. Li, K. Wang, W. Chen, and X. Yang, "A Maximum Efficiency Point Tracking Control Scheme for Wireless Power Transfer Systems Using Magnetic Resonant Coupling," *IEEE Trans. Power Electron.*, vol. 30, no. 7, pp. 3998–4008, Jul. 2015.

[223] T. Yeo, D. Kwon, S. Khang, and J. Yu, "Design of Maximum Efficiency Tracking Control Scheme for Closed-Loop Wireless Power Charging System Employing Series Resonant Tank," *IEEE Trans. Power Electron.*, vol. 32, no. 1, pp. 471–478, Jan. 2017.

[224] Y. Liu and H. Feng, "Maximum Efficiency Tracking Control Method for WPT System Based on Dynamic Coupling Coefficient Identification and Impedance Matching Network," *IEEE J. Emerg. Sel. Top. Power Electron.*, 2019.

[225] D.-H. Kim and D. Ahn, "Maximum Efficiency Point Tracking for Multiple-Transmitters Wireless Power Transfer," *IEEE Trans. Power Electron.*, 2019.

[226] D. H. Tran, V. B. Vu, and W. Choi, "Design of a High-Efficiency Wireless Power Transfer System With Intermediate Coils for the On-Board Chargers of Electric Vehicles," *IEEE Trans. Power Electron.*, vol. 33, no. 1, pp. 175–187, Jan. 2018.

[227] B. X. Nguyen *et al.*, "An Efficiency Optimization Scheme for Bidirectional Inductive Power Transfer Systems," *IEEE Trans. Power Electron.*, vol. 30, no. 11, pp. 6310–6319, Nov. 2015.

[228] W. Zhang and C. C. Mi, "Compensation Topologies of High-Power Wireless Power Transfer Systems," *IEEE Trans. Veh. Technol.*, vol. 65, no. 6, pp. 4768–4778, Jun. 2016.

[229] Q. Deng *et al.*, "Edge Position Detection of On-line Charged Vehicles With Segmental Wireless Power Supply," *IEEE Trans. Veh. Technol.*, vol. 66, no. 5, pp. 3610–3621, May 2017.

[230] N. Hasan, H. Wang, T. Saha, and Z. Pantic, "A novel position sensorless power transfer control of lumped coil-based in-motion wireless power transfer systems," in *Proc. IEEE Energy Conversion Congress and Exposition (ECCE)*, 2015, pp. 586–593.

[231] Y. Zhang, Z. Yan, J. Zhu, S. Li, and C. Mi, "A review of foreign object detection (FOD) for inductive power transfer systems," *eTransportation*, vol. 1, p. 100002, 2019.

[232] S. Y. Jeong, V. X. Thai, J. H. Park, and C. T. Rim, "Self-Inductance-Based Metal Object Detection With Mistuned Resonant Circuits and Nullifying Induced Voltage for Wireless EV Chargers," *IEEE Trans. Power Electron.*, vol. 34, no. 1, pp. 748–758, Jan. 2019.

[233] G. R. Nagendra, L. Chen, G. A. Covic, and J. T. Boys, "Detection of EVs on IPT Highways," *IEEE J. Emerg. Sel. Top. Power Electron.*, vol. 2, no. 3, pp. 584–597, Sep. 2014.

[234] A. Kamineni, M. J. Neath, A. Zaheer, G. A. Covic, and J. T. Boys, "Interoperable EV Detection for Dynamic Wireless Charging With Existing Hardware and Free Resonance," *IEEE Trans. Transp. Electrification*, vol. 3, no. 2, pp. 370–379, Jun. 2017.

[235] V. X. Thai, G. C. Jang, S. Y. Jeong, J. H. Park, Y.- Kim, and C. T. Rim, "Symmetric Sensing Coil Design for the Blind-zone Free Metal Object Detection of a Stationary Wireless Electric Vehicles Charger," *IEEE Trans. Power Electron.*, pp. 1–1, 2019.

[236] S. Fukuda, H. Nakano, Y. Murayama, T. Murakami, O. Kozakai, and K. Fujimaki, "A novel metal detector using the quality factor of the secondary coil for wireless power transfer systems," in *Proc. IEEE MTT-S Inter Microw Workshop Series. Innov Wireless Power Tran: Techno, Systems, and Appl*, 2012, pp. 241–244.

[237] S. Y. Jeong, H. G. Kwak, G. C. Jang, and C. T. Rim, "Living object detection system based on comb pattern capacitive sensor for wireless EV chargers," in *Proc. IEEE 2nd Annual Southern Power Electronics Conference (SPEC)*, 2016, pp. 1–6.

[238] M. R. Sonapreetha, S. Y. Jeong, S. Y. Choi, and C. T. Rim, "Dual-purpose non-overlapped coil sets as foreign object and vehicle location detections for wireless stationary EV chargers," in *Proc. IEEE PELS Workshop on Emerging Technologies: Wireless Power (WoW)*, 2015, pp. 1–7.

[239] "Typical Values for Driving Performance with Emphasis on the Standard Deviation of Lane Position: A Summary of the Literature," *Volpe - The National Transportation Systems Center*, 06-Jan-2014. [Online]. Available: https://www.volpe.dot.gov/safety-management-and-human-factors/surface-transportation-human-factors/typical-values-driving. [Accessed: 02-Mar-2017].

[240] "J2954A (WIP) Wireless Power Transfer for Light-Duty Plug-In/ Electric Vehicles and Alignment Methodology - SAE International," [Online]. Available: http://standards.sae.org/wip/j2954/. [Accessed: 13-Jan-2017].

[241] K. Fotopoulou and B. W. Flynn, "Wireless Power Transfer in Loosely Coupled Links: Coil Misalignment Model," *IEEE Trans. Magn.*, vol. 47, no. 2, pp. 416–430, Feb. 2011.

[242] S. G. Lee, H. Hoang, Y. H. Choi, and F. Bien, "Efficiency improvement for magnetic resonance based wireless power transfer with axial-misalignment," *Electron. Lett.*, vol. 48, no. 6, pp. 339–340, 2012.

[243] G. Ke, Q. Chen, W. Gao, S. Wong, C. K. Tse, and Z. Zhang, "Research on IPT Resonant Converters with High Misalignment Tolerance Using Multi-Coil Receiver Set," *IEEE Trans. Power Electron.*, pp. 1–1, 2019.

[244] D. Patil, M. Sirico, L. Gu, and B. Fahimi, "Maximum efficiency tracking in wireless power transfer for battery charger: Phase shift and frequency control," in *Proc. IEEE Energy Conversion Congress and Exposition (ECCE)*, 2016, pp. 1–8.

[245] A. N. Azad, A. Echols, V. A. Kulyukin, R. Zane, and Z. Pantic, "Analysis, Optimization, and Demonstration of a Vehicular Detection System Intended for Dynamic Wireless Charging Applications," *IEEE Trans. Transp. Electrification*, vol. 5, no. 1, pp. 147–161, Mar. 2019.

[246] I. Cortes and W. Kim, "Lateral Position Error Reduction Using Misalignment-Sensing Coils in Inductive Power Transfer Systems," *IEEE ASME Trans. Mechatron.*, vol. 23, no. 2, pp. 875–882, Apr. 2018.

[247] A. Gil, P. Sauras-Perez, and J. Taiber, "Communication requirements for Dynamic Wireless Power Transfer for battery electric vehicles," in *Proc. IEEE International Electric Vehicle Conference (IEVC)*, 2014, pp. 1–7.

[248] A. Echols, S. Mukherjee, M. Mickelsen, and Z. Pantic, "Communication Infrastructure for Dynamic Wireless Charging of Electric Vehicles," in *Proc. IEEE Wireless Communications and Networking Conference (WCNC)*, 2017, pp. 1–6.

[249] R. Bosshard and J. W. Kolar, "Inductive power transfer for electric vehicle charging: Technical challenges and tradeoffs," *IEEE Power Electronics Magazine*, vol. 3, no. 3, pp. 22-30, Sept. 2016.

[250] A. Rajagopalan, A. K. RamRakhyani, D. Schurig, and G. Lazzi, "Improving Power Transfer Efficiency of a Short-Range Telemetry System Using Compact Metamaterials," *IEEE Trans. Microw Theory. Techn,* vol. 62, no. 4, pp. 947-955, April 2014.

[251] M. Zucca *et al*., "Metrology for Inductive Charging of Electric Vehicles (MICEV)," *2019 AEIT International Conference of Electrical and Electronic Technologies for Automotive (AEIT AUTOMOTIVE)*, Torino, Italy, 2019, pp. 1-6.

[252] W. Zhang, J. C. White, A. M. Abraham, and C. C. Mi, "Loosely Coupled Transformer Structure and Interoperability Study for EV Wireless Charging Systems," *IEEE Trans. Power Electron.*, vol. 30, no. 11, pp. 6356-6367, Nov. 2015.

[253] G. R. Nagendra, G. A. Covic, and J. T. Boys, "Sizing of Inductive Power Pads for Dynamic Charging of EVs on IPT Highways," *IEEE Trans. Transp. Electrification*, vol. 3, no. 2, pp. 405-417, June 2017.

[254] W. Haibing, Z. Kehan, Y. Zhengchao, and S. Baowei, "Comparison of two electromagnetic couplers in an inductive power transfer system for Autonomous Underwater Vehicle docking application," in *OCEANS-Shanghai*, 2016, pp. 1–5

[255] S. Aldhaher, P. D. Mitcheson, J. M. Arteaga, G. Kkelis, and D. C. Yates, "Light-weight wireless power transfer for mid-air charging of drones," in *Proc. 11th European Conference on Antennas and Propagation (EUCAP)*, pp. 336-340, 2017.

[256] K. Mainali, R. Wang, J. Sabate, Y. Veer Singh, and S. Klopman, "Design of Gate Drive Power Supply with Air Core Transformer for High dv/dt Switching," in *Proc. IEEE Energy Conversion Congress and Exposition (ECCE)*, Portland, OR, 2018, pp. 5479-5484.

[257] W. Zhou and K. Jin, "Optimal Photovoltaic Array Configuration Under Gaussian Laser Beam Condition for Wireless Power Transmission," *IEEE Trans. Power Electron.*, vol. 32, no. 5, pp. 3662-3672, May 2017.

[258] M. Meng and M. Kiani, "Design and Optimization of Ultrasonic Wireless Power Transmission Links for Millimeter-Sized Biomedical Implants," *IEEE Trans.Biome Circuits. Syst*, vol. 11, no. 1, pp. 98-107, Feb. 2017.

[259] G. A. Putrus, P. Suwanapingkarl, D. Johnston, E. C. Bentley, and M. Narayana, "Impact of electric vehicles on power distribution networks," in *2009 IEEE Vehicle Power and Propulsion Conference*, 2009, pp. 827–831.

[260] E. L. Karfopoulos and N. D. Hatziargyriou, "Distributed coordination of electric vehicles providing V2G services," *IEEE Trans. Power Syst.*, vol. 31, no. 1, pp. 329–338, 2015.

[261] F. He, D. Wu, Y. Yin, and Y. Guan, "Optimal deployment of public charging stations for plug-in hybrid electric vehicles," *Transp. Res. Part B Methodol.*, vol. 47, pp. 87–101, 2013.

[262] Z. Chen, F. He, and Y. Yin, "Optimal deployment of charging lanes for electric vehicles in transportation networks," *Transp. Res. Part B Methodol.*, vol. 91, pp. 344–365, 2016.

[263] S. Debnath, A. Foote, O. C. Onar, and M. Chinthavali, "Grid Impact Studies from Dynamic Wireless Charging in Smart Automated Highways," *2018 IEEE Transportation Electrification Conference and Expo (ITEC)*, Long Beach, CA, 2018, pp. 950-955.

[264] S. Ruddell, U. K. Madawala, and D. J. Thrimawithana, "Dynamic WPT system for EV charging with integrated energy storage," *IET Power Electron.*, 2018.

[265] A. Azad, and Z. Pantic, "A Supercapacitor-Based Converter Topology for Grid-Side Power Management in Dynamic Wireless Charging Systems," in *2019 IEEE Transportation Electrification Conference and Expo (ITEC)*, 2019, pp. 1–5.

[266] S. Y. Chu and A. Avestruz, "Transfer-power measurement: A noncontact method for fair and accurate metering of wireless power transfer in electric vehicles," *in 2017 IEEE 18th Workshop on Control and Modeling for Power Electronics (COMPEL)*, pp. 1–8, July 2017

[267] S. Y. Chu and A. Avestruz, "A New Calibration Strategy for Transfer-Power Measurement of Wireless Charging of Electric Vehicles," *2019 IEEE Transportation Electrification Conference and Expo (ITEC)*, Detroit, MI, USA, 2019, pp. 1-5.

[268] Vincenzo, Cirimele, et al. "Challenges in the Electromagnetic Modeling of Road Embedded Wireless Power Transfer," *Energies* 12.14, 2019: 2677.

[269] Chen, Feng, et al. "Dynamic application of the Inductive Power Transfer (IPT) systems in an electrified road: Dielectric power loss due to pavement materials," *Construction and Building Materials* 147, 2017: 9-16.

[270] R. Tavakoli *et al*., "Magnetizable concrete composite materials for road-embedded wireless power transfer pads," *2017 IEEE Energy Conversion Congress and Exposition (ECCE)*, Cincinnati, OH, 2017, pp. 4041-4048.

[271] Beeldensa, Anne, Patrick Hauspiec, and Harold Perikd, "Inductive charging through concrete roads: a Belgian case study and application," 1st European Road Infrastructure Congress, 2016

[272] Marmiroli, Benedetta, Giovanni Dotelli, and Ezio Spessa. "Life Cycle Assessment of an On-Road Dynamic Charging Infrastructure," *Applied Sciences* 9.15, 2019: 3117.

[273] K. Harnett, B. Harris, D. Chin, and G. Watson "DOE/DHS/DOT Volpe technical meeting on electric vehicle and charging station cybersecurity report," i*n No. DOT-VNTSC-DOE-18-0 Report*, John A. Volpe National Transportation Systems Center (US), 2018.

[274] Y. Park, O. C. Onar, and B. Ozpineci, "Potential Cybersecurity Issues of Fast Charging Stations with Quantitative Severity Analysis," *2019 IEEE CyberPELS (CyberPELS)*, Knoxville, TN, USA, 2019, pp. 1-7.